STUDY OF MINIMUM PRESSURE LOSS IN HIGH VELOCITY DUCT SYSTEMS

by

C. R. Gerlach
E. C. Schroeder

Interim Technical Report No. 1
Contract No. NAS8-21133
Control No. DCN 1-7-52-20017 (IF)
SwRI Project No. 02-2119

Prepared for

National Aeronautics and Space Administration
George C. Marshall Space Flight Center
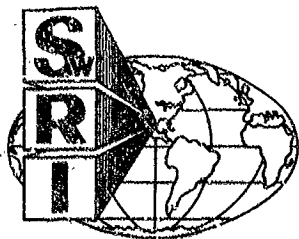Marshall Space Flight Center, Alabama   35812

16 July 1969

SOUTHWEST RESEARCH INSTITUTE
SAN ANTONIO   HOUSTON

SOUTHWEST RESEARCH INSTITUTE
8500 Culebra Road, San Antonio, Texas 78228

STUDY OF MINIMUM PRESSURE LOSS IN HIGH VELOCITY DUCT SYSTEMS

by

C. R. Gerlach
E. C. Schroeder

Prepared for

National Aeronautics and Space Administration
George C. Marshall Space Flight Center
Marshall Space Flight Center, Alabama   35812

16 July 1969

Approved:

H. Norman Abramson, Director
Department of Mechanical Sciences

TABLE OF CONTENTS

I. INTRODUCTION

This report summarizes all work which has been performed by the Southwest Research Institute during the past two-year period under Contract NAS8-21133, "Study of Minimum Pressure Loss in High Velocity Duct Systems". This study is being performed for the George C. Marshall Space Flight Center of the National Aeronautics and Space Administration and administered technically by the Propulsion and Vehicle Engineering Laboratory with Mr. R. H. Veitch serving as Technical Manager.

The general objective of this study is to perform a theoretical and experimental investigation of ducting and ducting components to minimize pressure drop, surge pressures and vibration levels and, thus, to generally improve flow conditions of gases and liquids in space vehicle feed systems. Because of NASA needs, much emphasis has been placed on the study of bellows flow-induced vibrations.

Summary of Results

A number of significant findings have been made throughout this study and are discussed in detail in this report; these are summarized below:

(a) Bellows Flow-Induced Vibrations - The fluid-elastic mechanism causing bellows flow excitation (vortex shedding) has been observed and described. Analytical models have been developed to allow a designer to predict when flow excitation may occur, and to estimate the severity of the bellows vibrations. All pertinent data, in the form of equations and curves, are presented in this report. The method is subject to certain current limitations which are discussed.

(b) Bellows Liner Design - A limited amount of information is presented to aid in the design of a conventional bellows liner which suppresses flow-induced vibrations.

(c) Bellows Pressure Loss - All available data has been compiled which gives bellows pressure loss for various convolution geometries, various sizes, and various flow media. Existing bellows pressure loss correlation methods have been reviewed, and while none are completely adequate, one is recommended for future use.

(d) Elbow Pressure Loss - A new elbow design has been
     discovered which results in a significant reduction in
     pressure loss, as confirmed by tests.

(e) External Damping Devices - Various bellows external
     damping devices have been tried as a means of suppressing
     bellows flow-induced vibrations. The results of these tests
     are presented to guide the designer in achieving vibration
     suppression by this means.

II. BELLOWS FLOW-INDUCED VIBRATIONS

II.1 Introduction

The occurrence of flow-induced vibrations of metal bellows contained in fluid ducting systems has, for some time, been a problem for aerospace applications. There are known instances where flow-induced vibrations of bellows have resulted in fatigue failures which forced the premature shutdown of some critical fluid systems. The most common methods for correcting unsuccessful bellows installations have been either to install an internal liner, where possible, or to use multiple plys or thicknesses of metal when constructing the bellows. Unfortunately, increasing the number of metal plys has not always cured the flow-induced vibration problem, and the use of a bellow's liner generally leads to an increase in component weight and cost. A major obstacle in the past has been that the flow mechanism which causes bellows vibration has not been described or understood so that flow-induced failures could be anticipated. From the standpoint of the designer, a desirable goal is to have available an analytical procedure which allows a prediction of critical fluid flow ranges for a given bellows configuration and, further, which gives a method for estimating stress levels resulting from the flow excitation in these critical ranges.

This chapter of the report is devoted to a comprehensive discussion of the bellows flow-induced vibration problem. As will be demonstrated, a fluid-elastic instability—coupling of vortex shedding from the bellows convolutions with the bellows structural vibration modes—is responsible for flow-induced failure problems. The conditions under which flow excitation is likely to occur are predictable, with acceptable accuracy, through the use of a simple analytical procedure. Further, good progress has been made in the development of a method for predicting magnitudes of the dynamic stresses which occur in the convolutions because of flow excitation. This refined stress prediction method is supplemented by a simple "stress indicator" procedure for quickly judging potential severity of bellows vibrations. A preliminary "stress indicator" versus number-of-cycles-to-failure curve has been compiled as a further aid to the engineer. Collectively, these various procedures represent a design or evaluation method which can be used to determine the adequacy of a given bellows application.

II.2 Background Information and Preliminary Test Results

A search of the open literature, conducted at the start of the project, revealed that no previous work had been reported on flow excitation of bellows. In fact, the only discussions found in the literature which deal with the related

problem of mechanically excited vibration characteristics of bellows are those of Daniels (1) and Lytle (2). A study of unpublished reports from the aerospace industry, however, revealed that bellows flow-induced fatigue failures had been observed for a variety of conditions, including liquid and gas flow, single- and multiple-ply bellows, and both free and wire braid-covered items.

In an effort to better understand the problem, several different bellows specimens were initially tested in a water-flow loop. Figure 1 shows a typical item mounted in the flow loop test section—in this case a free bellows with an internal diameter of 2-in. Each test bellows had one or more strain gages cemented on the bellows convolution crowns (see Figure 2 for bellows nomenclature) to allow flow-induced strain to be monitored. For each test bellows it was generally found that as the fluid velocity was slowly increased, starting from zero, successive longitudinal accordian vibration modes were excited. Figures 3 and 4 show typical strain data and Figure 5 illustrates the vibration modes observed. As may be seen from Figures 3 and 4, each vibration mode was excited over some well defined fluid velocity range with the peak excitation occurring near the center of this range. A Fourier analysis of the strain signal was made at each test point with a wave analyzer, which revealed that, in some instances, more than one mode was being excited at a given fluid velocity. The simultaneous existence of two modes has only been observed, however, where the resonant frequency of one mode is about twice the resonant frequency of the other. In Figure 4, for example, the second mode showed significant response over the same fluid velocity range for which the first mode was responding.

While the brief description above is not complete as to many fine points of other observations about bellows flow-induced vibrations, it should, at least, introduce the reader to the problem.

II.3   Flow Excitation Mechanism

Based on test data of the type discussed above, and on the results of some flow visualization experiments, evidence is now conclusive that vortex shedding from the bellows convolutions is the prime mechanism responsible for the flow excitation phenomena which are observed in practice. In every sense, the phenomena is a fluid-elastic instability (see References 3-7), since a mutual interaction or coupling occurs between the dynamics of the bellows (the elastic system) and the nonsteady flow near and between the convolutions (the dynamic fluid system). Many factors have an influence

4
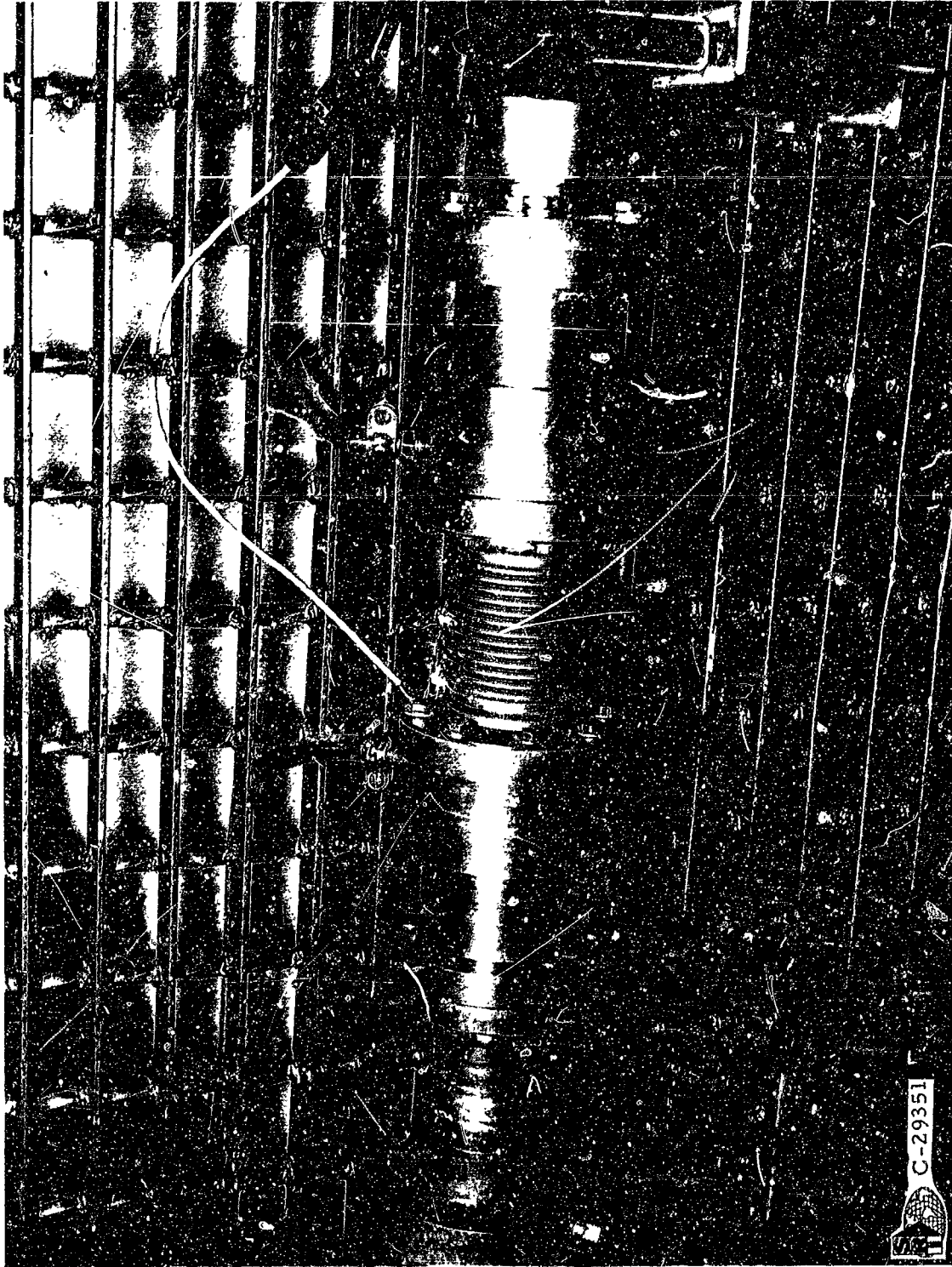
Figure 1. Installation Of Vibration Test Bellows In Flow Loop

C-29351

CONVOLUTION NOMENCLATURE

Crown

Trapped Fluid
(Added Mass)

Root

D_m

MECHANICAL MODEL AND NOMENCLATURE

A mass (m) is assigned each convolution crown
and root; the number of masses is $2N_C - 1$.
The value of m is $m_m + m_f$ where

$$m_m = \pi \rho_m t N_p D_m \mid \pi a + (h - 2a) \mid$$

The number of springs is $2N_C$ and

$$k = 2N_C k_A$$

where k_A is the overall bellows spring rate.
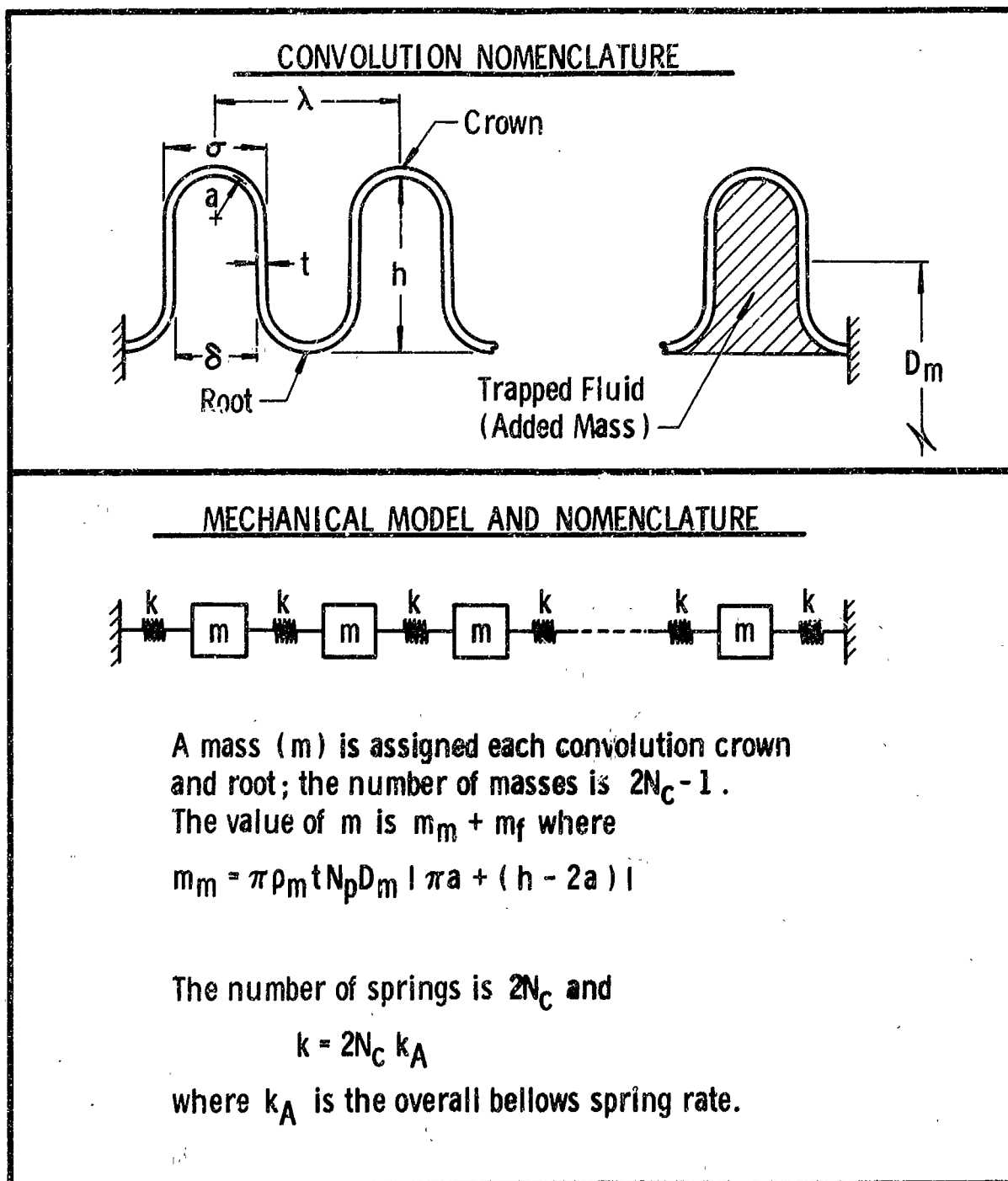
1870

Figure 2. Convolution Nomenclature And Mechanical Vibration Model

Figure 3. Bellows Stress As A Function Of Flow Rate For Four
Flow-Excited Modes Of Vibration - PN 08046

Figure 4. Bellows Stress As A Function Of Flow Rate For Two
Flow Excited Modes Of Vibration - PN 08047

Axial
Displacement
Of Convolutions

Envelope Of Axial Displacement

First Mode

Second Mode

Third Mode

2413

Figure 5. Observed Bellows Longitudinal Vibration
Mode Shapes

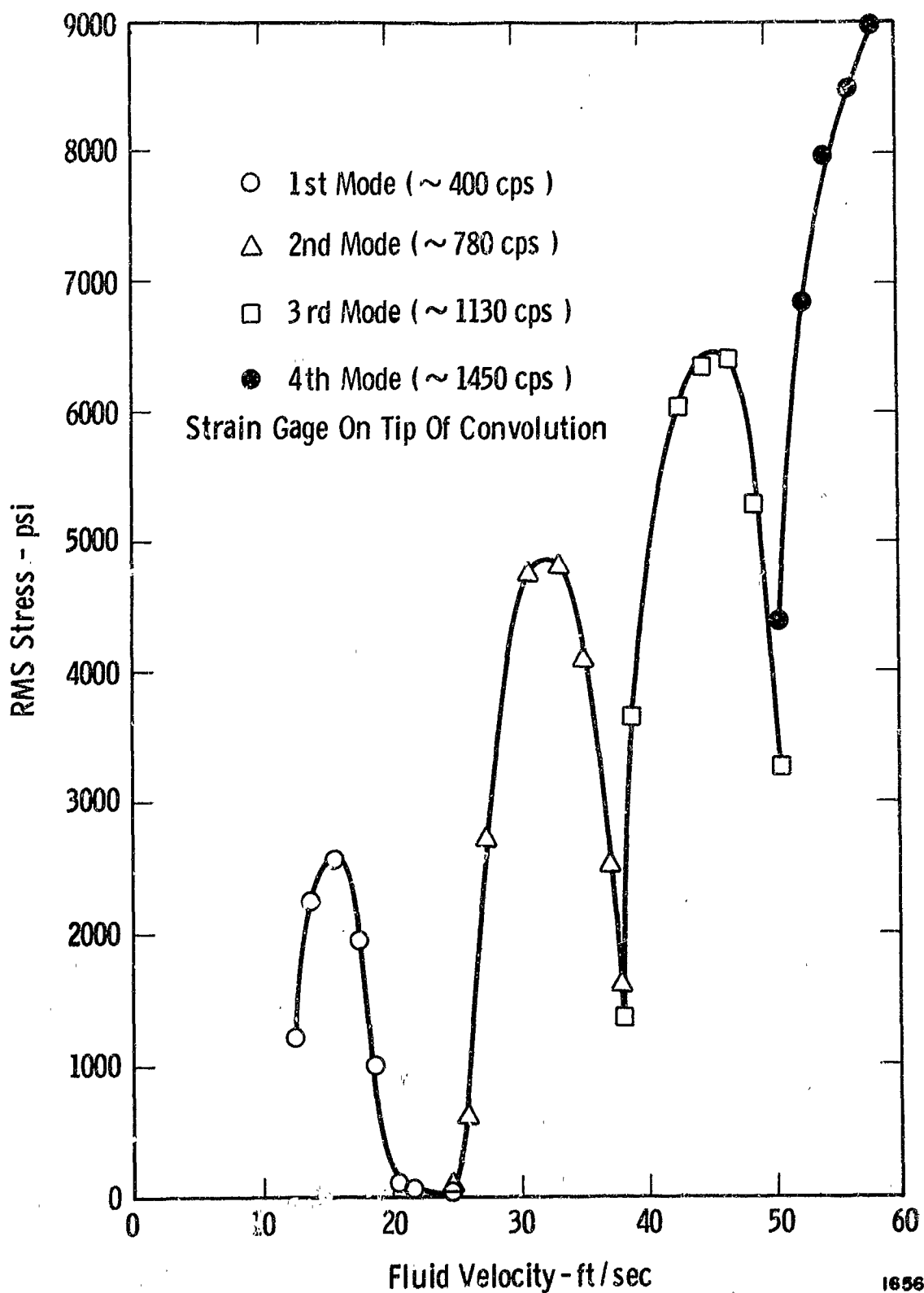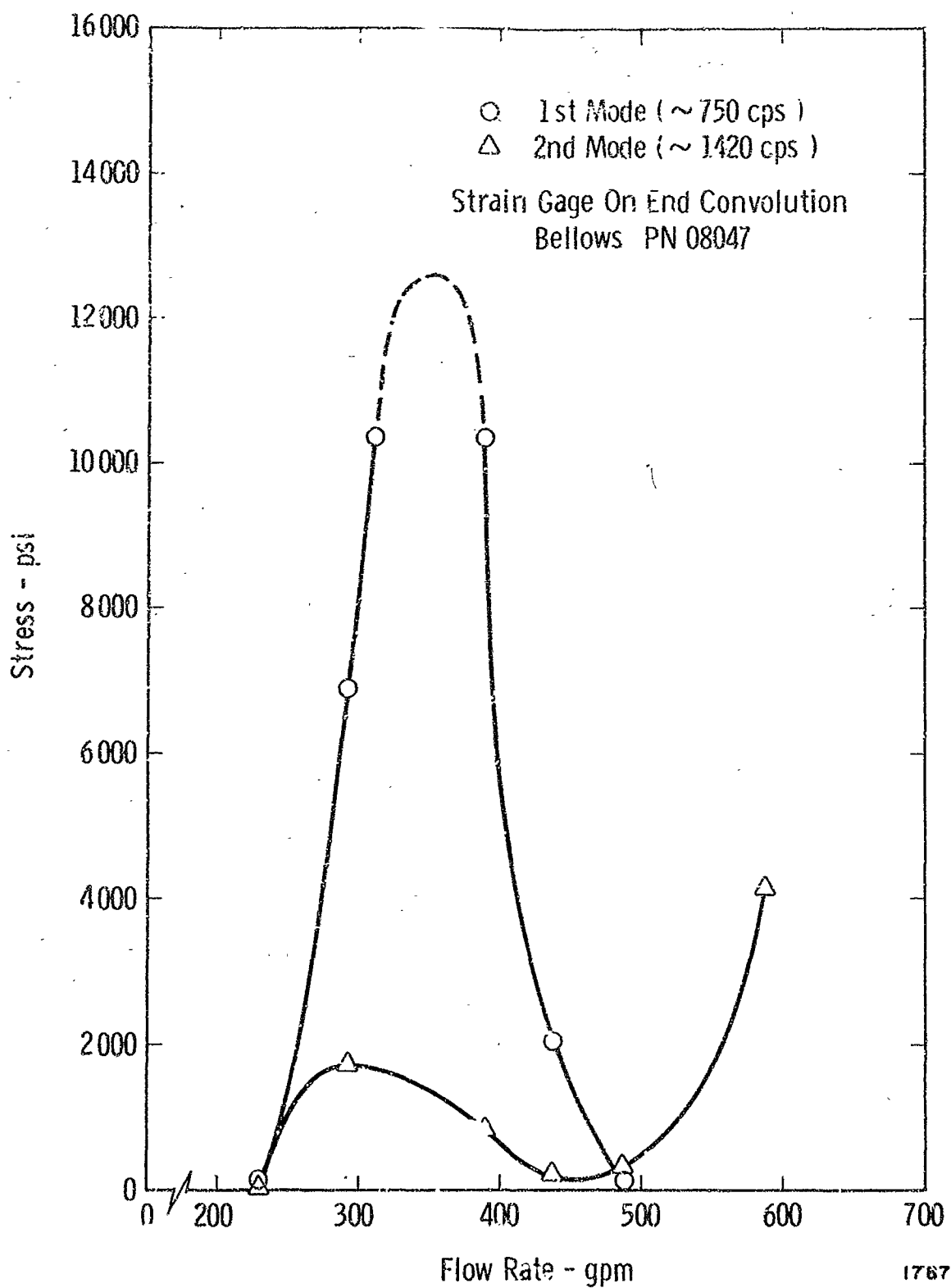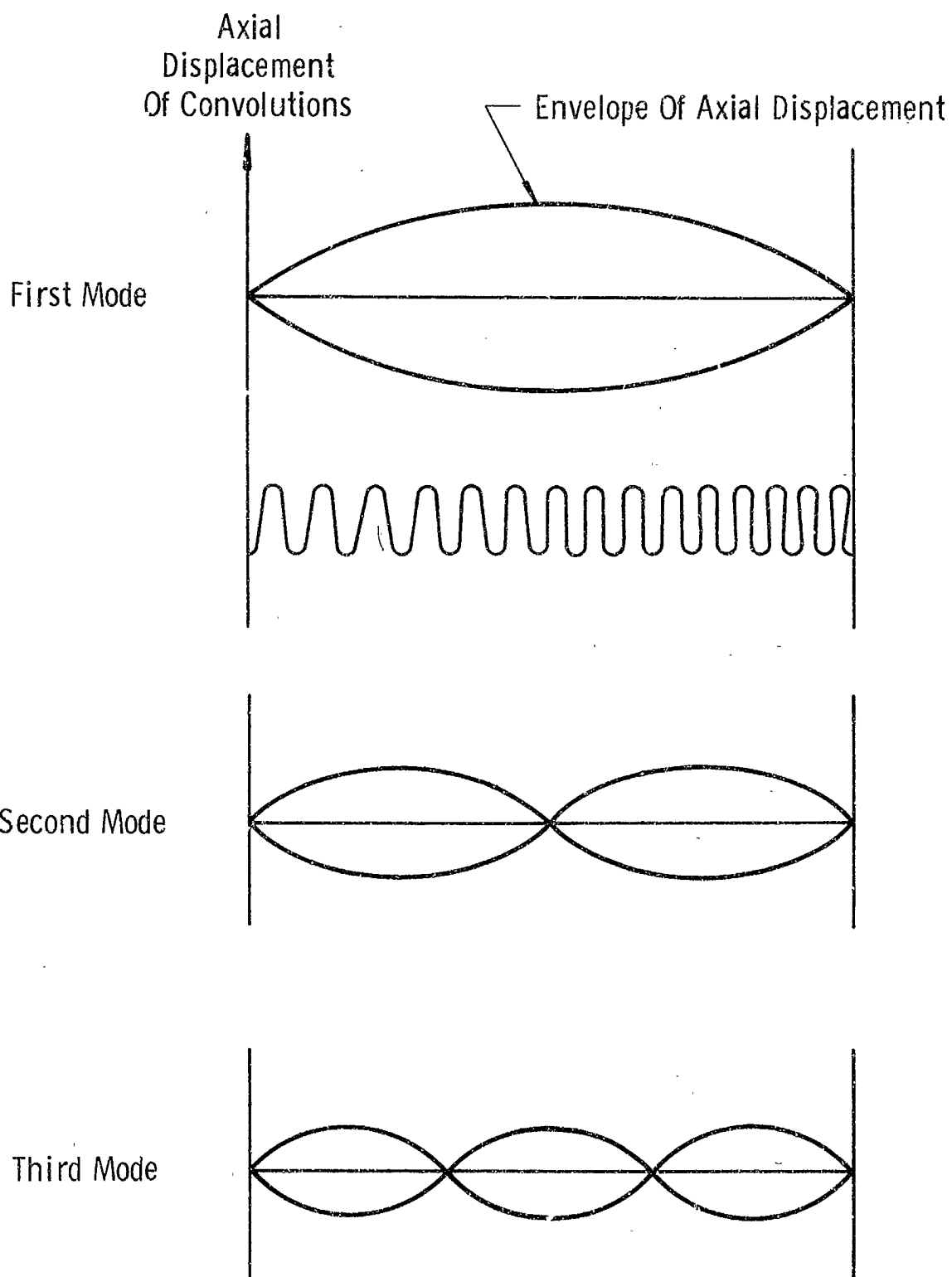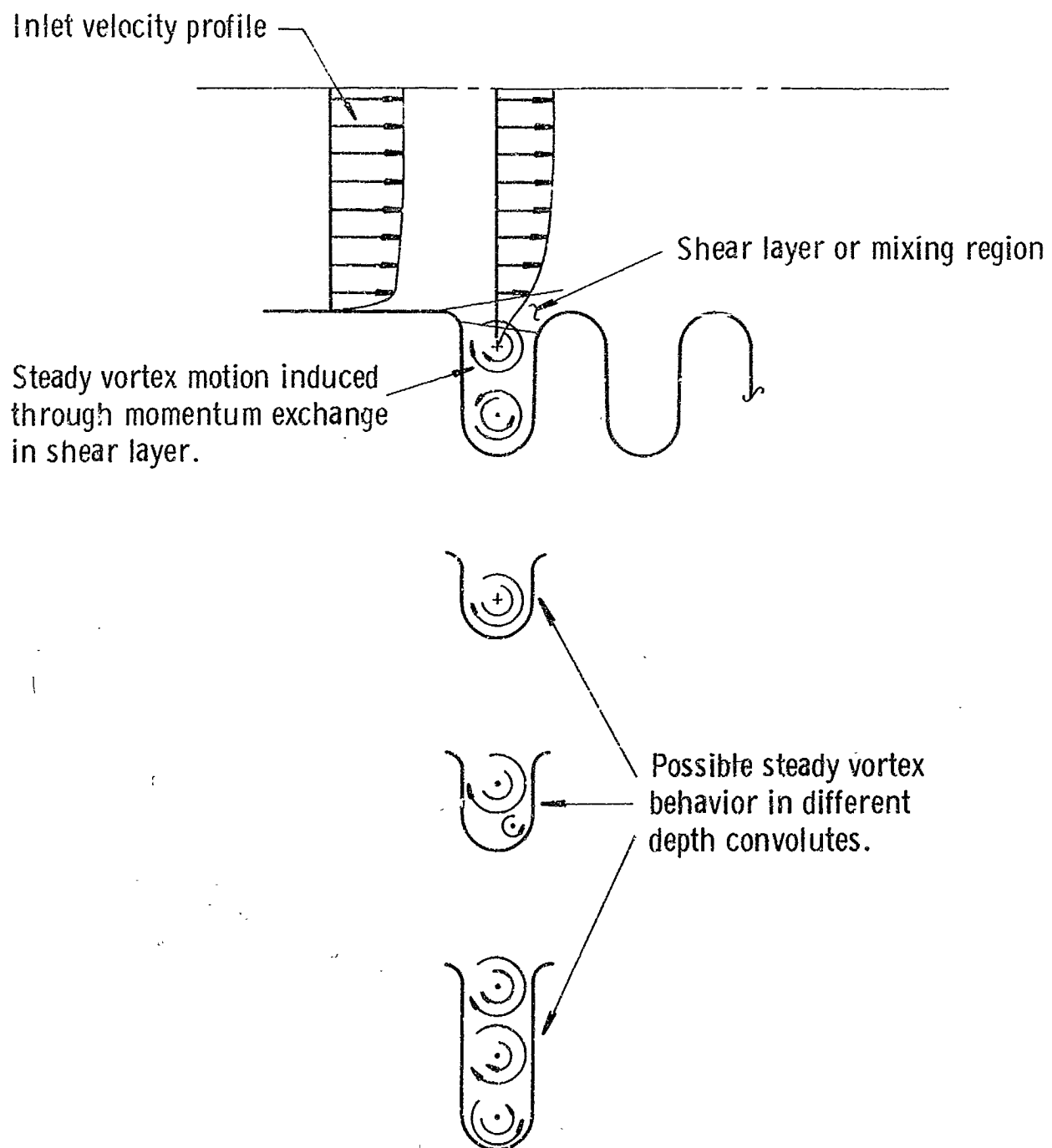on this coupling phenomena; these factors will be discussed in detail in later sections of this report. The purpose of this section is to describe the fluid and structural behavior when vibration occurs, and also for those conditions when it does not occur.

For flow through a convoluted section of bellows, with the convolutions fixed to prevent vibration, a steady turbulent flow situation exists throughout the bellows. Figure 6 illustrates the steady flow in a bellows with no convolution vibration; this is a physical picture formulated from our own flow visualization experiments, and from the information reported by Haugen and Dhanak (8), and Townes and Sabersky (9). Each convolution, in general, experiences an internal eddying flow because of a momentum transfer process. Energy is transferred into each convolution in a mixing zone or shear layer, indicated in Figure 6. The number and size of the steady vortices which exist in the convolutions are a function of the convolution geometry, also indicated in Figure 6. Very shallow convolutions may contain only one vortex, while two or more may exist in deep convolutions. As will be discussed in a later section of this report, it is this momentum transfer process and vortex motion which causes a bellows to have an extraordinarily high pressure loss.
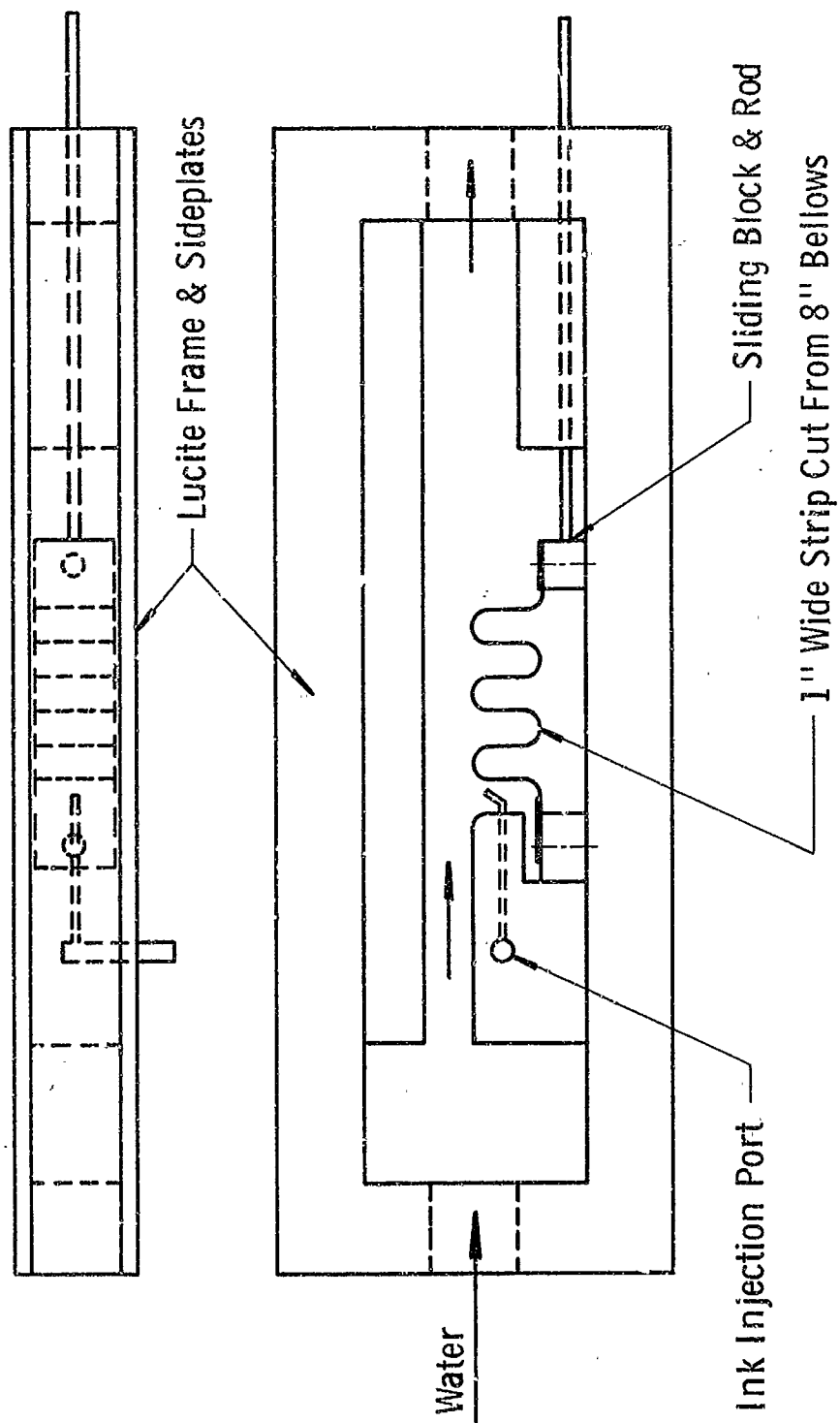
The physical picture described above is strictly for the case of no convolution motion or vibration. The only flow excitation which the bellows would experience with this type of flow behavior, would be random as a result of the turbulent pressure fluctuations experienced at the fluid-convolution boundary. This excitation mechanism would give forces of a much lower magnitude than the one really responsible for bellows flow excitation.

When the bellows is allowed to be flow excited, the physical picture of internal flow described above is no longer valid, in general. For this case, the flow now involves a large-scale periodic vortex formation and shedding process which has been visualized with the apparatus shown in Figure 7. The model consists of a two-dimensional clear plastic channel containing a short section of convoluted metal which is placed so that the convolution tips are exposed to the fluid flow, as in an actual bellows. One end of the convoluted segment is movable, in a longitudinal direction, so that the convolution pitch can be varied, as desired, by stretching or compressing the segment. When water is passed through the channel at the proper velocity, the segment is flow excited (if the conditions are right);

10

Inlet velocity profile —

Shear layer or mixing region

Steady vortex motion induced
through momentum exchange
in shear layer.

Possible steady vortex
behavior in different
depth convolutes.

2.395

Figure 6. Fluid Flow Behavior With Stationary Convolutions

Figure 7. Two Dimensional Bellows Flow Visualization Model

Lucite Frame & Sideplates

Sliding Block & Rod

1" Wide Strip Cut From 8" Bellows

Ink Injection Port

Water

2206

this vibration of the convoluted segment is easily viewed in a slowed-down manner with the aid of a strobe light. By injecting ink upstream from the convoluted segment, as indicated in Figure 7, the vortex shedding process can readily be visualized.

Both still and moving pictures of the vortex shedding have been made; Figure 8 shows several of the still pictures, which were taken at random times during the vortex shedding process. The presence of a vortex pattern is evident in each picture. The movie, of course, shows the interaction of the fluid motion and the segment much more clearly than do the still pictures.

Figure 9 shows the sequence of fluid and convolution events which have been observed in a frame-by-frame examination of the motion picture. Note, first of all, that the mode of vibration of the segment is one where each convolution moves out-of-phase with the adjacent convolution(s). The vortex shedding process on the vibrating segment, as shown by Figure 9, occurs as follows:

> Postion I - A large vortex (c) has formed between convolutions 1 and 2, and is being "pushed" out into the fluid stream by the pinching action of these two convolutions. A large, well-formed vortex (a) is moving across the tip convolution 3; the origin of this vortex will be made clear in the description of other events. Finally, a small vortex (b) is beginning to form on the downstream side of convolution 2.

> Postion II - Vortex (c) has been pinched from between convolutions 1 and 2 and has now moved out into the fluid stream, and will soon "detach" from convolution 1 and be swept downstream. Vortex (b), which is forming on the downstream side of convolution 2, is gaining in strength. Vortex (a), which in Position I was beginning to move over the tip of convolution 3, is now further downstream.

> Position III - The space between convolutions 1 and 2 is opening up, hence fluid is being drawn in, and vortex (d) is beginning to form on the downstream side of convolution 1. Vortex (c) has been swept over the top of convolution 2, with the timing being about right to reinforce vortex (b), which is being pinched from between convolutions 2 and 3; the combined vortex is labeled (b + c).
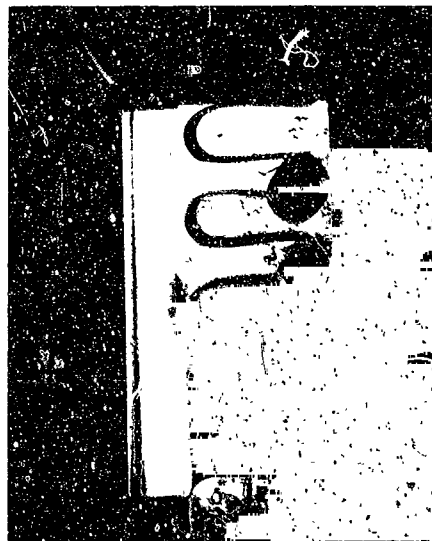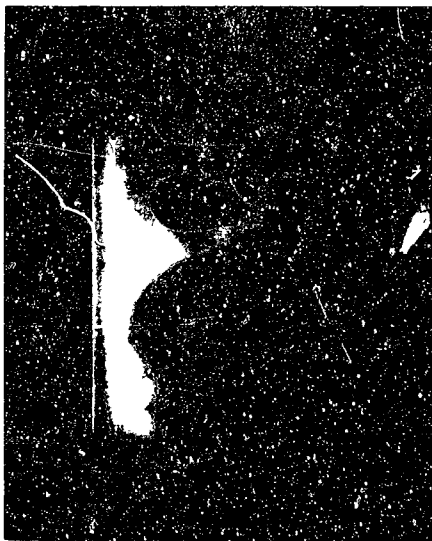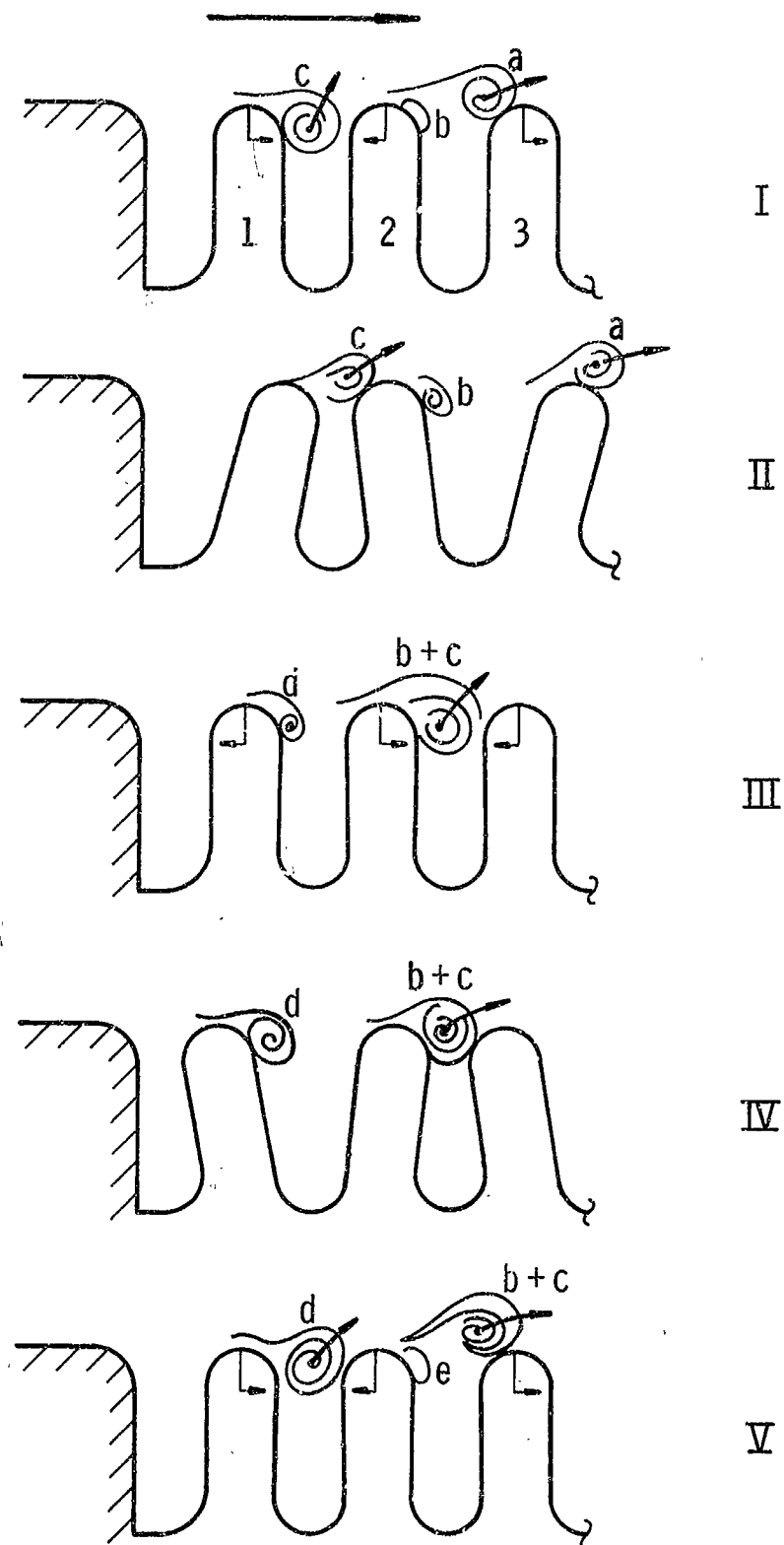
Figure 8. Series Of Photographs Showing Vortex Shedding From
Two-Dimensional Convoluted Metal Segment

14

Figure 9. Sequence Of Coupled Fluid – Convolution Events Observed
With Two-Dimensional Bellows Flow Visualization Model

2207

Position IV - Vortex (d) has gained in strength as it forms on the downstream side of convolution 1. Vortex (b + c) is being pinched out from between convolutions 2 and 3, and will begin to propagate downstream.

Position V - This position is the same as Position I, so the cycle is complete. Note that vortex (a) in Position I was a combination of two vortices, as is vortex (b + c) in Position V.

It must be emphasized that the series of fluid events described in the foregoing are probably not exactly descriptive of other situations. Probably the main difference seen from a comparison with other situations, would be that the phasing of vortices propagating downstream would not always be correct, with respect to a vortex forming at a point downstream, to give a reinforcement condition, as was seen here. We have some evidence to suggest that there might be optimum convolution geometries, for a given mode of vibration, which yields a peak excitation amplitude. This might be caused by a vortex reinforcement phenomena.

It has been shown in the foregoing discussion that two different fluid flow regimes exist; one occurs when the convolutions are constrained and, consequently, no organized large scale vortex shedding is seen, only a steady-state turbulent situation. The other flow regime occurs when the convolutions are vibrating as a result of flow excitation; here a large-scale vortex shedding process does exist. Therefore, the bellows flow excitation can be described as a mutual or coupled instability between the bellows structure and the fluid vortex shedding process. One cannot exist without the other.

The primary condition which must be satisfied for this coupling to occur is that the bellows structural frequency and the ideal vortex shedding frequency be equal, or about equal within certain limits. This limit of vortex-structure coupling can be called a "lock-in" range, and as shown in Figures 3 and 4, it can exist over a rather broad velocity range.

II.4 Prediction of Flow-Excitation Lock-In Range

The purpose of this section is to discuss how the occurrence of the vortex shedding and bellows structure coupling can be predicted. Basically, this involves calculating the ideal vortex shedding frequency and the bellows vibration mode frequencies, and then comparing the two. Also, some allowance must be made for the fact that a "lock-in" range exists.

Vortex Shedding Frequency

For a given bellows, having some particular convolution geometry and structural mode frequencies, there are certain optimum fluid velocities which result in a maximum amplitude bellows excitation of each mode (see again Figure 3). It is at these velocities that the vortex shedding process is best able to feed energy from the fluid stream into the vibration process. In other words, the vibration frequency and fluid velocity conditions are "optimum" from a vortex shedding standpoint. It has been found that the use of a Strouhal number is an excellent means of correlating the vibration frequency, fluid velocity and geometry under these optimum conditions, as is true for any vibration phenomena involving vortex shedding.

In general terms, a Strouhal number is a dimensionless quality of the form

$$S = f \, \ell / V \qquad\qquad (1)$$

where f is a frequency, ℓ is a length quantity, and V a fluid velocity. For the case of bellows flow-induced vibrations, the only problem in using this correlation parameter is in selecting a satisfactory length quantity. Referring back to the discussion of the vortex formation and shedding process illustrated in Figures 8 and 9, it would seem that two length quantities may be primarily involved; these are the convolution pitch and the convolution tip width σ. While neither of these quantities has been found entirely satisfactory, that is neither gives a precisely constant value of S for all conditions, we have chosen to use σ in making Strouhal number calculations.

Figures 10 and 11 show example data of the Strouhal number calculated at the optimum flow excitation condition for two different bellows. The pitch of these bellows were changed by stretching and compressing them from their original configuration. Strouhal number values based on both the tip width σ and the pitch λ have been plotted. Note how neither of the two dimensionless numbers is constant as pitch changes. Based on a composite of all test data, a single curve of Strouhal number (based on tip width σ) as a function of the ratio of pitch to tip width (λ/σ) has been prepared and is believed valid for a general case. This curve is shown in Figure 12; also shown are dotted curves defining the limits of the lock-in range. Using this data, it is possible to calculate the fluid velocity V at which a given bellows longitudinal vibration mode (defined by a frequency value) will most likely be excited and, also, to estimate the total lock-in range of a given mode. To make this calculation it is necessary to know
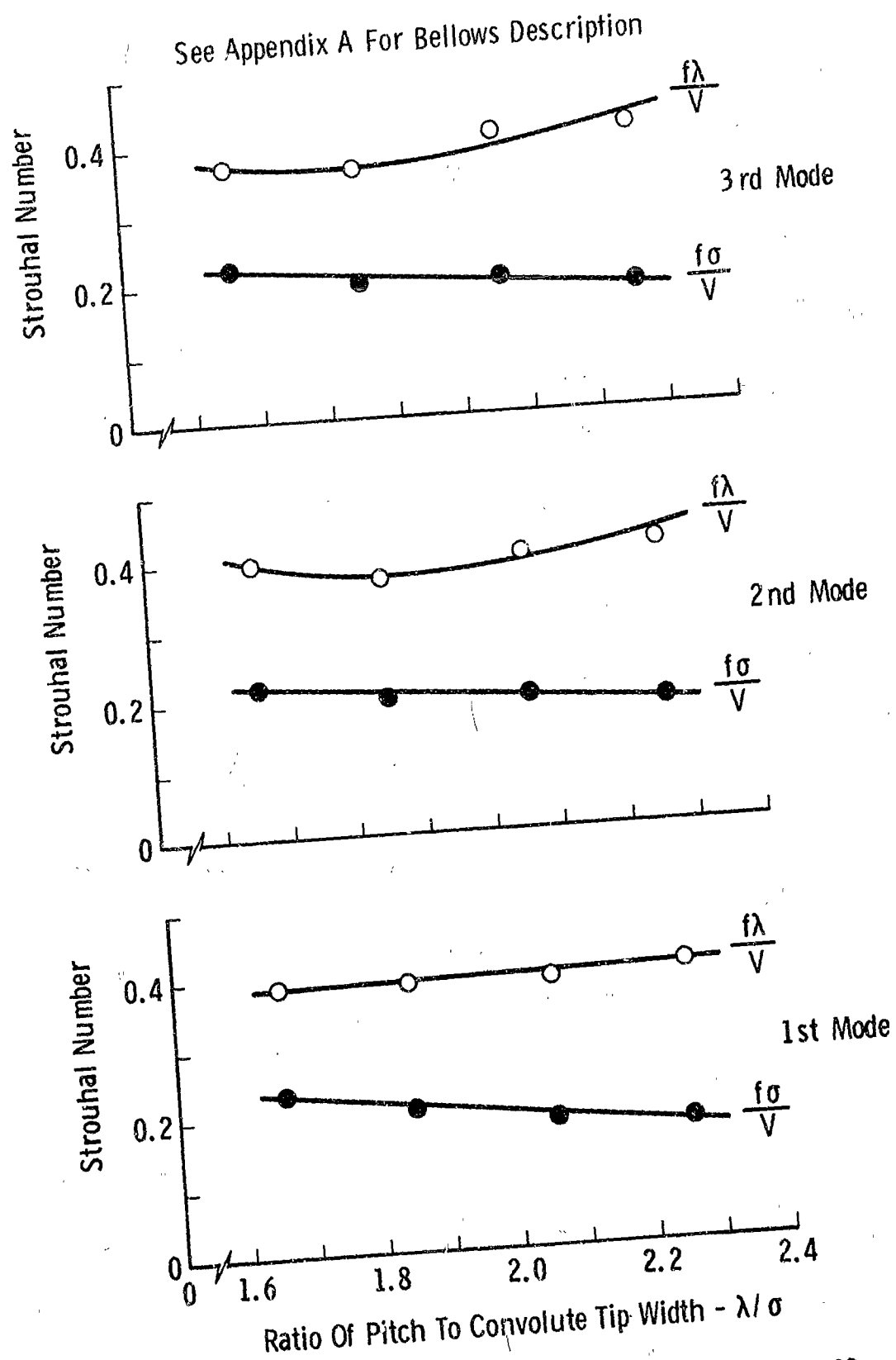
17

See Appendix A For Bellows Description

Figure 10. Strouhal-Number Correlation For Bellow #113

2409

18

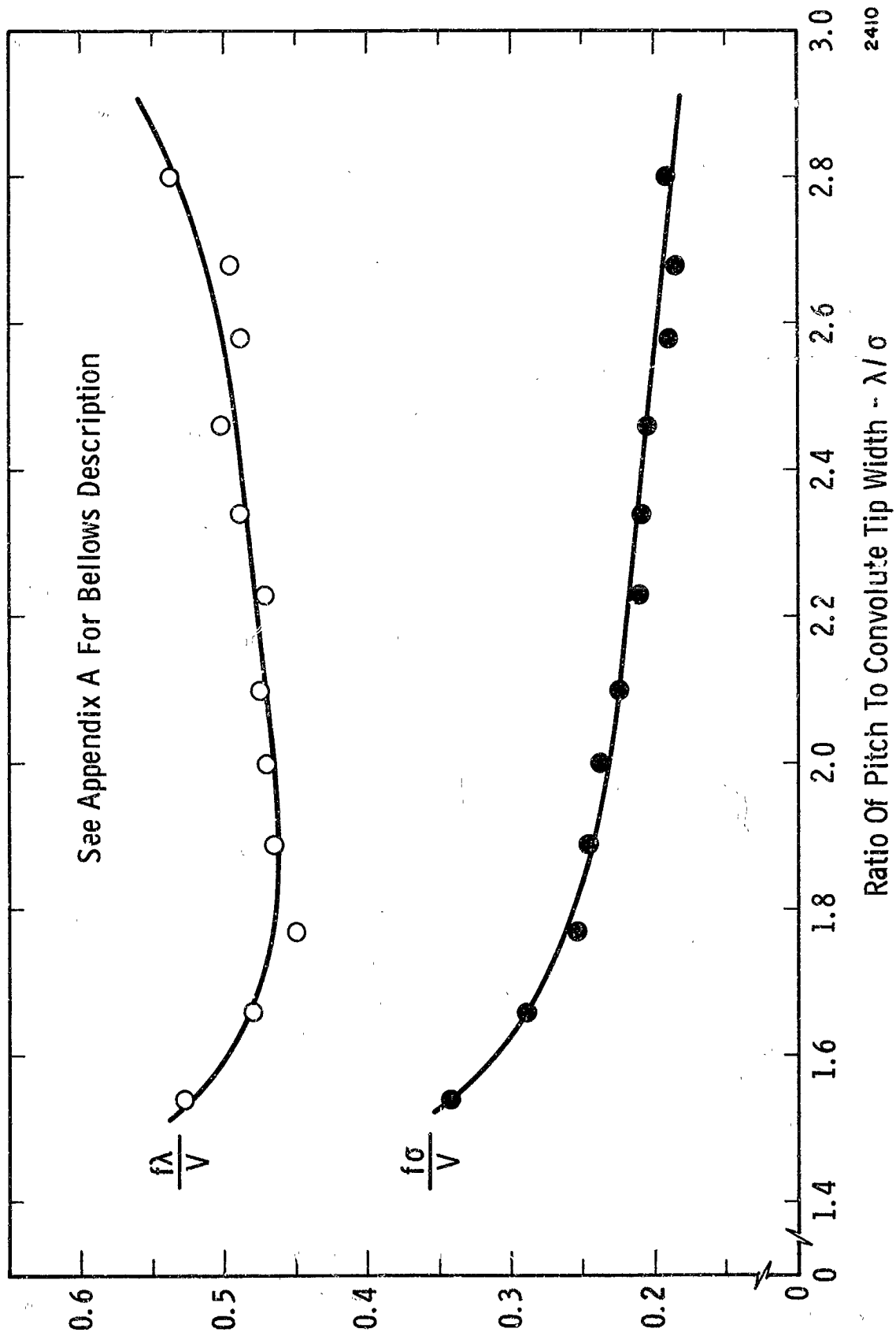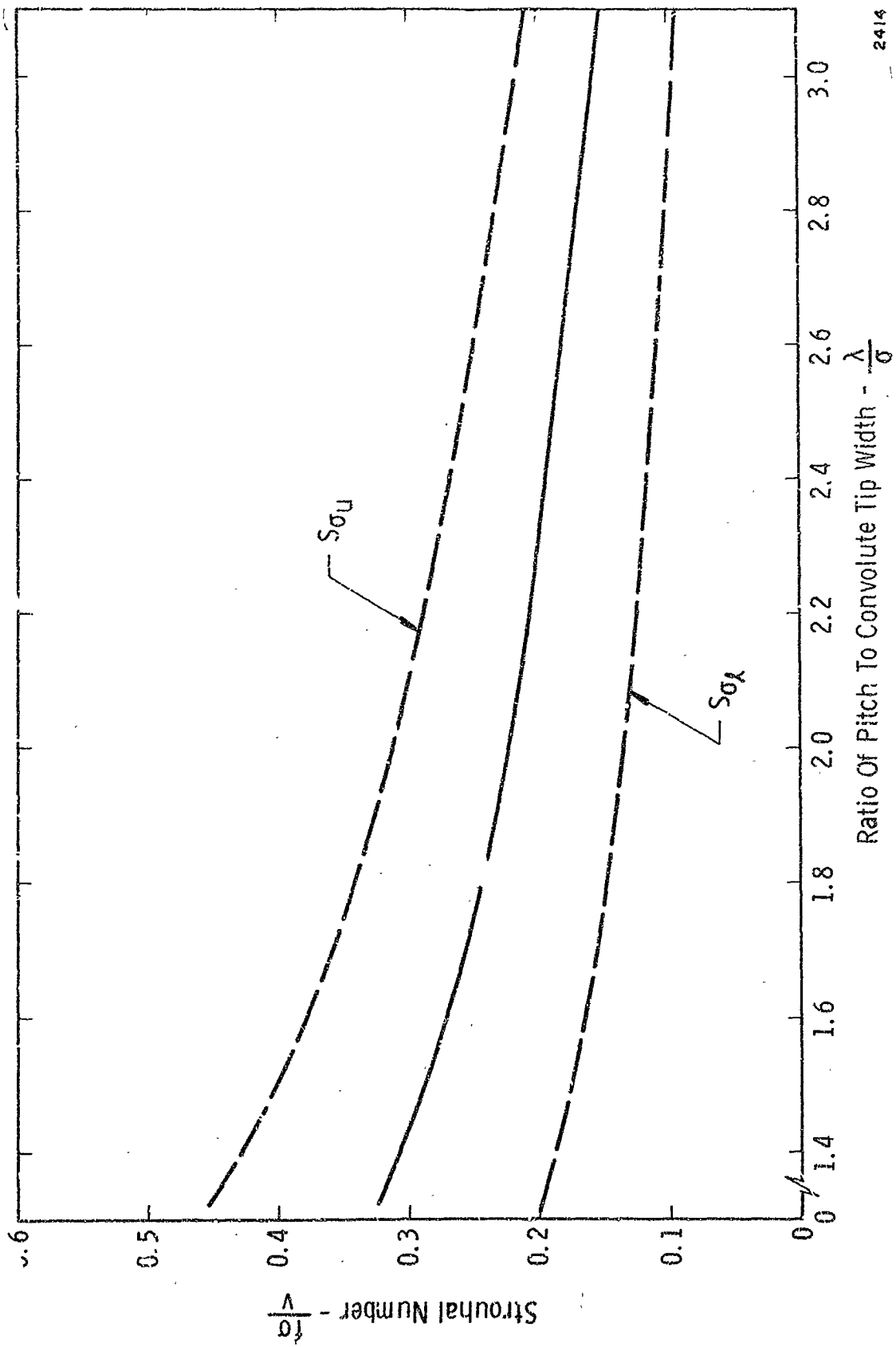Figure 11. Strouhal Number Correlation For Bellows #105 (first mode)

Figure 12. Composite Of All Strouhal Number Correlation Data

$S\sigma_u$

$S\sigma_\ell$

Ratio Of Pitch To Convolute Tip Width – $\dfrac{\lambda}{\sigma}$

Strouhal Number – $\dfrac{f\sigma}{V}$

2414

20

three quantities; namely, the pitch λ, the convolution tip width σ and the mode frequency f_m. The value of this critical velocity is, then

$$V = \frac{f_m \sigma}{S_\sigma} \qquad (2)$$

where S_σ is obtained from Figure 12.

Bellows Structural Frequencies

In order to calculate the fluid velocity range(s) over which bellows excitation will occur by the procedure described in the foregoing section, it is necessary to know the frequencies of all bellows modes which may be flow excited. Therefore, some method must be used to calculate these frequencies. A method, based on an analogous mechanical model, has been developed and will be discussed below. Because the structural bellows modes cannot be considered independent of fluid loading, this influence is discussed also.

It has been determined from experiments that three different kinds of structural modes can be flow excited, these are; axisymmetric longitudinal or accordian modes, longitudinal antisymmetric or cocking modes, and local convolution bending modes. These different kinds of bellows modes are illustrated in Figure 13. The longitudinal modes (both symmetric and antisymmetric) involve vibrations where there is longitudinal motion of the roots and/or crowns of the convolutions. The higher order local bending modes will involve no longitudinal motion of roots and crowns, only local flexural distortion of the convolutions. In our experiments, we have observed only one type of higher order bending mode; it is the one shown in Figure 13 and again in Figure 14. It is doubtful that many, if any, other higher order bending modes can couple with vortex shedding to produce a bellows flow-induced vibration; this has not been confirmed experimentally. For the purposes of this report, we will assume that the higher order bending mode illustrated in Figure 14 is the highest which can be excited by vortex shedding. The reader should keep in mind, however, that this does not rule out the possibility of other higher order local convolution bending modes being excited.

During the course of the present study, the mechanical model shown in Figure 2 has been found to yield adequate predictions of the longitudinal symmetric mode frequencies of a free bellows, if the overall spring rate is accurately known. The model consists of $(2N_c - 1)$ elemental masses m and $2N_c$ elemental springs k connected alternately in series, giving
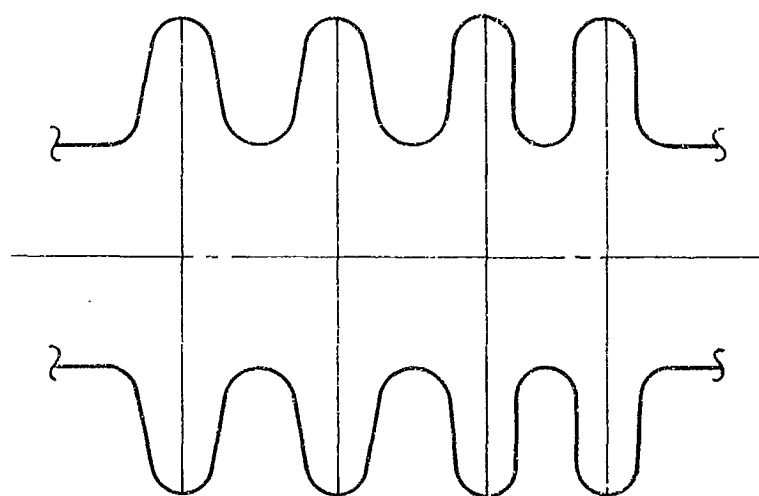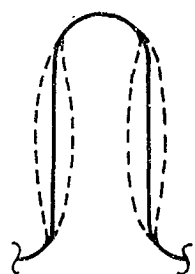
Axisymmetric
Longitudinal Modes
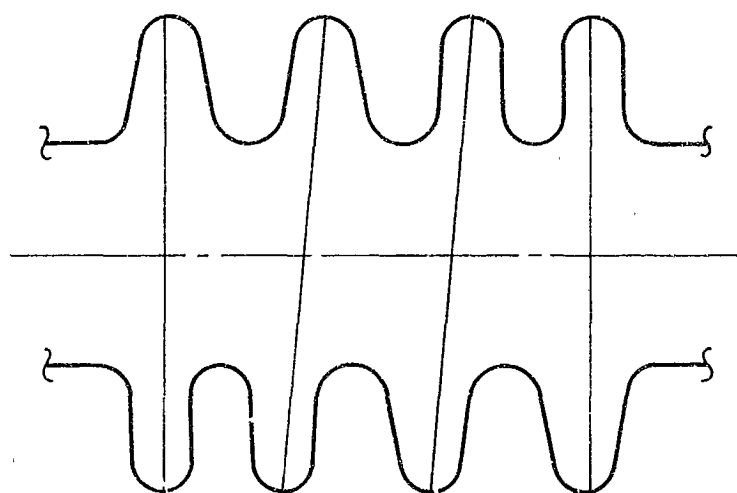
Nonsymmetric
Longitudinal (Cocking)
Modes

Higher Order
Local Convolute
Bending Mode

2396

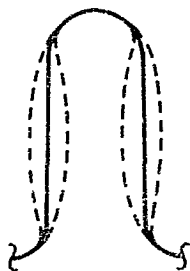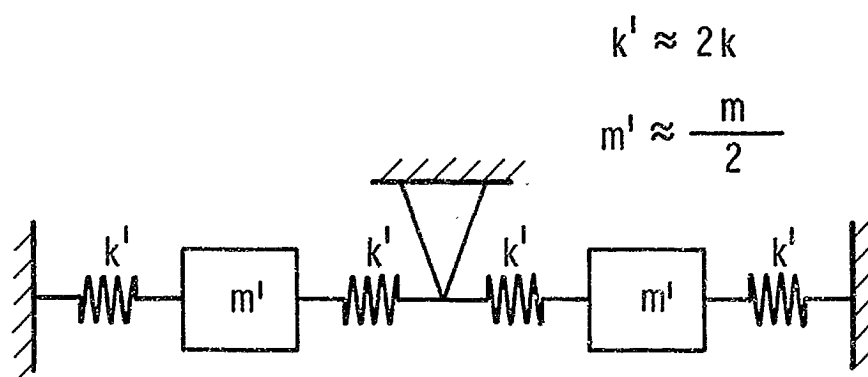Figure 13. Kinds Of Bellows Modes

22

Illustration Of First Local Convolute Bending Mode

$$k' \approx 2k$$

$$m' \approx \frac{m}{2}$$

Approximate Mechanical Model Of First Local Bending Mode

2397

Figure 14. Only Observed Higher Order Mode

23

an $N = 2N_c-1$ degree-of-freedom system; N_c is the number of bellows convolutions. Each elemental mass represents one-half of the mass of metal contained in each bellows convolution plus some fluid added mass, and k represents the spring rate of one-half of a convolution. A tabulation of dimensionless frequencies obtained for this model up to 25 degrees of freedom is shown in Table I; the normalizing frequency is

$$f_o = \frac{1}{2\pi} \left(\frac{k}{m}\right)^{1/2}$$

For use in the mechanical model, the values of the elemental spring rate k and the elemental metal mass m_m may be estimated by the following procedure. The value of k is defined in terms of the overall bellows spring rate K_A as

$$k = 2N_c K_A \tag{3}$$

where K_A is known either from a spring rate test or from some analytical calculation.* The value of the elemental metal mass m_m is equal to one-half of the mass of one complete convolution and may be satisfactorily approximated by the expression

$$m_m = \pi \rho_m t \, N_p \, D_m \left[\pi a + (h-2a)\right] \tag{4}$$

where (see Figure 2)

ρ_m = mass density of bellows metal

t = thickness per ply of metal

N_p = number of bellows plys

D_m = mean diameter of bellows convolution. $D_m = (D_i + D_o)/2$.

a = mean radius of convolution

h = convolute height

The frequencies obtained using the information given above are for the symmetric longitudinal modes only. An analysis has been made to determine the cocking mode frequencies and the results show that these

---

* Appendix B gives a review of existing bellows spring rate information. In general, it has been found that experimentally obtained spring rate data is the most satisfactory.

24

Model\Mode	1	2	3	4	5	6	7	8	9	10	11	12	13	14	15	16	17	18	19	20	21	22	23	24	25
1	1.414																								
2	1.806	1.732																							
3	0.765	1.414	1.85																						
4	0.520	1.175	1.620	1.900																					
5	0.520	1.000	1.414	1.732	1.980																				
6	0.445	0.868	1.247	1.554	1.802	1.950																			
7	0.390	0.765	1.111	1.414	1.663	1.848	1.962																		
8	0.347	0.684	1.000	1.286	1.532	1.732	1.879	1.970																	
9	0.314	0.618	0.908	1.176	1.414	1.618	1.782	1.902	1.975																
10	0.285	0.563	0.831	1.082	1.310	1.511	1.682	1.819	1.919	1.980															
11	0.264	0.518	0.765	1.000	1.217	1.414	1.587	1.732	1.848	1.932	1.983														
12	0.246	0.479	0.709	0.929	1.136	1.326	1.497	1.646	1.771	1.870	1.942	1.985													
13	0.226	0.445	0.661	0.868	1.064	1.247	1.414	1.563	1.693	1.802	1.888	1.950	1.987												
14	0.213	0.416	0.618	0.834	1.000	1.176	1.338	1.486	1.618	1.732	1.827	1.902	1.956	1.988											
15	0.199	0.390	0.583	0.765	0.942	1.111	1.269	1.414	1.546	1.663	1.764	1.848	1.913	1.952	1.990										
16	0.185	0.367	0.547	0.722	0.891	1.052	1.205	1.347	1.478	1.596	1.700	1.790	1.864	1.923	1.966	1.991									
17	0.174	0.347	0.518	0.684	0.845	1.000	1.147	1.285	1.414	1.532	1.638	1.732	1.812	1.879	1.931	1.969	1.992								
18	0.165	0.329	0.491	0.649	0.803	0.952	1.093	1.228	1.354	1.471	1.578	1.674	1.758	1.831	1.891	1.938	1.972	1.993							
19	0.157	0.317	0.467	0.618	0.765	0.908	1.044	1.175	1.298	1.414	1.520	1.618	1.705	1.782	1.847	1.902	1.944	1.975	1.993						
20	0.149	0.298	0.445	0.590	0.731	0.868	1.000	1.126	1.246	1.360	1.466	1.563	1.652	1.732	1.801	1.861	1.911	1.948	1.977	1.994					
21	0.142	0.285	0.425	0.563	0.695	0.831	0.958	1.081	1.198	1.309	1.414	1.511	1.601	1.682	1.755	1.819	1.873	1.918	1.954	1.979	1.994				
22	0.136	0.272	0.407	0.540	0.670	0.797	0.920	1.039	1.153	1.262	1.365	1.461	1.551	1.633	1.708	1.775	1.834	1.884	1.925	1.958	1.981	1.995			
23	0.131	0.262	0.390	0.518	0.643	0.765	0.885	1.000	1.111	1.217	1.318	1.414	1.503	1.586	1.662	1.732	1.793	1.847	1.893	1.931	1.961	1.982	1.995		
24	0.126	0.251	0.375	0.497	0.618	0.736	0.852	0.964	1.071	1.175	1.274	1.369	1.457	1.541	1.618	1.688	1.753	1.809	1.859	1.902	1.937	1.964	1.984	1.996	
25	0.12	0.241	0.361	0.479	0.595	0.709	0.821	0.929	1.034	1.136	1.233	1.326	1.414	1.497	1.574	1.645	1.711	1.770	1.823	1.870	1.909	1.941	1.967	1.985	1.996

MODEL NUMBER N = 2N$_c$ - 1

Table I - Dimensionless Frequencies For Bellows Mechanical Model

new modes are always within the frequency limits of the symmetric longitudinal modes. Therefore, a calculation of the range of symmetric longitudinal modes can be considered to include any cocking modes which may occur. Cocking modes have been observed only for bellows with quite deep convolutions, and will probably not occur in most instances.

The higher order local bending mode shown in Figure 14 may be modeled with the mechanical analog shown in the same figure.

Fluid Loading Effects

The previous discussion concerning calculation of structural bellows mode frequencies made no mention of possible fluid loading effects. The presence of the fluid can, however, cause some changes in the structural frequencies and even add more degrees of freedom to the system (increase the number of possible modes).

When a bellows is being excited by a flowing fluid, two basic classes of forces are present; namely, active forces which are vortex shedding derived, and passive fluid forces which are present regardless of the excitation source. For the idealized case of an incompressible fluid, only two types of passive fluid forces are possible and these give rise to an added-mass and damping influence; they result because the fluid must be moved in and out from between the convolutions and, to some extent, back and forth longitudinally as the bellows vibrates. If only added-mass and damping effects are introduced, the number of degrees of freedom of the bellows (that is, the number of possible vibration modes) does not necessarily change. One exception to this are in-phase and out-of-phase flex hose modes to be discussed later.

For a compressible fluid, the complexity of the situation is greatly increased, because the bellows' vibrations may couple with various system acoustic modes. Generally, this increases the number of degrees of freedom, or the number of possible vibration modes of the bellows. This phenomena is illustrated in Figure 15 which shows the response characteristic of a single convolution test model as influenced by an acoustic loading effect. One curve in this figure shows the frequency response amplitude of the test convolute where no significant ducting longitudinal acoustic resonance occurred; the response is clean, and has a single peak at the expected frequency of 600 cps. The mechanical analog for the convolute with no acoustic effect is also shown in Figure 15; additional mass and damping have been added to simulate these fluid loading effects. The other

△ No acoustic effect-simple mass loading and fluid damping equivalent mechanical model below

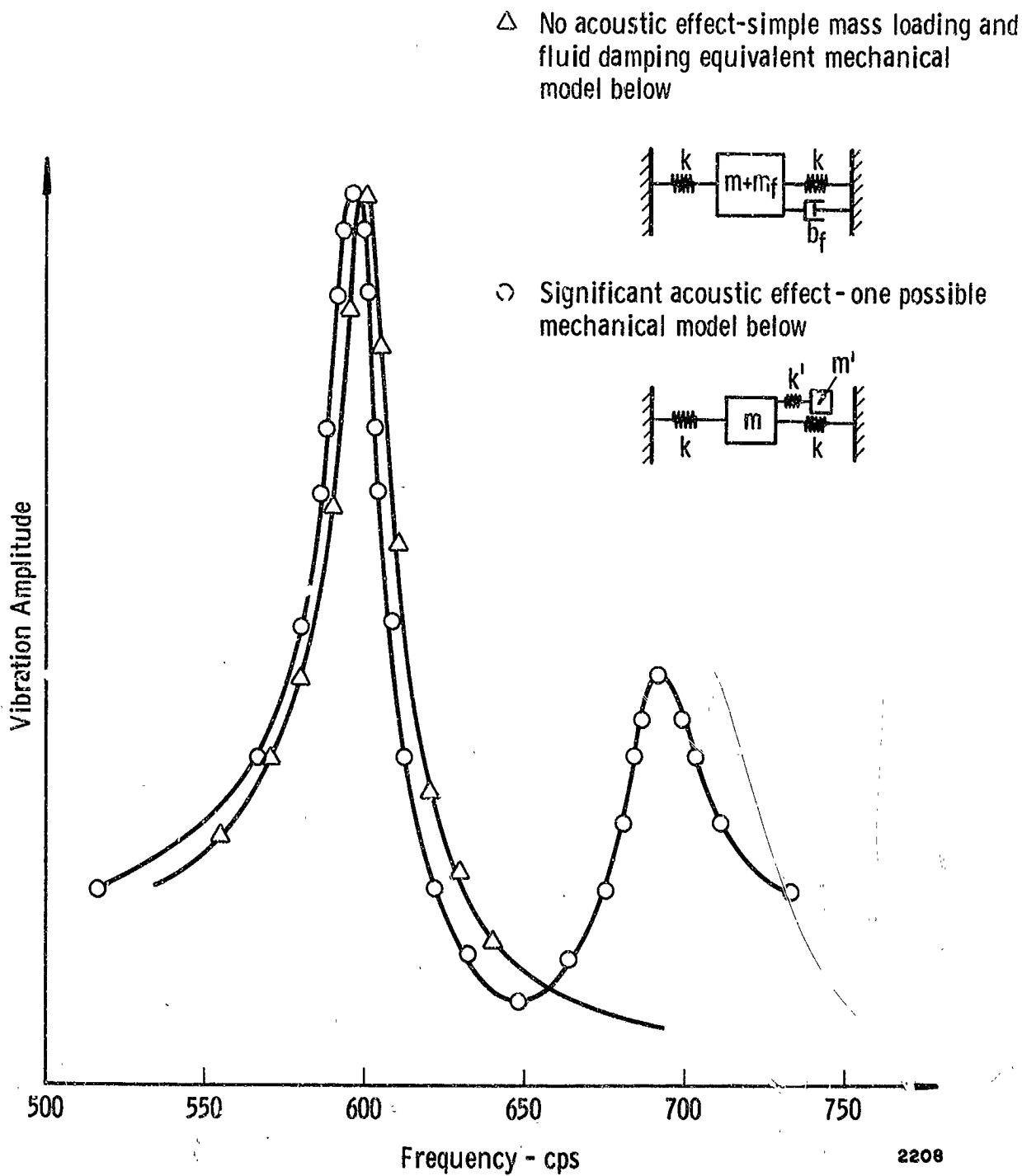○ Significant acoustic effect - one possible mechanical model below

Figure 15. Vibration Response Of Convolution Test Model Ring Number 2 In Water (No Flow). With And Without Ducting Acoustic Resonance - Ring Excited Electromagnetically

curve in Figure 15 shows the response of the test ring where the effect
of a duct acoustic resonance was significant. Note that two distinct
resonant frequencies are present. In this case, a description of the
convolute dynamics must include the line acoustic loading effect. While
the system was ordinarily considered representable by a single-degree-
of-freedom second order system, it must now be considered as at least
a two-degree-of-freedom system; a possible mechanical analog is shown
in Figure 15.

For the present, only incompressible fluid loading effects will
be considered in regard to coupled bellows-fluid mode frequency calcu-
lations. Further, because the fluid damping is small enough to give a
very small change in the system resonant frequencies, it will be dis-
regarded in all frequency calculations. Later, however, damping will
be shown to be of great importance in calculating bellows flow-induced
stress levels.

For the first few modes of a free bellows (more precisely, where
the mode number N is small with respect to the number of convolutions
N_c), it has been determined by comparing calculated with observed
frequencies that the fluid added mass is adequately represented by setting
it equal to the total amount of fluid trapped between adjacent convolutions;
see Figure 2. Physically this makes sense since the first few modes
involve a gross back-and-forth motion of adjacent convolutions with the
trapped fluid carried along with the convolutions. This means, then, that
each elemental mass of the mechanical model must include one-half of
the mass of fluid trapped between two adjacent convolutions, or approximately

$$m_f = \frac{\pi}{2} \rho_f D_m h (2a - tN_t)$$ (5)

with, now, the elemental model mass becoming

$$m = m_f + m_m$$ (6)

where the value of m_m is the metal mass discussed previously. In
Equation (5), ρ_f is the fluid mass density; other symbols were defined
previously.

For the higher modes of a free bellows, it is not adequate to
consider the fluid added mass as being simply that amount of fluid trapped
between convolutions. The fluid behavior for the higher modes is rather

28

more of a "squeezing in-and-out" from between the convolutions type of motion. This acceleration of the fluid out of and back into the convolutions results in alternating pressure forces which may be interpreted as an added-mass effect with respect to the bellows vibrations. In Appendix C this added mass is analytically estimated to be

$$m_f = \frac{\pi D_m \rho_f h^3}{3\delta} \qquad (7)$$

where δ is the gap width between adjacent convolutions as shown in Figure 2.

Comparison of Calculated and Observed Frequencies

Comparison of observed and calculated frequencies for several different free bellows specimens has verified the validity of the free bellows frequency calculation model described in the foregoing. If the spring rate of a given bellows is accurately known from a force-deflection test, the calculated frequencies, where the fluid added mass is small, are surprisingly accurate; generally the error is no greater than 10 percent and often no more than 5 percent compared with experimental values. When the fluid added mass is of the same order of magnitude as the metal mass or greater, the errors begin to increase in some instances, particularly where the bellows geometry is unusual. For example, if the convolution is an extreme "open" design, the added fluid mass is overestimated by the equations given previously. This is understandable since the fluid cannot be readily "held" between the convolutions as they vibrate back and forth.

Table II gives examples of experimental and calculated frequencies for many different cases. In most instances the accuracy obtained from using the mechanical model described above is completely adequate. More sophisticated computational methods could well be employed, however, because of uncertainties in various bellows dimensional data when comparing "blueprint" information and real bellows dimensions, very little, if any, additional accuracy can be achieved. The largest source of error in using the mechanical model for calculating frequencies, is an inaccurate knowledge of the bellows spring rate; see Appendix B.

Flex Hose Modes

The difference between the convolution vibrations of a flexible hose and a free bellows is that the allowed modes are limited by the wire braid covering. In most cases this covering clamps tightly around the

Bellows Number	Internal Media	Excitation	Frequency (cps)		
			Calculated	Experimental	Error
#101	Water	Flow	504	494	2.0%
#104	Water	Flow	770	813	5.3%
#105	Water	Flow	527	515	2.3%
#106	Air @ 30 psig	Shaker	790	935	15.5%
#106	Water @ 30 psig	Shaker	616	700	12.0%
#106	Water	Flow	616	764	19.4%
#110	Water	Flow	780	836	6.7%
#112	Air @ 30 psig	Shaker	635	620	2.4%
#112	Water @ 30 psig	Shaker	521	461	13.0%
#112	Methanol @ 20 psig	Shaker	541	478	13.0%
#112	Methanol @ 30 psig	Shaker	1065 (2nd Mode)	914	16.5%
#112	Water	Flow	521	521	---
#114	Water	Flow	774	754	2.7%
#114	Water	Flow	1512	1435	5.4%

Note: See Appendix A for Bellows Dimensions

TABLE II
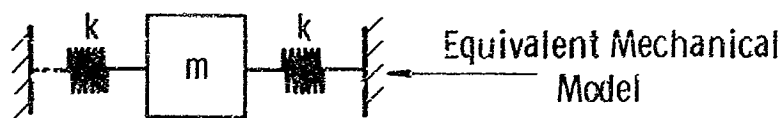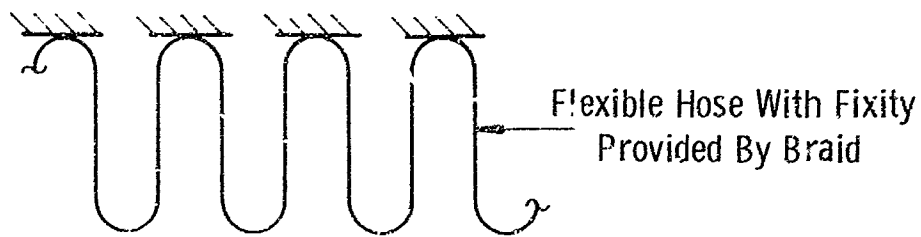Calculated and Experimental Frequencies

bellows when the hose is pressurized, preventing longitudinal motion of the convolution crowns. Except for special instances where not all convolutions crowns are in contact with the wire braid, it is believed that the only purely structural longitudinal mode which can exist is the one shown in Figure 16(a). Because of fluid added-mass effects, however, two coupled fluid-structural longitudinal modes appear possible, and these are shown in Figure 16(b) and (c). Note that both of the coupled fluid structural modes are possible for the single allowed structural mode.

The primary difference between the two coupled fluid-structural modes shown in (b) and (c) of Figure 16 is the fluid mass loading involved. For the case in Figure 16(b), the in-phase mode, the fluid-added mass corresponds to a portion of fluid contained between adjacent convolutions and may be estimated from Equation (4). This quantity of mass accounts for the fact that fluid is accelerated back and forth with the convolutions as they vibrate in the in-phase mode. For the out-of-phase mode, the fluid added mass does not correspond to some real quantity of fluid, but is an apparent mass which results from the fluid being accelerated in and out from between the convolutions as discussed in the foregoing for the free bellows. This quantity of added mass may be estimated from Equation (7).
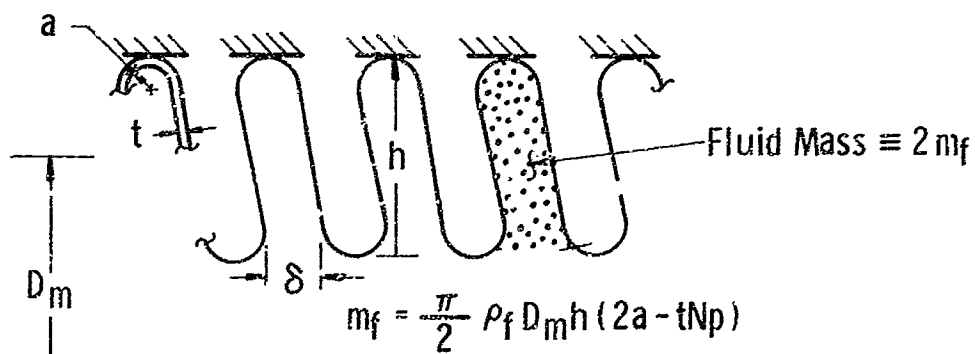
In addition to the longitudinal flex hose modes discussed above, it is believed possible for the higher order local bending mode shown in Figure 14 to also exist.

Thus far, only one flexible hose has undergone extensive flow testing. This particular item, a 1.5-in-id specimen, was placed in the water flow loop and subjected to a slowly increasing internal fluid velocity while bellows response was noted. Because the convolutions were covered on the outside with the wire braid, it was impractical to measure convolution strain, or even observe the convolution motion stroboscopically as had been done with the free bellows. The bellows response was therefore detected indirectly by three methods; external acoustic emission, dynamic fluid pressure downstream, and acceleration of the duct adjacent to the hose were observed. The external acoustic emission technique gave the most reasonable results for this test but, of course, gave only a qualitative indication of response.
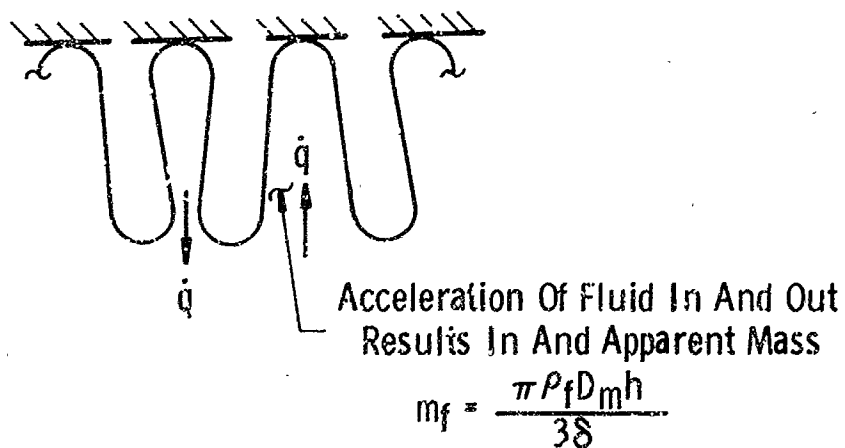
Prior to the test, calculation of the in-phase and out-of-phase mode frequencies gave values of 6720 cps and 3420 cps, respectively. The measured spring rate was used in this frequency calculation. Notice that, by coincidence, the ratio of these two frequencies is about 2 to 1. All of the output data from each monitor was subjected to a Fourier analysis to allow the bellows response modes to be clearly seen. In general, two

31

Flexible Hose With Fixity Provided By Braid

Equivalent Mechanical Model

(a) Structural Mode For Flexible Hose

Fluid Mass $\equiv 2\,m_f$

$$m_f = \frac{\pi}{2}\,\rho_f\,D_m h\,(2a - tNp)$$

(b) In - Phase Mode

Acceleration Of Fluid In And Out Results In And Apparent Mass

$$m_f = \frac{\pi \rho_f D_m h}{3\delta}$$

2003

(c) Out - of - Phase Mode

Figure 16.   Summary Of Flexible Hose Longitudinal Vibration Modes

flow-induced modes were observed, one at about 3300 cps and the other at twice this value or 6600 cps. Figure 17 shows a plot of typical spectral data obtained from the external acoustic monitor to show how these modes responded as the flow velocity was increased. Figure 18 shows a corresponding plot of acoustic emission level as a function of Strouhal number.

The fact that two modes were observed in this test of a flexible hose, very close to the calculated values for the in-phase and out-of-phase modes, substantiates to some extent the existence of these two types of modes. The fact that one happened to have twice the frequency of the other was pure coincidence; they were both apparently excited simultaneously because of the multiple-frequency content of the vortex shedding.

Estimating Flow Excitation Range

The foregoing discussions have described how the conditions for bellows excitation can be correlated with a Strouhal number, and, further, how the modal frequencies of a bellows can be calculated. The purpose of this section is to summarize how this information can be used to predict possible bellows flow-excitation ranges.

As we have seen, a given bellows will have a number of structural modes which may be flow excited. These modes may be defined in terms of a number of modal frequencies denoted by

$$f_{m1}, \quad f_{m2}, \quad f_{m3} \cdots \cdots f_{mn}$$

Here f_{m1} denotes the first or lowest modal frequency and f_{mn} denotes the highest. For the case of a free bellows, f_{m1} will represent the first longitudinal mode and f_{mn} will denote the convolute bulging mode; the total number of modes will depend on the number of convolutions. For a flex hose, there are, so far as we presently know, only three possible modes; these are the in-phase and out-of-phase longitudinal modes shown in Figure 16, and the convolution bulging mode shown in Figure 14. Tables III and IV summarize the frequency calculation procedure for free bellows and flex hose.

Each of the bellows modes may experience flow excitation over a fluid velocity range defined by

$$V_\ell = \frac{f_{m\sigma}}{S_{\sigma u}} \tag{8}$$

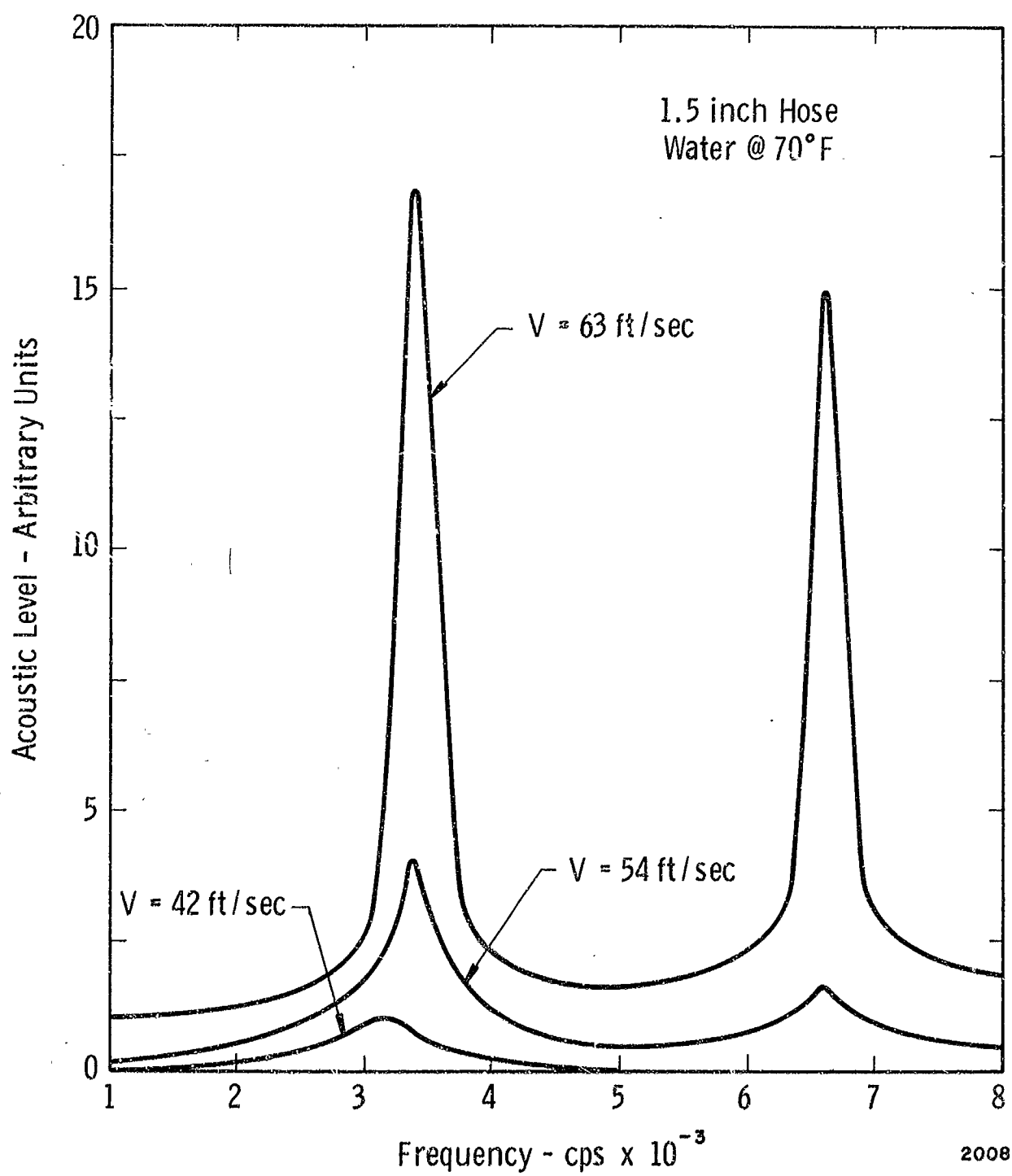$$V_u = \frac{f_{m\sigma}}{S_{\sigma\ell}} \tag{9}$$

33

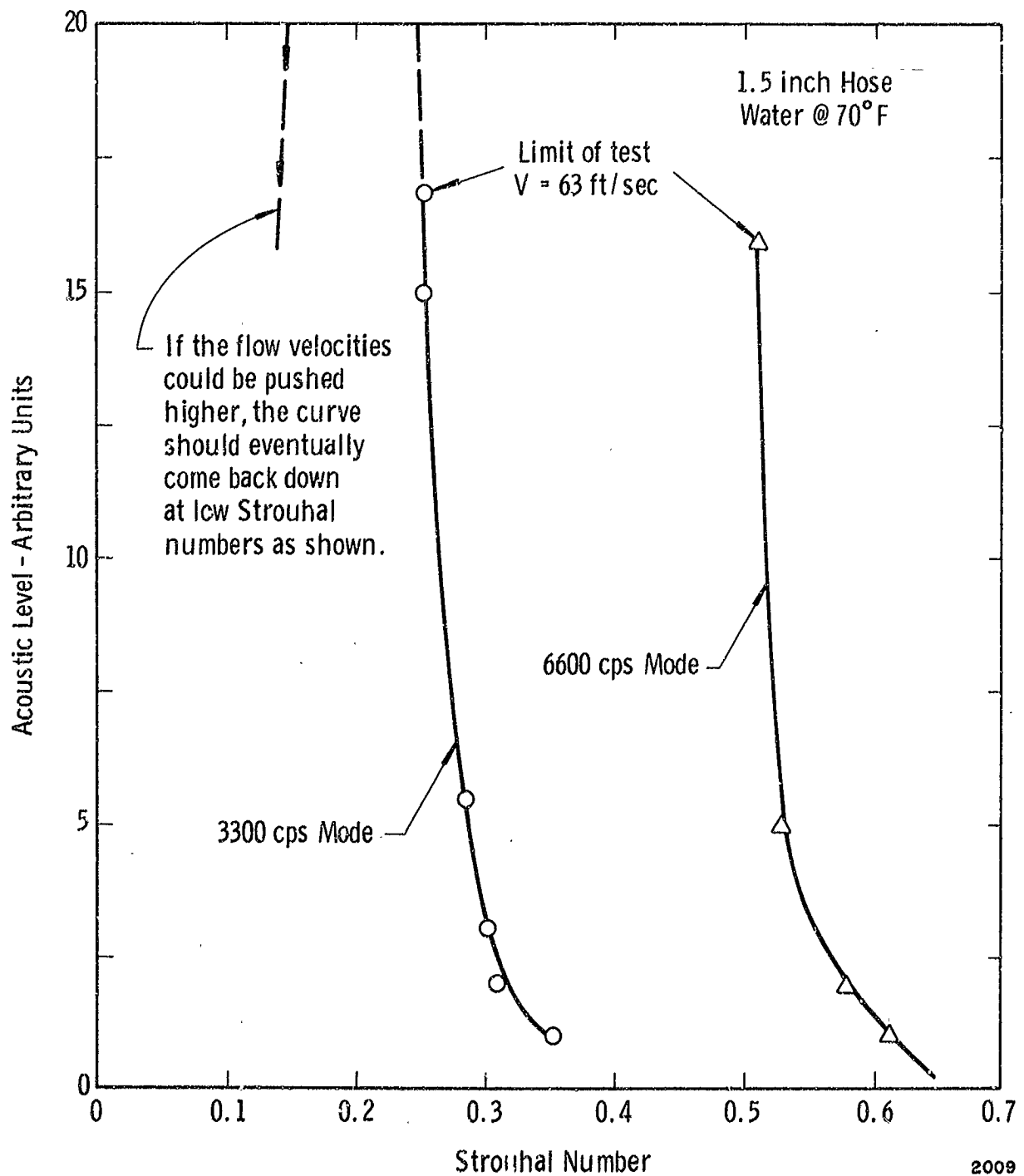Figure 17. Plot Of A Few Of The Acoustic Emission Spectral Traces
For Flexible Hose Test

34

**Figure 18. Acoustic Level As A Function Of Strouhal Number
For Flexible Hose Modes**

The figure shows acoustic level (arbitrary units, 0 to 20) versus Strouhal Number (0 to 0.7).

1.5 inch Hose
Water @ 70°F

Limit of test
V = 63 ft / sec

If the flow velocities could be pushed higher, the curve should eventually come back down at low Strouhal numbers as shown.

6600 cps Mode

3300 cps Mode

2009

Step A   -   Consider the bellows structure representable by the lumped mass-spring mechanical model shown in Figure 2.

Step B   -   Calculate the elemental spring rate value k from the expression

$$k = 2N_c K_A$$

where K_A is the overall spring rate determined from a method given in Appendix A or from a force-deflection test.

Step C   -   Calculate the elemental metal mass m_m from Equation (4) or

$$m_m = \pi \rho_m t \, Np \, D_m \left[\pi a + (h-2a) \right]$$

Step D   -   Calculate the fluid added mass m_f, using Equation (5) for the first few longitudinal modes (N values) and Equation (7) for the higher longitudinal modes; thus

$$m_f = \frac{\pi}{2} \rho_f D_m h \, (2a - tN_p) \Big\} \qquad \text{First few N values}$$

and

$$m_f = \frac{\pi D_m \rho_f h^3}{3\delta} \Big\} \qquad \text{Higher N values}$$

Step E   -   Calculate the reference frequency f_o from the expression

$$f_o = \frac{1}{2\pi} \sqrt{\frac{k}{m}}$$

where

$$m = m_m + m_f$$

Step F   -   Look up proper dimensionless frequencies in Table I (corresponding to given N_c value) and then calculate the true mode frequencies by multiplying by the reference frequency. This gives all of the longitudinal mode frequencies.

Step G   -   Calculate the first bending mode frequency from the information in Figure 14, or

$$f = \frac{1}{2\pi} \sqrt{\frac{2k'}{m'}} = \frac{1}{2\pi} \sqrt{\frac{8k'}{m}}$$

where

$$k' = 2k$$

and

$$m' = m/2 = \frac{m_m + m_f}{2}$$

For the value of m_f use

$$m_f = \pi D_m \rho_f h^3 / 3\delta$$

TABLE III - SUMMARY OF FREE BELLOWS FREQUENCY CALCULATION PROCEDURE (ASSUMED INCOMPRESSIBLE FLUID)

36

Step A	–	Consider the hose convoluted structure representable by the mass-spring model shown in Figure 16.

Step B – Calculate the elemental spring rate value k from the expression

$$k = 2K_A$$

where K_A is the overall spring rate of one complete convolution.   The value of K_A may be determined by a method given in Appendix A or from a force-deflection test.

Step C – Calculate the elemental metal mass m from the expression

$$m_m = \pi \rho_m t \, N_p \, D_m \left[\pi a + (h-2a) \right]$$

Step D – Calculate the in-phase mode and out-of-phase longitudinal mode fluid masses from

$$m_f = \frac{\pi}{2} \, \rho_f D_m h \, (2a - t N_p) \Big\} \qquad \text{in-phase mode}$$

$$m_f = \frac{\pi D_m \rho_f h^3}{3\delta} \quad \Big\} \qquad \text{out-of-phase mode.}$$

Step E – Calculate the in-phase and out-of-phase longitudinal frequencies from

$$f = \frac{1}{2\pi} \sqrt{\frac{2k}{m}}$$

where

$$m = m_m + m_f$$

Step F – Calculate the first bending mode frequency from the information in Figure 14, or

$$f = \frac{1}{2\pi} \sqrt{\frac{2k'}{m'}} = \frac{1}{2\pi} \sqrt{\frac{8k}{m}}$$

where

$$k' = 2k$$

and

$$m' = \frac{m}{2} = \frac{m_m + m_f}{2}$$

For the value of m_f use

$$m_f = \pi D_m \rho_f h^3 / 3\delta$$

TABLE IV – SUMMARY OF FLEX HOSE FREQUENCY
CALCULATION PROCEDURE

and the optimum or most severe excitation will occur at a velocity equal to

$$V = \frac{f_m \sigma}{S_\sigma} \tag{10}$$

In Equations (8) to (10), we have

f_m = a bellows mode frequency

$S_{\sigma u}$ = upper limit Strouhal number

$S_{\sigma \ell}$ = lower limit Strouhal number   see Figure 12

S_σ = optimum Strouhal number

V_ℓ = velocity at lower limit of lock-in range

V_u = velocity at upper limit of lock-in range

σ = convolution tip width

Because of the lock-in range phenomena, and the closeness of successive bellows modes, it is best to assume that flow excitation can occur continuously over a velocity range from the minimum velocity for the lowest mode to the maximum velocity for the highest mode. Therefore, if f_{m1} and f_{mn} are the lowest and the highest mode frequencies, the extreme possible limit of flow excitation is defined by the limiting velocities

$$V_\ell = \frac{f_{m1} \sigma}{S_{\sigma u}} \tag{11}$$

and

$$V_u = \frac{f_{mn} \sigma}{S_{\sigma \ell}} \tag{12}$$

In summary, the range of possible bellows flow excitation may be predicted as follows:

(a) Calculate the lowest and highest bellows mode frequencies, f_{m1} and f_{mn}. The procedure for doing this is summarized in Tables III and IV.

(b) Calculate the limits of fluid velocity corresponding to these two frequencies. This is done with Equations (11) and (12), and with the values of the Strouhal numbers $S_{\sigma \ell}$ and $S_{\sigma u}$ obtained from Figure 12.

38

(c)   Compare this flow excitation fluid velocity range with the known operating range of the bellows. If an overlap of these ranges exists, then excitation may occur.

A graphical method of predicting bellows excitations ranges is illustrated in Figure 19. This method involves preparing a plot of frequency versus fluid velocity which contains both the bellows mode frequency information and the possible vortex shedding frequency limits. The upper and lower bellows frequencies are represented by horizontal lines on the plot (constant frequency lines), as shown in Figure 19. Also, lines of constant slope which pass through the origin are drawn in to represent the vortex frequency limits (as a function of velocity), defined by the expressions

$$f_\ell = \frac{S_{\sigma\ell} V}{\sigma} \tag{13}$$

and

$$f_u = \frac{S_{\sigma u} V}{\sigma} \tag{14}$$

The range of possible flow excitation is clearly seen from this plot.

II.5   General Discussion of Bellows Forced Vibration

All previous discussion has been directed to the problem of determining when a bellows may be flow excited, based on a coincidence of coupled bellows-liquid frequencies and the vortex shedding frequency. This coincidence of frequencies does not guarantee that the bellows will vibrate, however, or indicate the severity of vibration. It is desirable, therefore, to be able to predict vibration amplitudes and corresponding stress levels for a given bellows and given flow conditions.

Figure 20 illustrates the fluid and structural dynamics involved in bellows flow excitation. The process of periodic vortex formation and shedding causes a corresponding periodic pressure to be exerted on the convolutions. The amplitude of this alternating pressure is proportional to the free-stream stagnation pressure $(1/2 \ \rho_f V^2)$. So far as the bellows structure is concerned, the effect of this alternating pressure may be considered as a
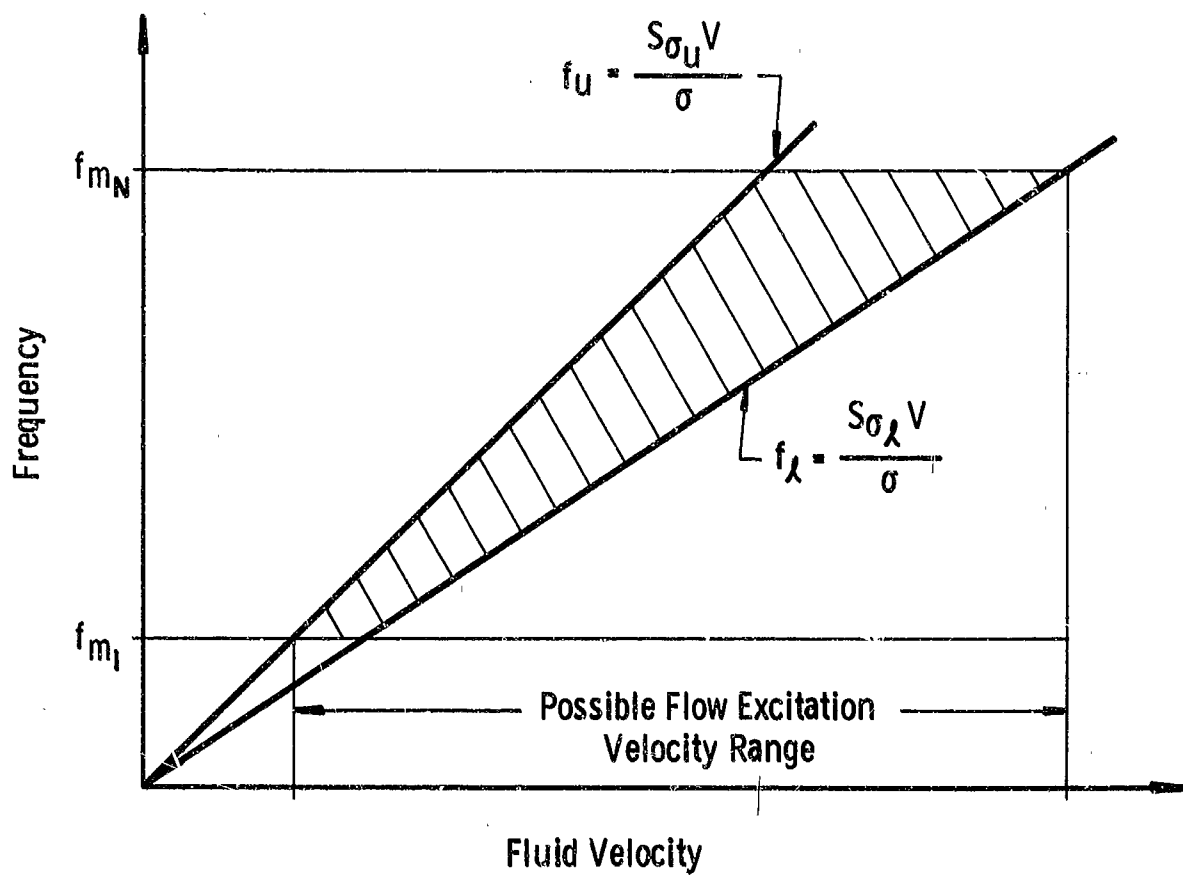
Figure 19. Frequency versus Velocity Plot To Illustrate
Bellows Flow Excitation Region

40

net force applied at the tip of each convolution, as shown in Figure 20. The amplitude of this force is assumed to be of the form

$$F = C_F A_P (1/2 \ \rho_f V^2) \qquad (15)$$

where C_F is a vortex force coefficient (a dimensionless coefficient) and A_P is the projected convolute height area* over which the pressure acts (the fluctuating pressure producing the force).

If the frequency of the vortex shedding coincides with some bellows mode frequency, then a resonance will occur and the bellows convolutions will experience a vibratory displacement, as illustrated in Figure 20, of the form

$$x = \frac{C_m F Q}{K_A} \qquad (16)$$

In Equation (16), C_m is a dimensionless factor dependent on the bellows mode of vibration (mode factor), F is the vortex shedding force defined in Equation (15), K_A is the bellows overall spring rate, and Q is the dynamic amplification factor (damping). This convolution vibratory displacement x will cause a corresponding stress, and the magnitude of this stress is dependent on the convolution geometry, as illustrated in Figure 20.

Accepting this simple concept of bellows vibration resulting from a coupling with the vortex shedding, the problem of calculating resultant stress levels boils down to one of requiring a forehand knowledge of the various "factors" illustrated in Figure 20. The primary factors are: C_F, a vortex force coefficient; C_m a vibration mode factor; Q a dynamic amplification factor; and C_s, a geometric stress factor**. Other factors may also be introduced to account for various unique situations. For example, when an elbow is located upstream of a bellows, this can have an effect and cause higher-than-normal stress levels for a given flow

---

* In earlier reports we used the convolution projected tip area as the area over which the vortex shedding fluctuating pressures act; we have since found that the convoluted projected height area is more realistic.

** The stress model indicated in Figure 20 results from the analytical form presented by Salzmann (10), and is only representative of a number of stress prediction methods (see Appendix B).
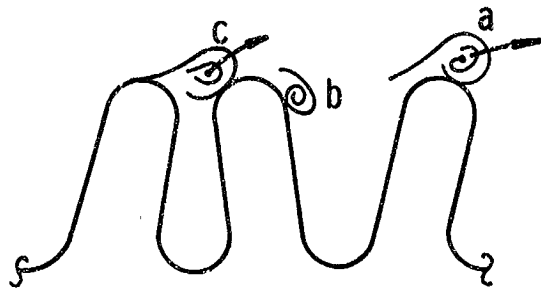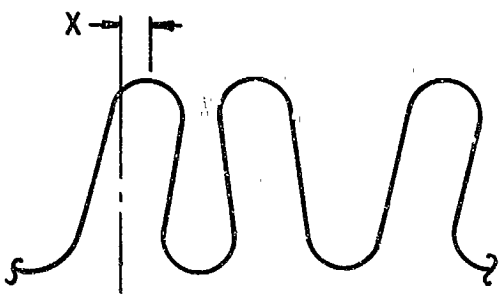
Vortex Shedding From Convolutions
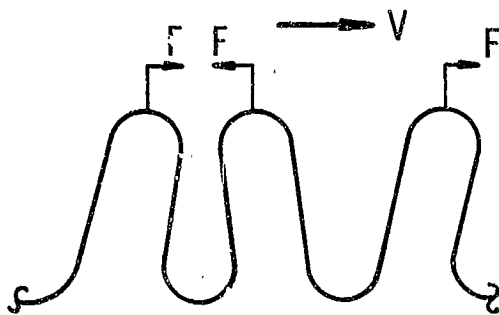
Vortex Force

$$F = C_F C_E A_p \left(\frac{1}{2} \rho V^2 \right)$$

Convolution Displacement

$$X = \frac{C_m F Q}{k_A}$$

The resultant stress is

$$\text{Stress} = \frac{C_S E t x}{h^2}$$

In the above equations

C_F = vortex force coefficient
C_E = elbow factor
C_m = vibration mode factor
Q = dynamic amplification (damping)
C_S = geometric stress factor

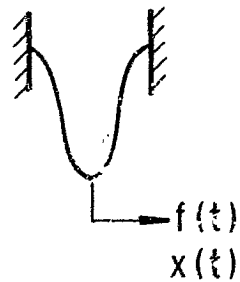2331

Figure 20. Illustration Of Stress Resulting From Vortex Force

velocity. This can be accounted for by an "elbow factor" C_E, as indicated in Figure 20. If an acoustic resonance exists, this can change the picture, also. The objective of the next several sections is to give detailed results of studies of these various factors.

II.6 Vortex Force Coefficient - Idealized Test Model

The initial study of the nature and magnitude of the vortex shedding force was undertaken with a special single convolution test model which is illustrated in Figure 21. A bellows convolution is simulated in this test model by a flexible ring which is geometrically quite similar to a convolution. The ring was constructed from steel and had a coating of lead on the flexible web section to provide sufficient damping to prevent early fatigue failure during actual testing; this happened with the first several rings which were constructed without added damping. The test ring or simulated convolution is clamped in a special housing between a pair of exciter coils; also, a displacement probe is built into the apparatus to allow ring vibration amplitudes to be monitored.

With this apparatus the following types of tests have been performed: (a) frequency response of the ring in air with excitation provided by the coils; (b) frequency response of the ring in water with excitation provided by the coils; and (c) response of the ring as a result of flow excitation with internal water flow. Also, a calibration of static force versus deflection was made for the ring. From these tests and the force-deflection calibration, several kinds of information were obtained. First, the forced vibration test in air gave essentially the ring-only natural frequency and damping (neglecting air loading). Second, the forced vibration test in water allowed the water added-mass and water damping to be calculated. Finally, the flow-induced vibration data allowed an effective vortex force coefficient to be obtained over the lock-in range. This effective vortex coefficient was reduced from the ring flow-induced vibration data in the following manner:
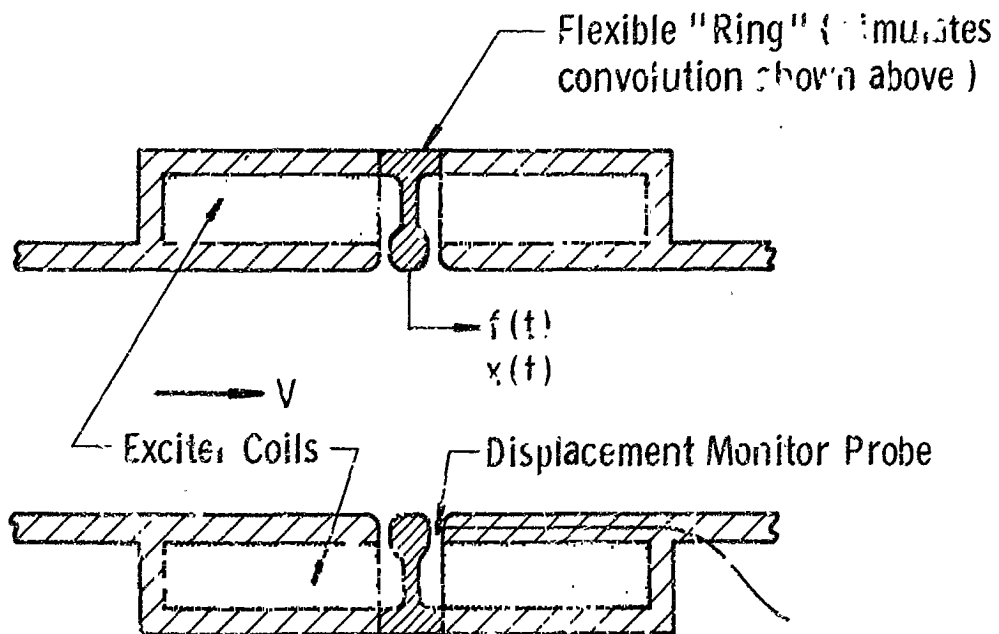
(a) The vibration amplitude (as a function of fluid velocity) was converted to an apparent force through the use of the force-deflection calibration.

(b) This apparent force was converted to a true vortex force by dividing by the Q value reduced from the forced vibration test data (in water).

(c) This true force was converted to a force coefficient through the use of Equation (15).

43

SINGLE BELLOWS CONVOLUTION
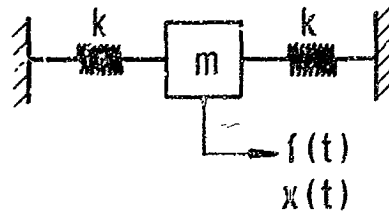
MECHANICAL MODEL OF CONVOLUTION

Flexible "Ring" (imulutes convolution shown above)

CONVOLUTION VIBRATION TEST MODEL

Excite Coils — Displacement Monitor Probe

1868

Figure 21. Diagram Of Convolution Vibration Test Model And Equivalent Bellows And Mechanical Model Representations

44

Vortex coefficient data was obtained in this manner for two different convolution geometries and the results are shown in Figure 22. Notice the great reduction in the force coefficient as the convolution pitch is "opened up".

II.7 Vibrations of Real Bellows

Bellows Mode Factor

Having available the results of the experiments with the single convolution test model, discussed in the previous section, the next logical step was to use this force coefficient information, along with the equivalent mechanical model concept, to predict flow-induced vibration amplitudes of real bellows. This was done by assigning one force per mass point[*], as shown in Figure 23, and then calculating the forced amplitude of the mechanical model. Comparing the resultant vibration amplitudes with observed values showed the predictions to be high by a factor about equal to the number of convolutions involved in each "half wavelength" of bellows vibration. This suggested, therefore, that there was only one effective vortex force per mode number of the vibration. Further detailed comparison of calculated and observed vibrations of bellows confirmed this idea. Also, reexamination of the visualized vortex shedding activity (illustrated typically in Figure 8) and reconsideration of the pressure forces involved, showed how this must happen.

Figure 24 depicts the action of a bellows with several convolutions vibrating in the first longitudinal mode. As shown, the vortex shedding causes fluctuating pressure forces on each side of each convolution. Because of the phasing of these pressure forces, however, only one effective vortex force exists per mode number of vibration. The first mode has one effective force point, the second mode, two, et . Each of these effective forces is exerted a the central convolution of each mode half wavelength, or at the point(s) of maximum displacement of each mode.

---

[*] By assigning one force per mass point, where each mass point represented one-half of a convolution, it was necessary to take each force equal to one-half of the force in Equation (15).
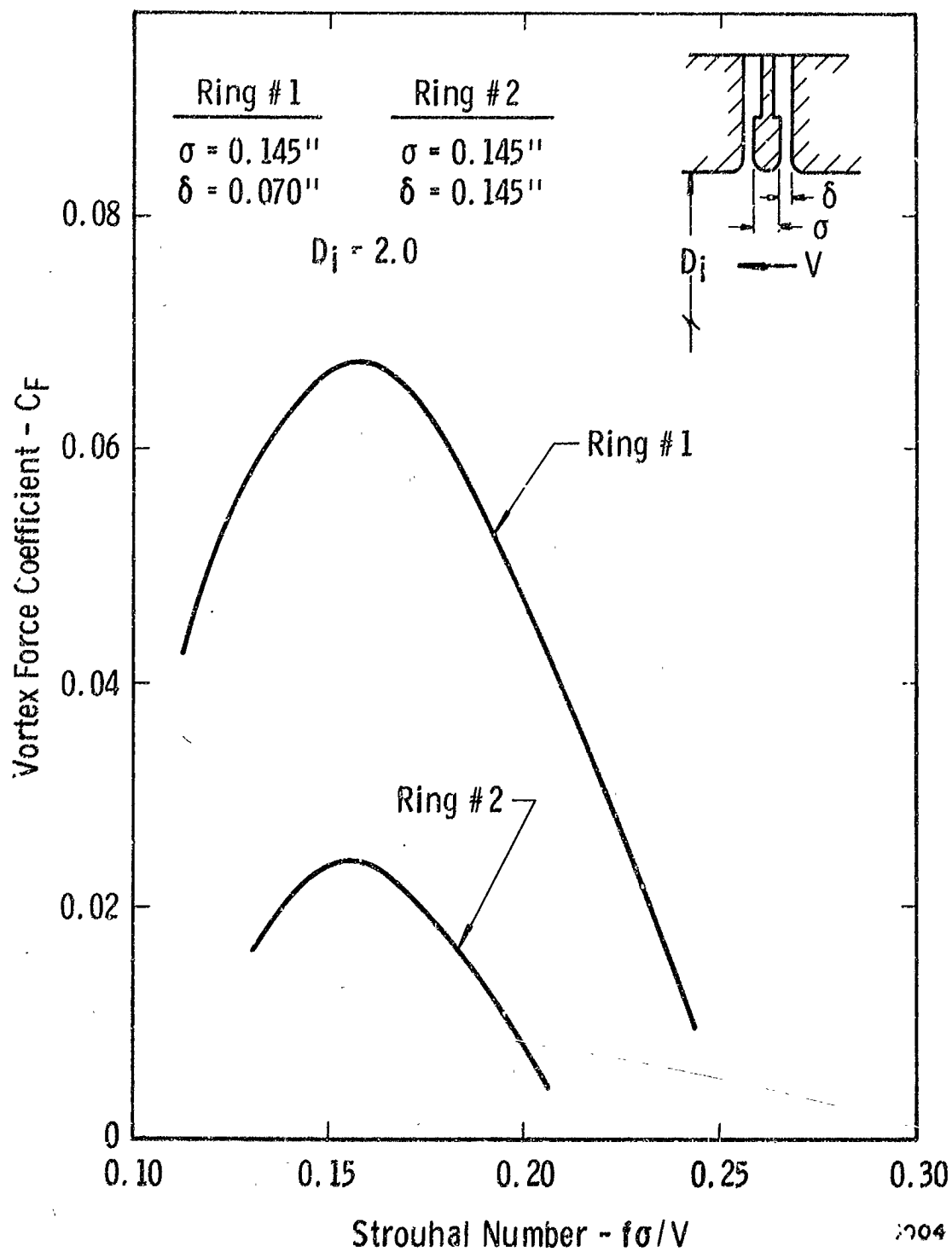
Figure 22. Vortex Shedding Force Coefficients From Tests Of
Two Simulated Convolution Geometries

46

All forces are of the form $f_n = f_0 \sin(\omega t + \Phi_n)$
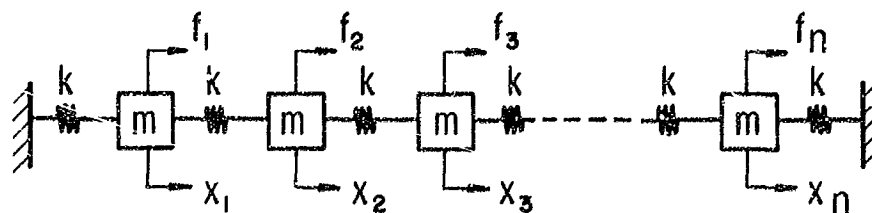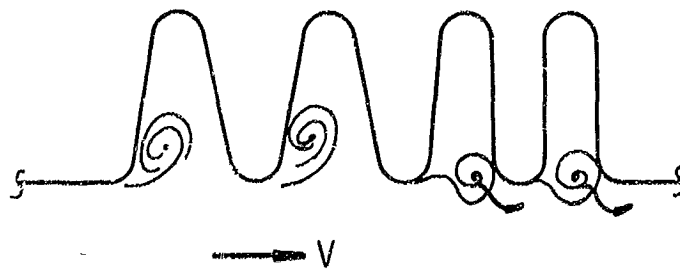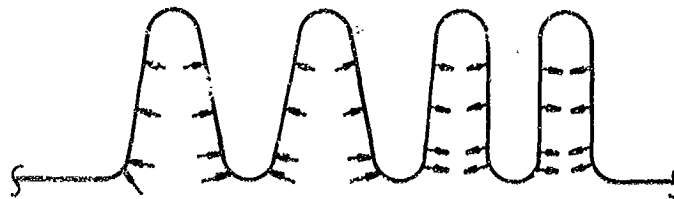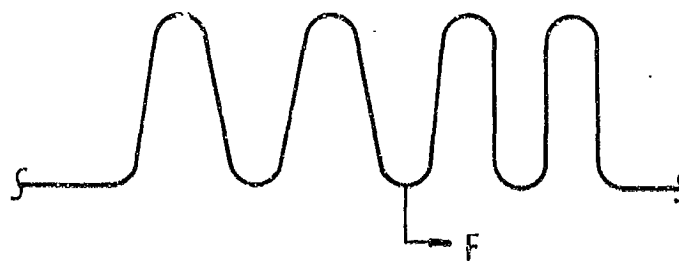where ρ depends on mode of vibration

Figure 23. Mechanical Model With One Force Per Mass Point-
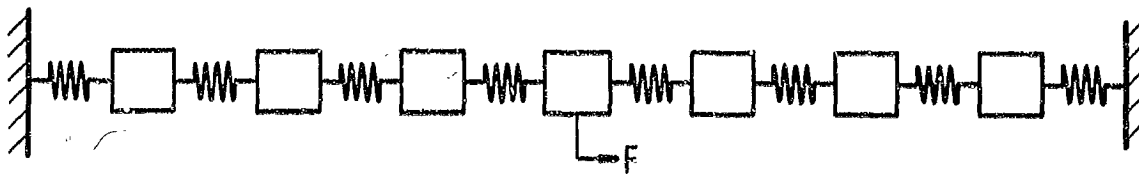All Forces Are Of Equal Magnitude

Vortex Activity On
Bellows Vibrating In
1st Mode

Resultant Pressure
Forces On Convolutions

Net Effective Force
On Convolutions

Equivalent Mechanical Model

2333

Figure 24. Effective Vortex Force On Bellows Vibrating
In The First Longitudinal Mode

Using the one-force-per-half-wavelength concept illustrated in Figure 24, we can now proceed with the derivation of a value for the mode factor C_m which relates displacement and force during a resonant condition. The following assumptions will be made:

(a) The shape of the longitudinal bellows modes is intermediate between a linear and a sinusoidal form. This is a very good assumption as comparison of the exact mode shapes with this approximation has shown.

(b) The maximum deflection for a given mode is equal to the static deflection times Q, the dynamic amplification factor.

(c) The maximum stress point for a given vibration mode occurs at the convolution with the maximum relative displacement; this is the end convolution for each half-wave mode shape, in general.

The first assumption noted above implies that the mode shape is of the form illustrated in Figure 25, or over the first quarter wavelength

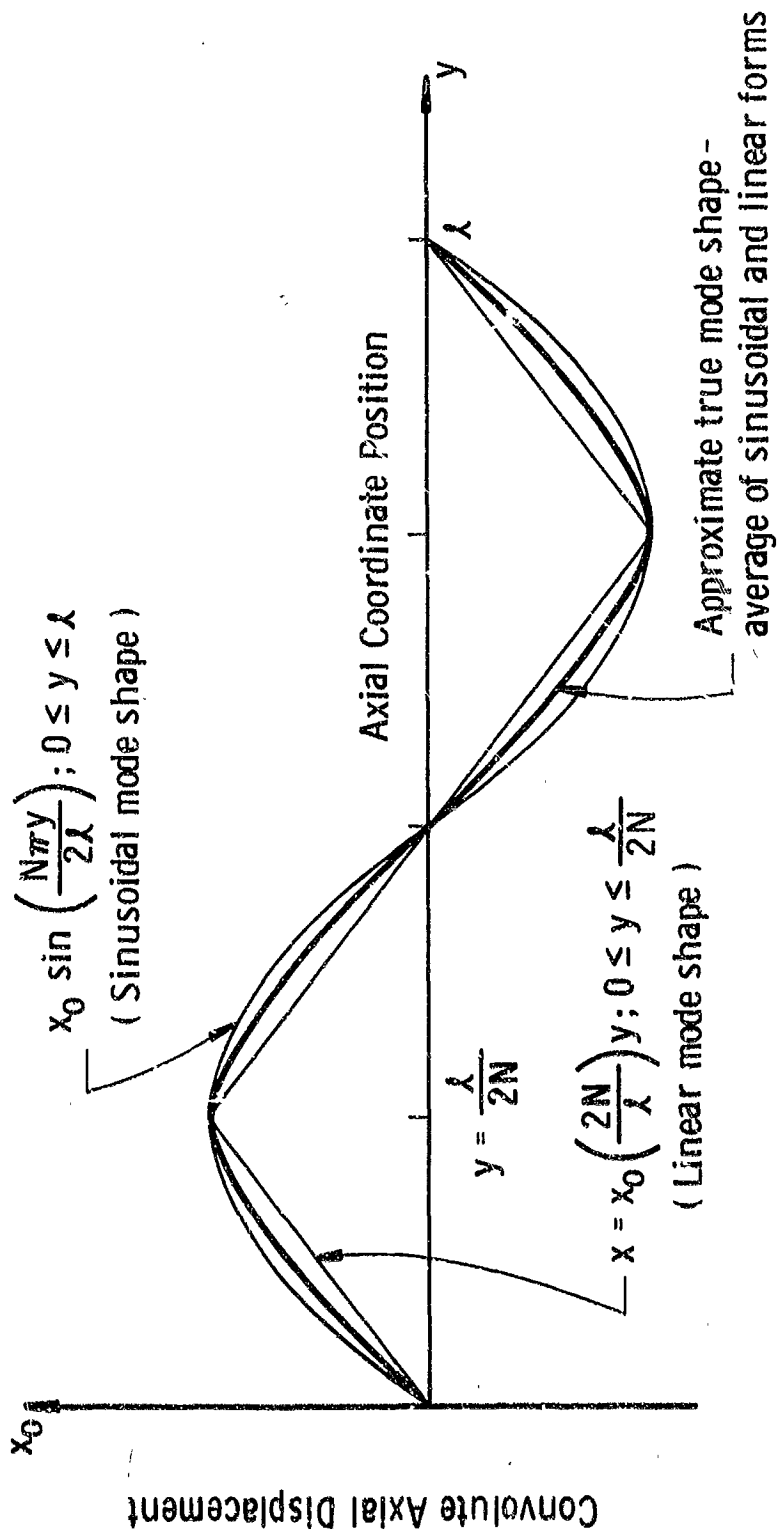$$x = \frac{x_0}{2} \left\{ \left(\frac{N}{\ell} \right) y + \sin \left(\frac{N \pi y}{\ell} \right) \right\} \tag{17}$$

where x denotes the axial absolute displacement of a given point along the bellows defined by the axial position coordinate y; N is the mode number.

The second assumption given above, when considered in light of the one-force-per-half-wavelength concept, implies that the maximum absolute displacement x_0 (see Figure 25) is

$$x_0 = \frac{FQ}{4Nk_A} \tag{18}$$

where F is the amplitude of the vortex shedding force applied as was illustrated in Figure 24. Again, Q is the dynamic amplification factor and K_A is the overall bellows spring rate.

From the third assumption given above, the point of maximum relative displacement x_{mr} for a given bellows, and a given mode of vibration, occurs at a point where $y = \ell/2N_c$. Therefore, from

49

Figure 25. Illustration Of Approximate True Bellows Mode Shapes

The figure shows a plot with the vertical axis labeled "Convolute Axial Displacement" (x_0) and the horizontal axis labeled "Axial Coordinate Position" (y).

Curves shown:

$$x_0 \sin\left(\frac{N\pi y}{2\lambda}\right) ; \ 0 \leq y \leq \lambda$$
(Sinusoidal mode shape)

$$x = x_0\left(\frac{2N}{\lambda}\right)y ; \ 0 \leq y \leq \frac{\lambda}{2N}$$
(Linear mode shape)

$$y = \frac{\lambda}{2N}$$

Approximate true mode shape - average of sinusoidal and linear forms

2399

50

Equation (17),

$$x_{mr} = \frac{x_o}{2} \left\{ \frac{N}{N_c} + \sin\left(\frac{\pi}{2} \frac{N}{N_c}\right) \right\} \qquad (19)$$

Combining Equations (18) and (19) yields

$$x_{mr} = \frac{FQ}{8NK_A} \left\{ \frac{N}{N_c} + \sin\left(\frac{\pi}{2} \frac{N}{N_c}\right) \right\} \qquad (20)$$

and comparison with Equation (16) shows that the "mode factor C_m" defined in Equation (16), or

$$x = \frac{C_m FQ}{K_A} \qquad (21)$$

now becomes

$$C_m = \frac{1}{8N} \left\{ \frac{N}{N_c} + \sin\left(\frac{\pi}{2} \frac{N}{N_c}\right) \right\} \qquad (22)$$

and refers to the maximum relative displacement point (maximum stress point) along the bellows.

At this stage, we are about in a position to estimate bellows flow-induced vibration amplitudes using Equations (15), (21) and (22), plus the data from Figure 22. We still need, however, values of Q, the amplification factor. A comprehensive discussion of bellows damping and the resultant Q values will be delayed until a later section of this report; for the present we will assume the damping values are known.

Test Data for Real Bellows

The analysis method described in the foregoing has been used to correlate data from a number of flow-induced vibration tests of bellows. These tests were conducted in the following manner:

(a) Strain gages were installed on the tips of the end convolutions of all test bellows. On all bellows, one strain gage was oriented to monitor longitudinal strain and, on a few bellows, a gage to monitor circumferential strain was also installed.

(b) Each test bellows was subjected to a static load test, during which both deflection and strain were monitored. This allowed force-deflection and force-strain curves to be plotted for each bellows.

(c) Each bellows type was subjected to a mechanical vibration test (to be discussed later) and the damping was determined.

(d) Each test bellows was installed in the water-flow system, and flow-induced stress levels were monitored as a function of flow velocity.

(e) This data was finally correlated with the analysis described earlier.

The following discussion describes these various steps, and the results, in more detail.

A typical strain gage installation on a bellows is shown in Figure 26. For most cases 1/32-inch gages were used, while some 1/64-inch gages were installed on those bellows with small width convolutions. Actual gage installation was straightforward, however, particular care was needed in lead installation to prevent fatigue. It was found that very small lead wire worked best (say about 0.005-0.010 inch) and that the best procedure was to glue the wires down along the sides of the end convolution with rubber cement. The amount of cement used was kept to a minimum to ensure that the damping of the bellows was not significantly increased.

Following strain gage installation, each bellows was tested to obtain force-deflection and strain-deflection curves. The reasons for doing this were twofold; first, it was desirable to have experimental spring rate values to allow more accurate mode frequency calculations and, second, by having a strain-deflection "calibration" along with the spring rate value, the flow-induced strain amplitudes could be directly interpreted as vortex shedding forces after suitable data reduction to account for the dynamic amplification, and mode factor. By this procedure, errors inherent in trying to analytically relate strain (or stress), and vibration amplitudes and forces, were eliminated. This allowed a more realistic judgment of the validity of the bellows flow-induced vibration analysis presented earlier in this report. Some typical force-deflection and strain-deflection data are shown in Figures 27 and 28*.

---

* Appendix A gives dimensional data for all bellows used throughout the study; refer to this appendix for data on numbered bellows in all figures.
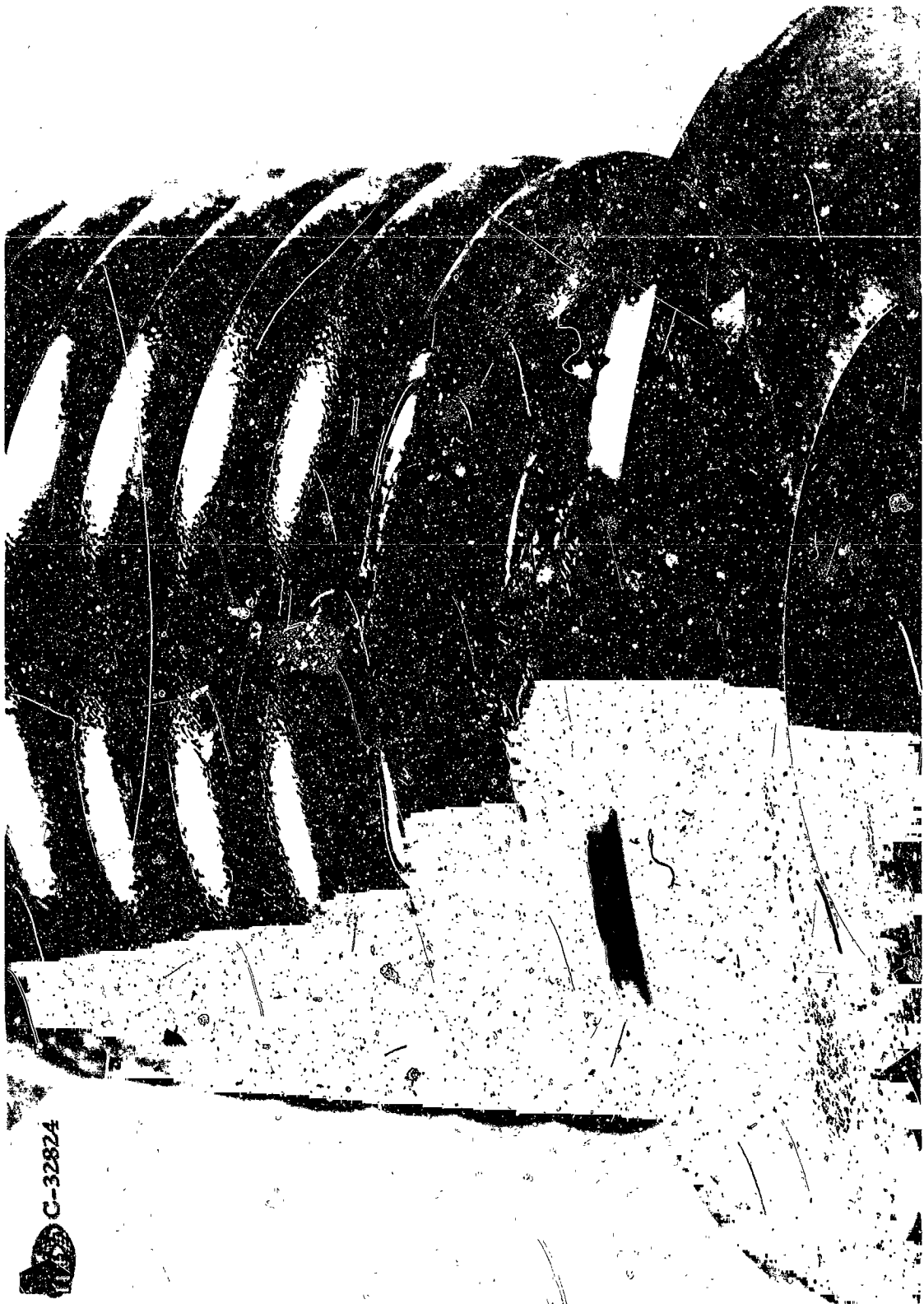
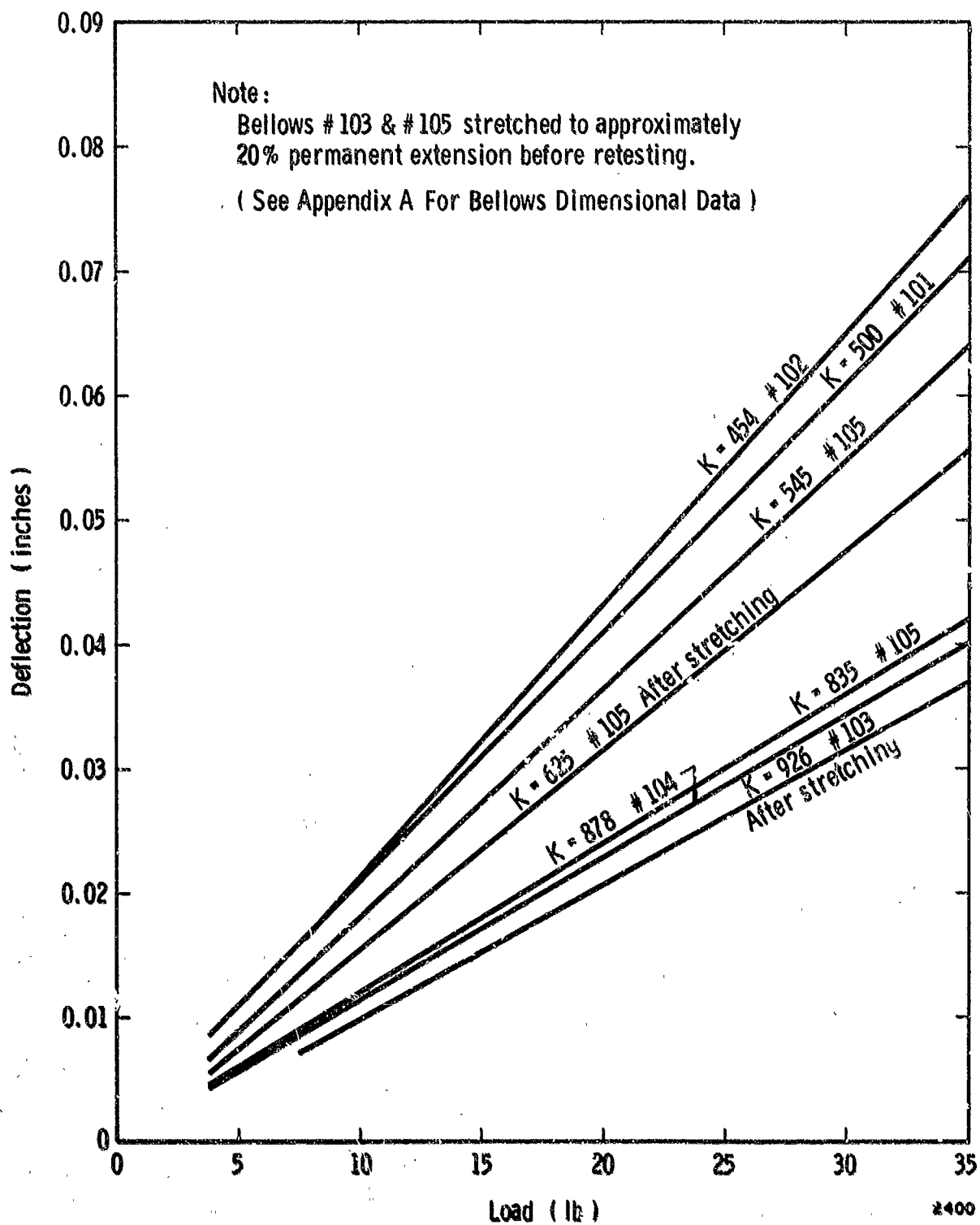Figure 26. Typical Strain Gage Installation

C-32824

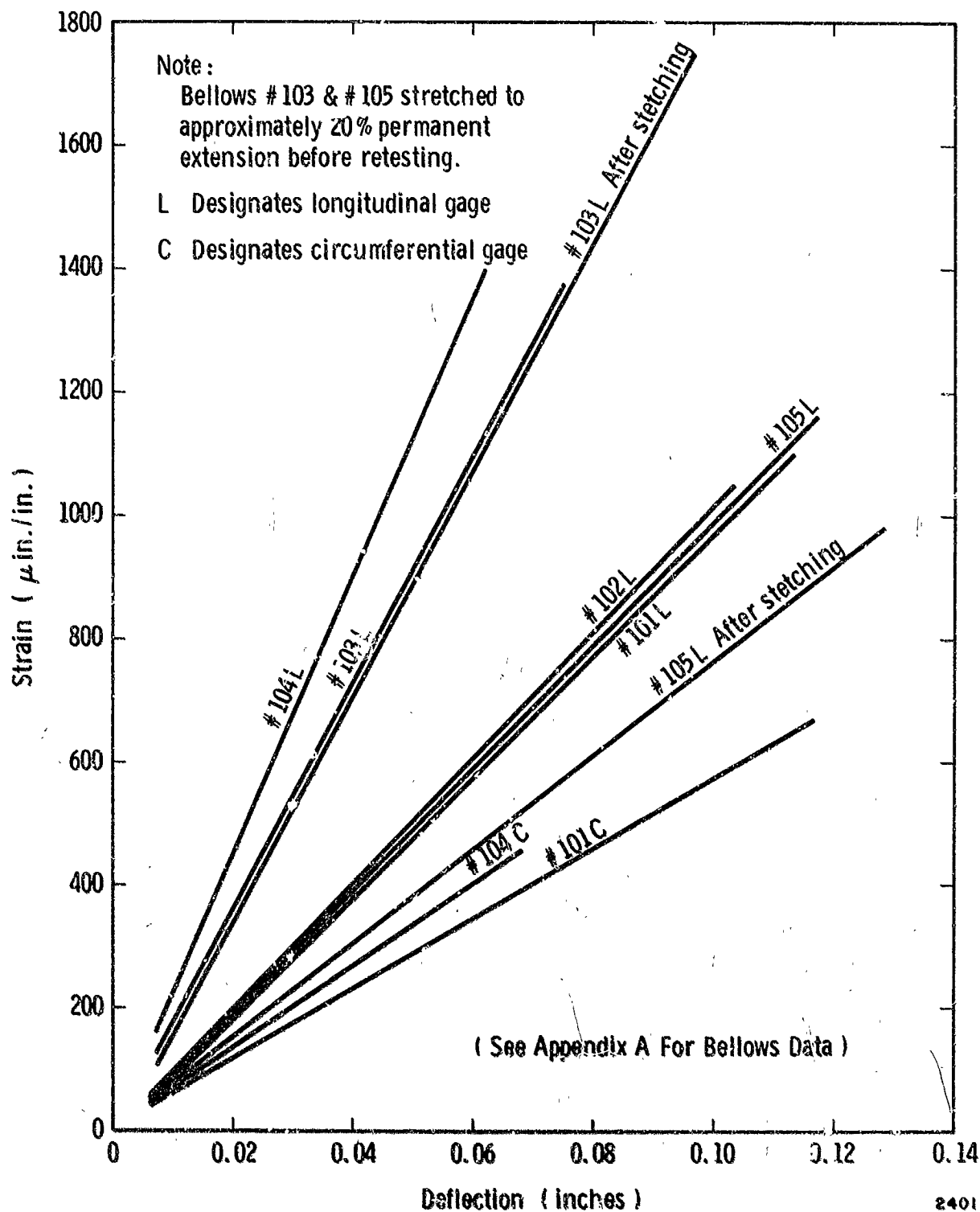Figure 27. Typical Load-Deflection Data For Test Bellows

Figure 28. Typical Strain – Deflection Data For Test Bellows

The next step in the bellows test procedure was to subject one bellows of each particular type to mechanical vibration and thereby obtain a forced response plot for various conditions (various internal media, various internal pressures, different peak strain levels, etc.). This mechanical vibration test procedure will be discussed in much more detail in a later section. The important point here is to realize that the result of these tests was a tabulation of Q values for each bellows for the various test conditions.

The final step in testing each bellows was to mount it in the water flow loop and monitor vibratory strain levels as a function of internal fluid velocity. Figures 29, 30 and 31 illustrate typical flow-induced strain data for three different bellows types. In Figure 29, data for three supposedly identical test bellows is given, however, variations in vibration characteristics are readily evident. The main reason for this difference in the vibration characteristics is that the force-deflection and strain-deflection calibrations of these supposedly identical bellows were quite dissimilar, also. As will be shown, however, correlation of the apparently dissimilar data in Figure 29 for "identical" bellows using the flow-induced vibration analysis discussed earlier gives very consistent results.

This correlation for all data was carried out in the following manner:

(a) The peak flow-induced strain data, as exemplified by the data in Figures 29, 30 and 31, was converted to equivalent maximum relative convolution displacement (x_{mr}) values. The equation giving this conversion is

$$x_{mr} = \frac{S}{2N_c} (dS/dx)^{-1}$$ (23)

where S is the measured peak strain and dS/dx is the slope of the overall bellows strain-deflection curve (see Figure 28).

(b) Next, these maximum relative displacement values were used to calculate the quantity FQ from Equation (20), or

$$FQ = \frac{8NK_A \, x_{mr}}{\left\{ \frac{N}{N_c} + \sin\left(\frac{\pi}{2} \frac{N}{N_c} \right) \right\}}$$ (24)

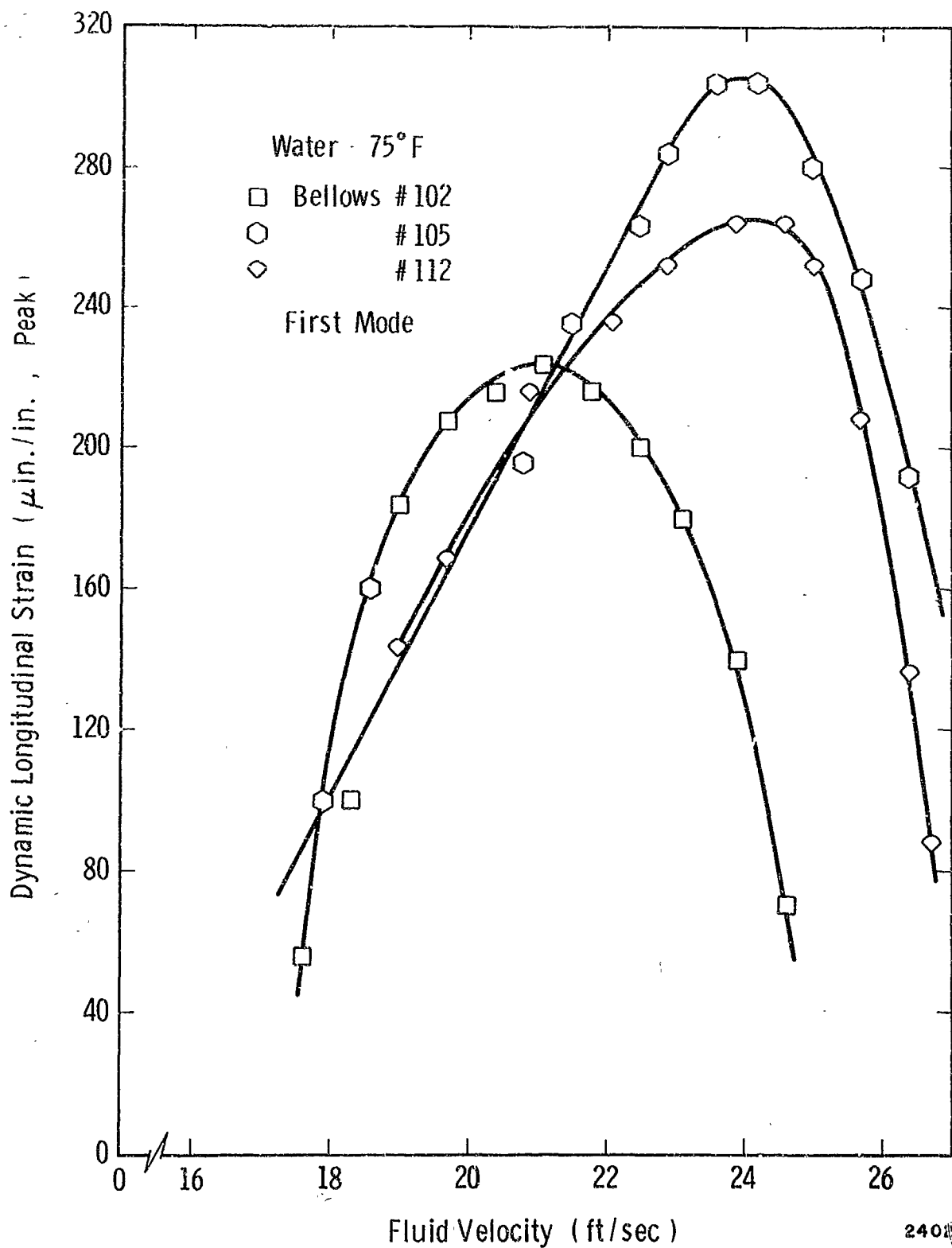Here, F is the peak vortex shedding force and Q is the dynamic amplification factor.

56

Figure 29. Peak Flow-Induced Strain For Three Supposedly
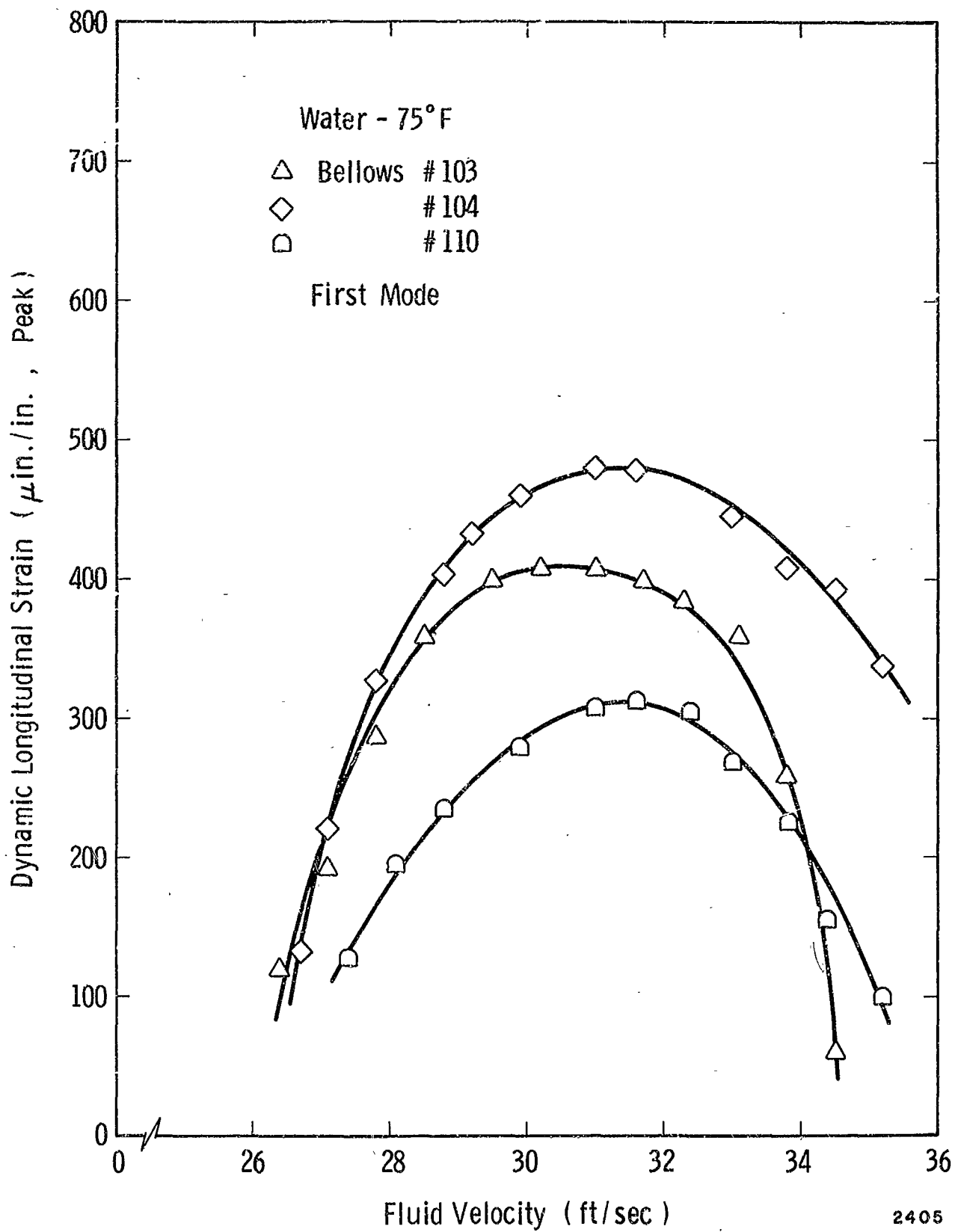Identical Test Bellows

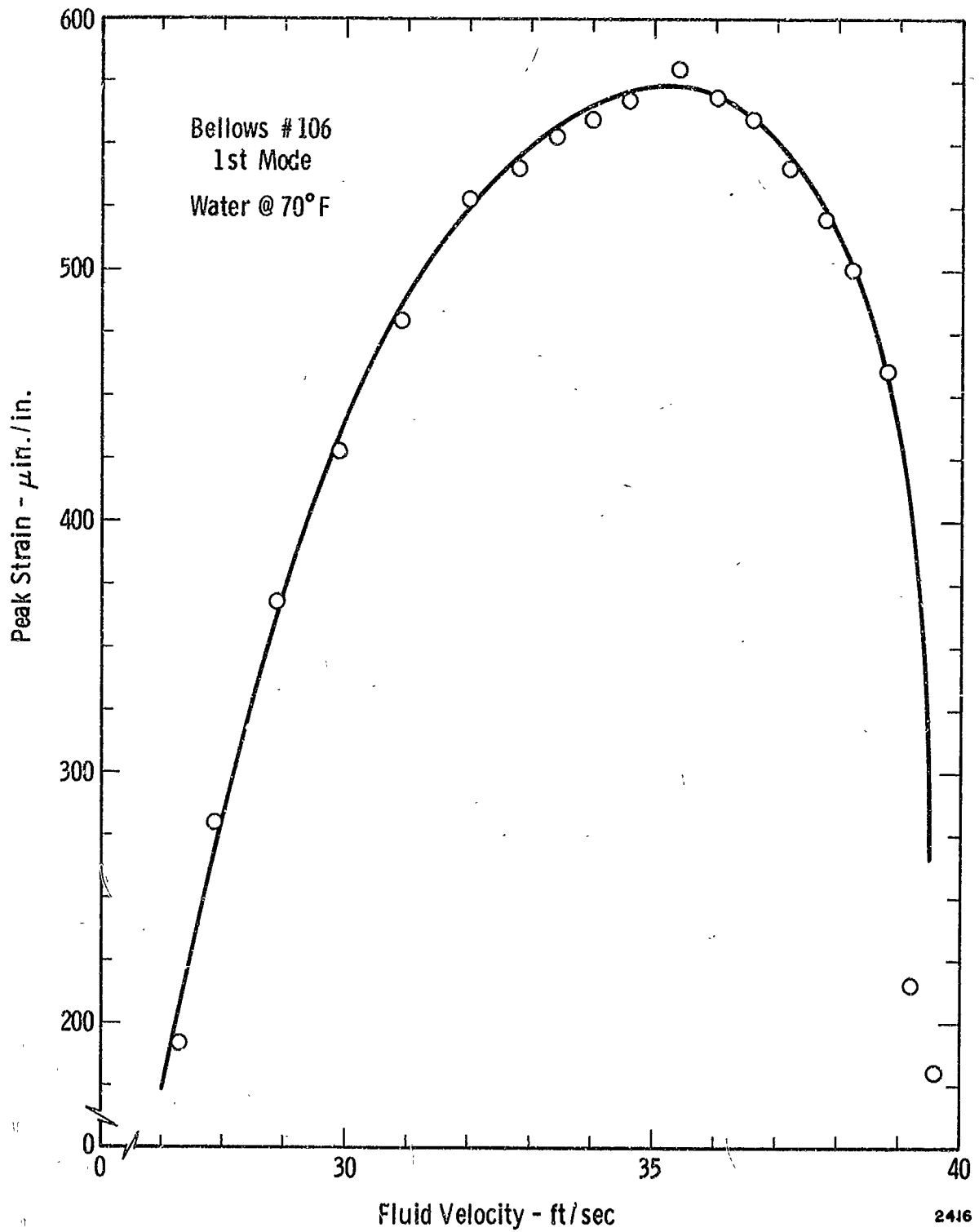Figure 30. Peak Flow-Induced Strain Of Three Test Bellows

Figure 31. Peak Flow-Induced Strain As A Function Of Fluid Velocity For Bellows #106

2416

59

(c) From the results of the bellows damping study (to be discussed in a later section) the value of Q was known from the conditions of the test, therefore, the vortex force F was readily found from the results of (b) above.

(d) Finally, the value of vortex shedding force F was used to calculate an effective vortex force coefficient C_F from Equation (15), or

$$C_F = \frac{F}{(1/2 \rho V^2)(A_p)}$$ (25)

where

$$A_p = \pi(D_i h + h^2)$$

Figures 32 and 33 show the result of this data reduction process as applied to the flow-induced strain data of Figures 29 and 31. The independent variable in Figures 32 and 33 is the Strouhal number based on convolution tip width. Note how much better the data for the supposedly identical bellows is correlated when reduced to the form shown in Figure 32 than it was in Figure 29.

The flow-induced strain data from all test bellows was reduced to the form shown in Figures 32 and 33. Because of differences in the convolution geometry, the peak C_F values varied somewhat from item to item. In general, the greater the ratio of pitch to convolution tip width (λ/σ), the smaller the peak C_F value. This trend was also seen in the results of the single convolution test model discussed earlier, see Figure 22. Unfortunately, the bellows tests discussed above did not provide the range of convolution geometry required to adequately determine C_F as a function of geometry. Therefore, a special test procedure was developed to allow a better study of geometry effect.

Bellows Geometry Effects

Several tests have been performed in which the effect of bellows convolution geometry on the vortex force was determined. This was accomplished in a rather unique manner by step-wise stretching and compressing the test bellows so as to alter the convolution pitch. The advantages of this method are at least twofold; first, it allows geometry to be varied rather independent of other property variations, and second, it results in a hardware savings since more data can be obtained from a single test item.
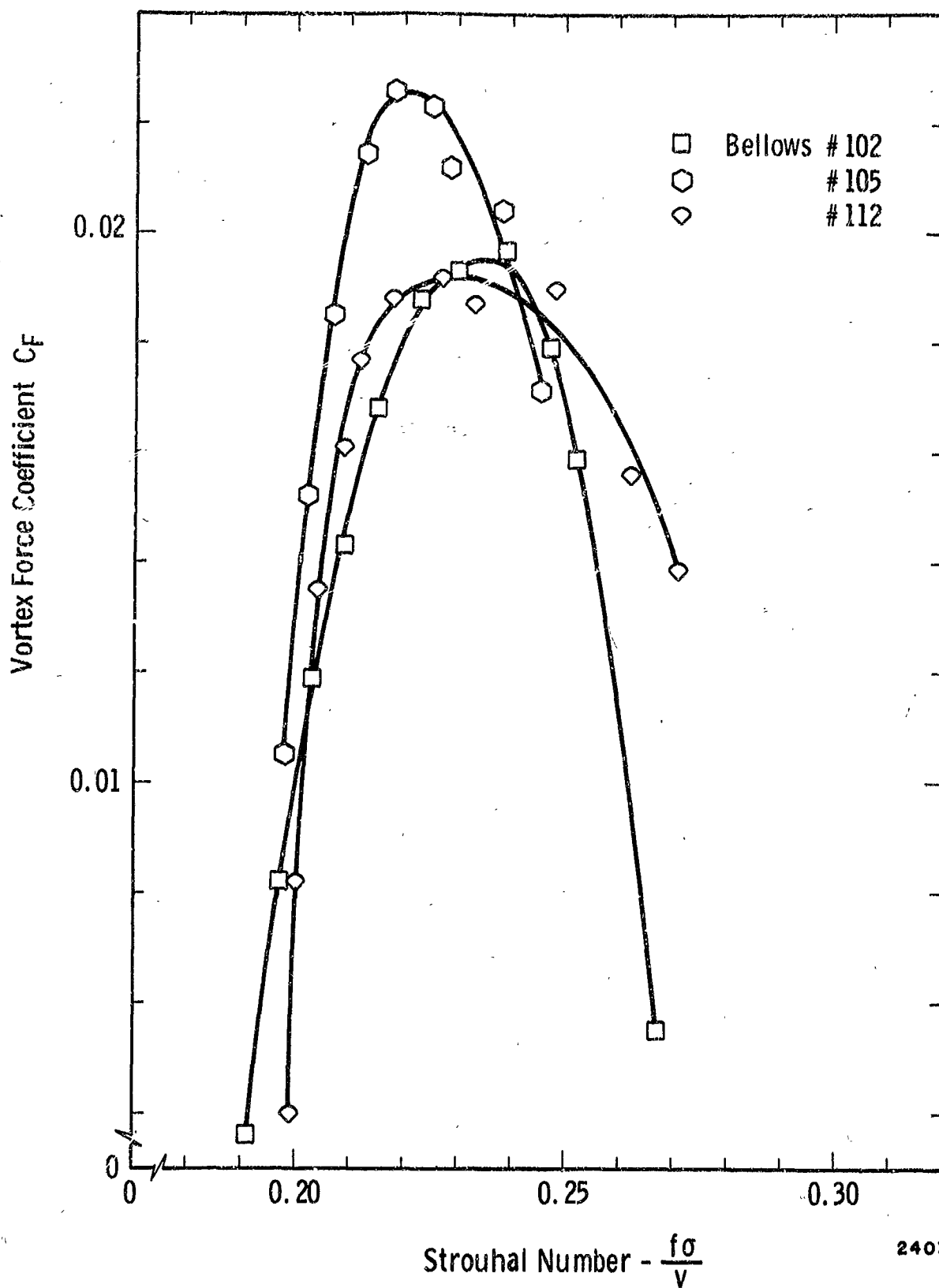
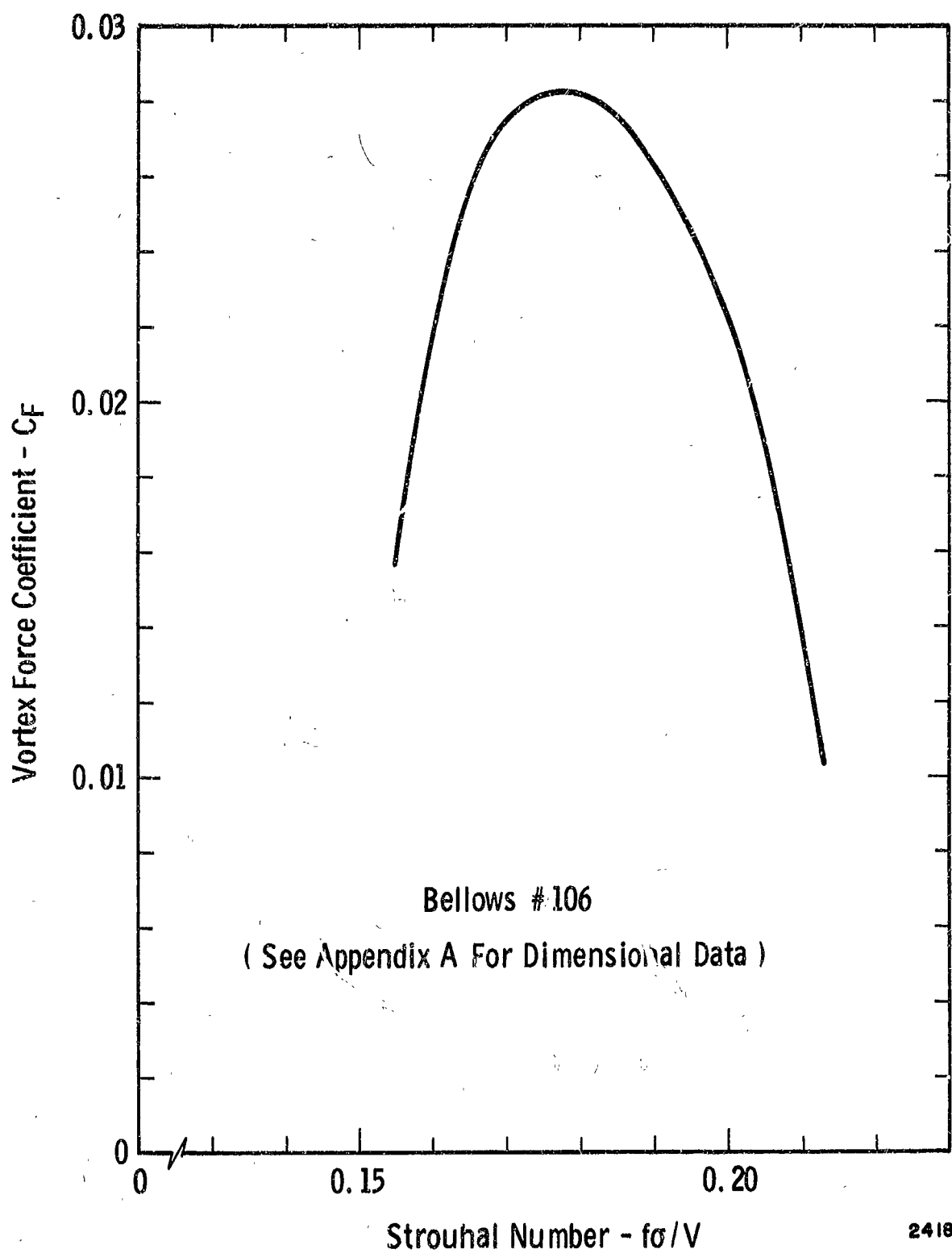Figure 32. Force Coefficient Data Reduced From Strain Data Of Figure 29

Figure 33. Vortex Force Coefficient Data For Bellows Number 106

62

Figure 34 shows a series of photographs of a sectioned bellows mounted in a stretching fixture and positioned in three different pitch configurations. Figure 35 gives flow-induced strain data taken from a bellows identical to the one shown in Figure 34. The data represents the observed peak flow-induced strain for each pitch setting. Figure 35 also shows this same data reduced to the vortex force coefficient form. Notice that the force coefficient generally decreases as the pitch increased; this trend is in agreement with the single convolution test model results (see Section II.6) and other bellows tests. Also, however, Figure 35 shows an obvious trend of "optimum" pitch values which produce minimum local C_F values. This trend has been observed in several bellows tests and can probably be explained by vortex reinforcement as noted in Figure 9. These "optimum" pitch values can be correlated with the parameter λ/σ and are most pronounced for the first few modes of a free bellows. The higher modes of a free bellows and flex hose modes don't seem to have these "optimum" pitch values; they apparently operate in a "vortex reinforcement condition" for all λ/σ values by a natural, and slight, "tuning" of the shedding frequency.

Summary of Force Coefficient Data

In the foregoing sections, vortex shedding force coefficient data has been presented as derived from essentially three different kinds of tests. First, the results of the idealized single convolution model tests were given in Section II.6. These tests yielded force coefficient data for two different convolution configurations; the two configurations had the same convolute height h and the same tip width, but different pitches. Second, complete force coefficient data was obtained from tests of a number of "calibrated" bellows having various convolution geometries. Finally, a limited amount of test data was obtained by a bellows stretch-compression pitch changing scheme. Comparison of all of this force coefficient data shows consistent results which gives credence to the bellows flow-induced vibration model developed in the previous sections.

Figure 36 shows two different curves representative of all available force coefficient data which we have obtained from the various sources. One curve is for use with the first few modes of a free bellows, and reflects the apparent vortex reinforcement trend discussed above. The other curve is for the higher longitudinal free bellows modes, flex hose modes and the convolute local bending mode.

This data represents, then, our state-of-the-art knowledge of vortex shedding force coefficients for bellows. It must be emphasized that this data can only be considered strictly valid for liquid flows through bellows of a size not too different from those tested to date (1.5 and 2.0 inch). We do not anticipate that these coefficients will vary much, if any, for other size ranges, however, the user of this data should be aware of a potential limitation. Larger bellows will be tested in the very near future to extend our knowledge of vortex force coefficients.
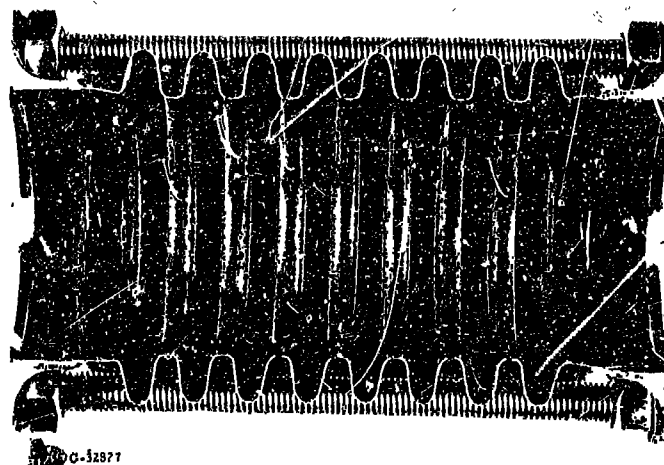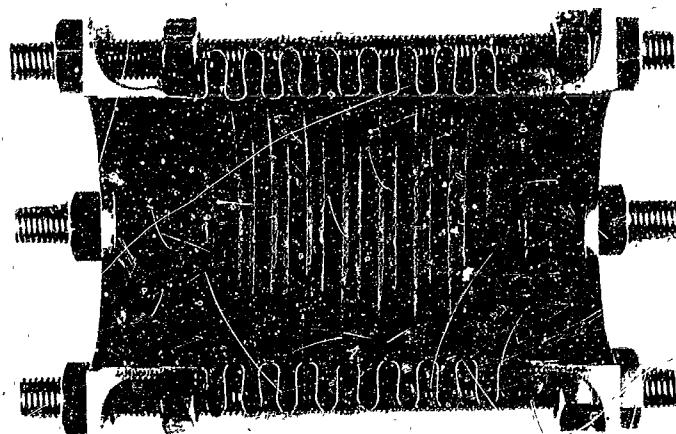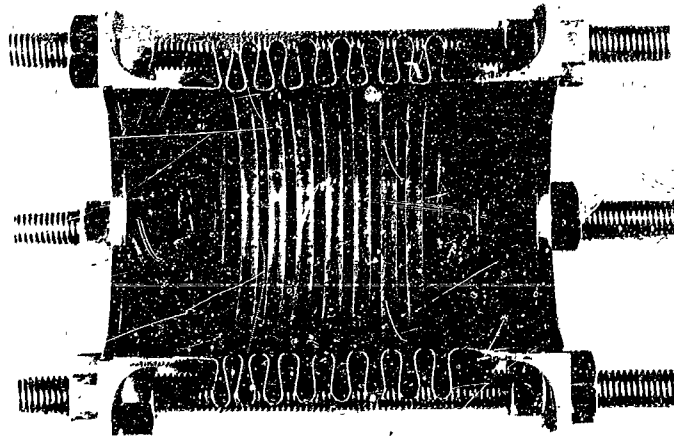
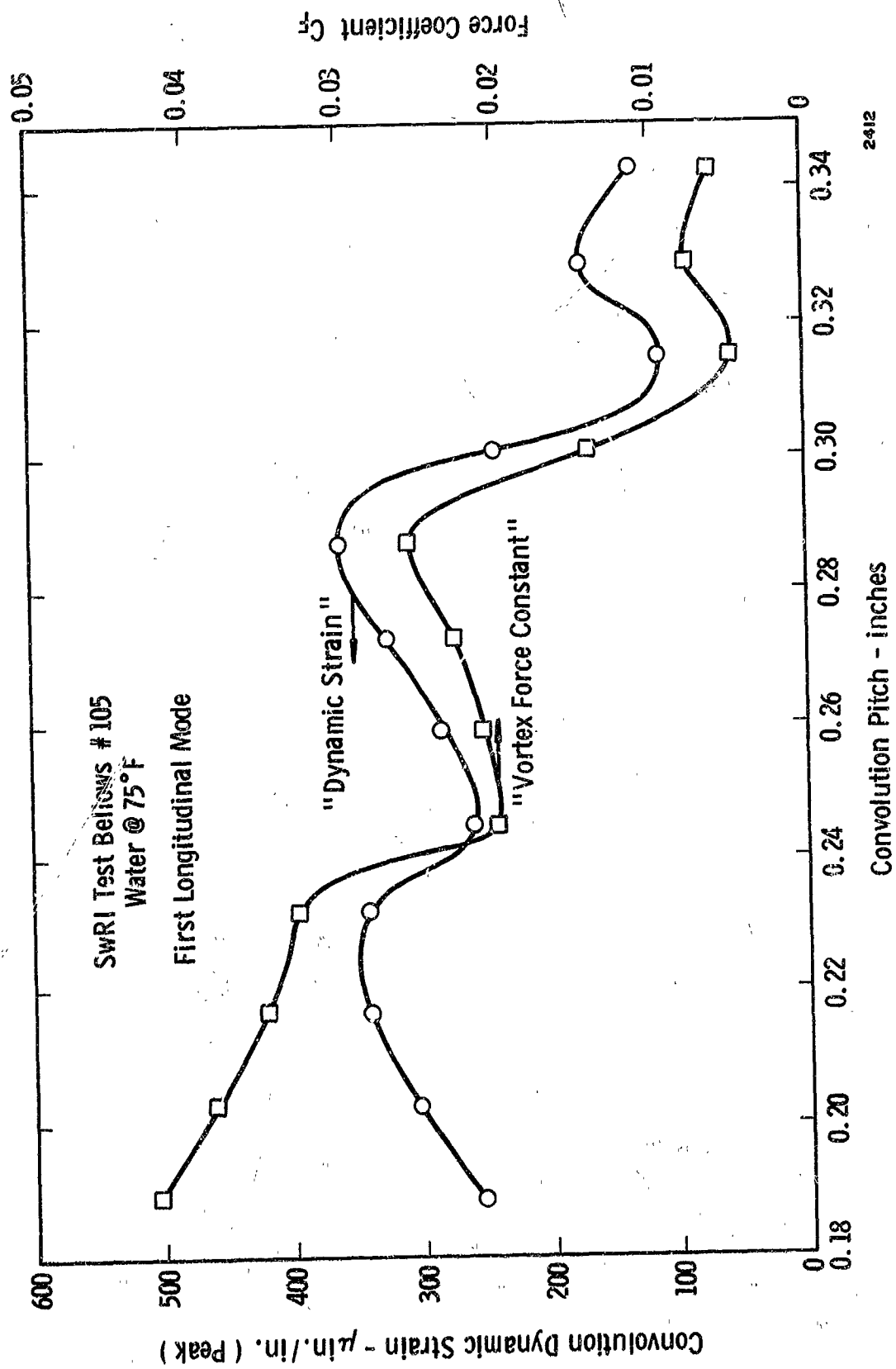Figure 34. Photographs Of Stretched And Compressed Bellows

Figure 35. Response Of Test Bellows As A Function Of Pitch – Bellows
Stretched To Change Pitch

Vortex Force Coefficient - Cf

Use this curve for higher longitudinal free bellows modes, flex hose longitudinal modes, and convolute bending mode

Use this curve for first few free bellows longitudinal modes

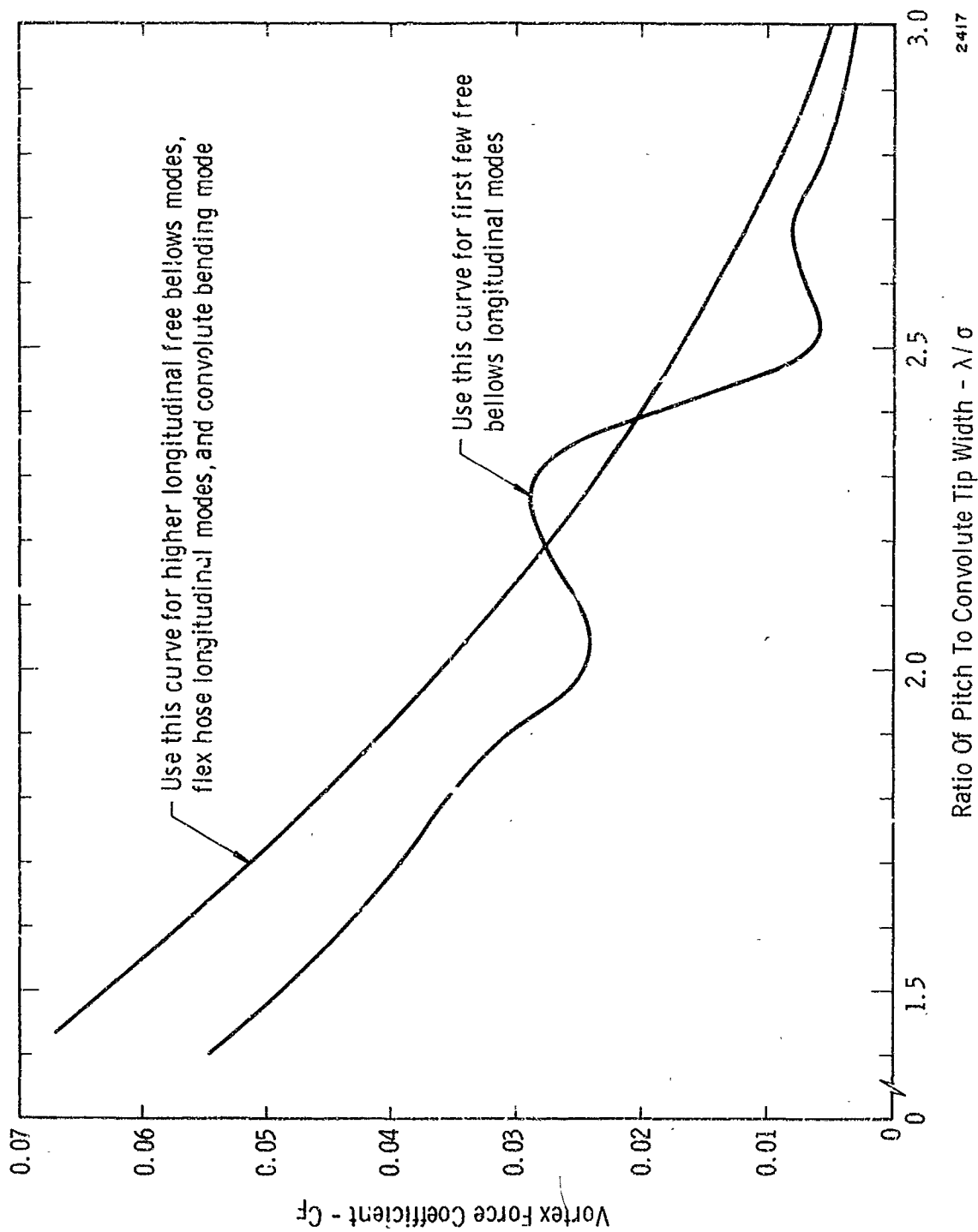Ratio Of Pitch To Convolute Tip Width – λ/σ

2417

Figure 36. Summary Of Bellows Vortex Force Coefficient Experimental Data

II.8   Bellows Damping

An extremely important factor, which provides a limiting condition
i the amplitude of the vibrations resulting from bellows flow excitation,
is the damping of the coupled bellows-fluid system. The vortex force
and mechanical model concept discussed earlier and illustrated in Figure 24
includes no damping so that, ideally, the vibration amplitudes would be
infinite. Some damping is present, however, in all real structures and
it serves to limit the vibration amplitudes to finite values.

By way of review, consider the elementary linear second-order
system shown in Figure 37. The forced response amplitude of this system,
subject to a harmonic excitation $F_o \sin \omega t$, is of the form

$$x(\omega) = \frac{F_o/k}{\left\{ \left[1 - \left(\frac{\omega}{\omega_o} \right)^2 \right]^2 + 4\zeta^2 \left(\frac{\omega}{\omega_o} \right)^2 \right\}^{1/2}} \tag{26}$$

where

$$\omega_o = (k/m)^{1/2}, \qquad \zeta = b/2 \, (km)^{-1/2}$$

At resonance (the frequency ω_r for which $x(\omega)$ is a maximum, the
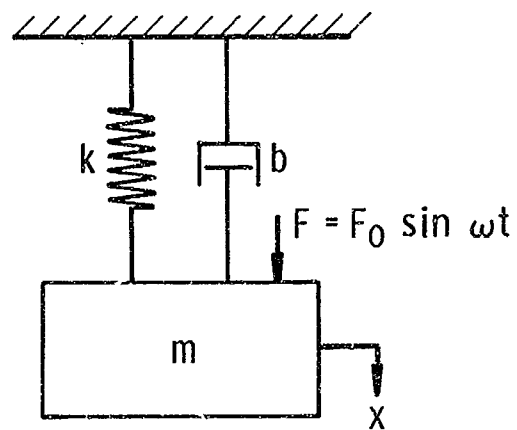amplitude may be written as

$$x(\omega_r) = \frac{F_o Q}{k} \tag{27}$$

where

$$Q = \left\{ \left[1 - \left(\frac{\omega_r}{\omega_o} \right)^2 \right]^2 + 4\zeta^2 \left(\frac{\omega_r}{\omega_o} \right)^2 \right\}^{-1/2} \tag{28}$$

In terms of the values of the mechanical elements of the system in
Figure 37, Q may also be written as

$$Q = \frac{1}{2\zeta} = \frac{(km)^{1/2}}{b} \tag{29}$$

$$m\ddot{x} + b\dot{x} + kx = F_0 \sin \omega t$$

2407

Figure 37. Linear Second-Order System

Figure 38 illustrates a typical response curve for the system shown in Figure 37 where the amplitude of the force F_o has been held constant, and the frequency of excitation varied. As shown, the value of Q physically represents the ratio of the vibration amplitude at resonance to the vibration amplitude in the limit of zero frequency. Also, the value of Q may be expressed in the form

$$Q = \frac{f_r}{\Delta f} \qquad (30)$$

where f_r is the system resonant frequency and Δf is the bandwidth at the halfpower point (0.707 times the resonant amplitude); see Figure 38.

Because the value of Q is so important in the prediction of bellows flow-induced vibration amplitudes, and even for proper data reduction as discussed earlier, a large number of bellows mechanical vibration tests were conducted from which Q values could be obtained. Figure 39 shows the test set-up used for the mechanical vibration tests. Each bellows was mounted in a special fixture which rigidly connected the end flanges. The reason for this was to ensure that the vibration modes excited would be the same as those observed in the flow-excitation tests.

Figures 40 and 41 show Q values obtained from the forced vibration tests. In general, the following trends are noted (see also Figure 42):

(a) The bellows damping is generally most sensitive to peak strain amplitudes, with the damping increasing as strain increases.

(b) Single-ply bellows of different configurations, tested under similar conditions (same strain level, same internal media, etc.) do not necessarily have the same Q values.

(c) For one configuration of bellows, increasing the number of plies from one to two significantly increases the damping (reduces Q); however, going to three plies adds little more damping, if any, over the two-ply configuration.

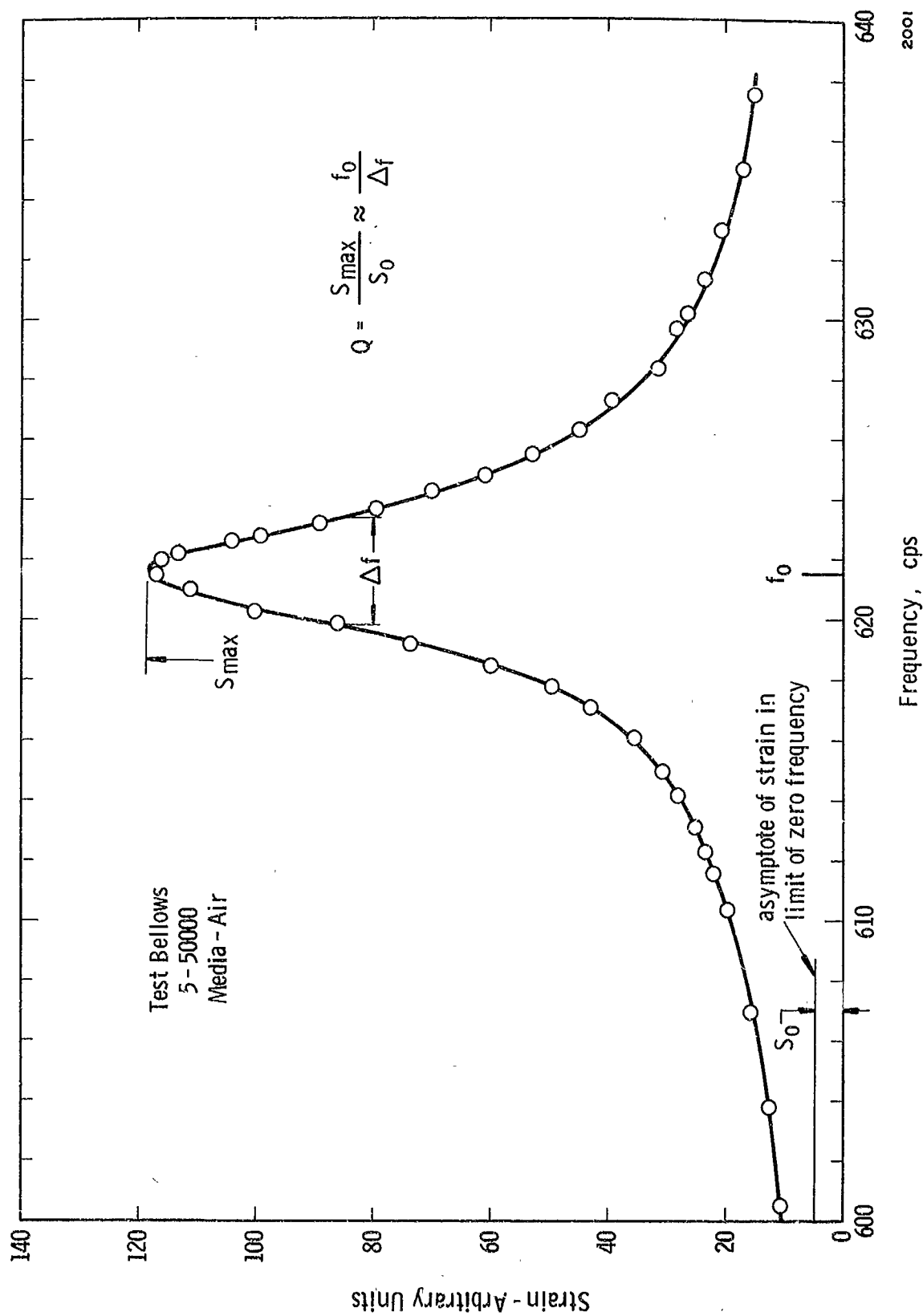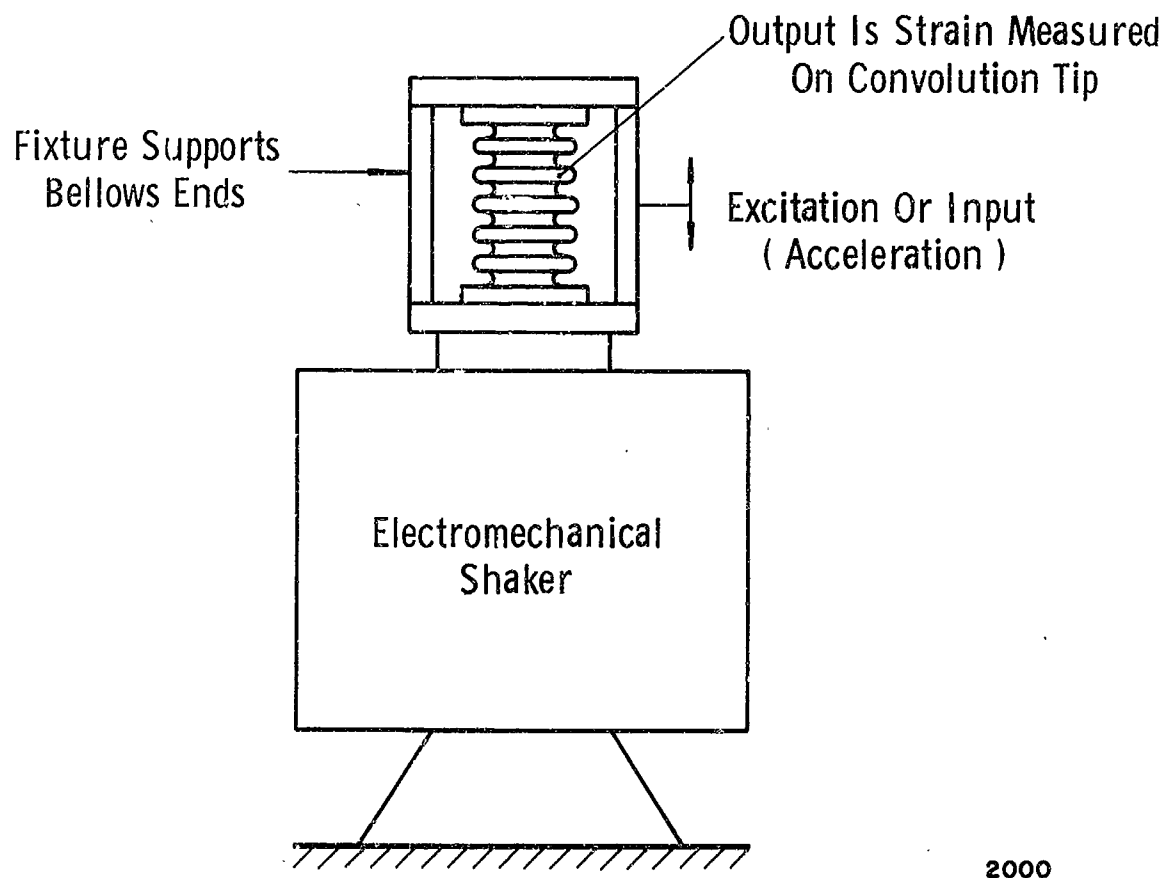(d) For bellows with a liquid as the contained media, damping may greatly increase at low absolute pressures.

69

Figure 38. Example Bellows Forced Response Data For Constant Level Acceleration Input

$$Q = \frac{S_{max}}{S_0} \approx \frac{f_0}{\Delta f}$$

Test Bellows
5 - 50000
Media - Air

Strain - Arbitrary Units

Frequency, cps

S_{max}

Δf

f_0

S_0

asymptote of strain in
limit of zero frequency

70

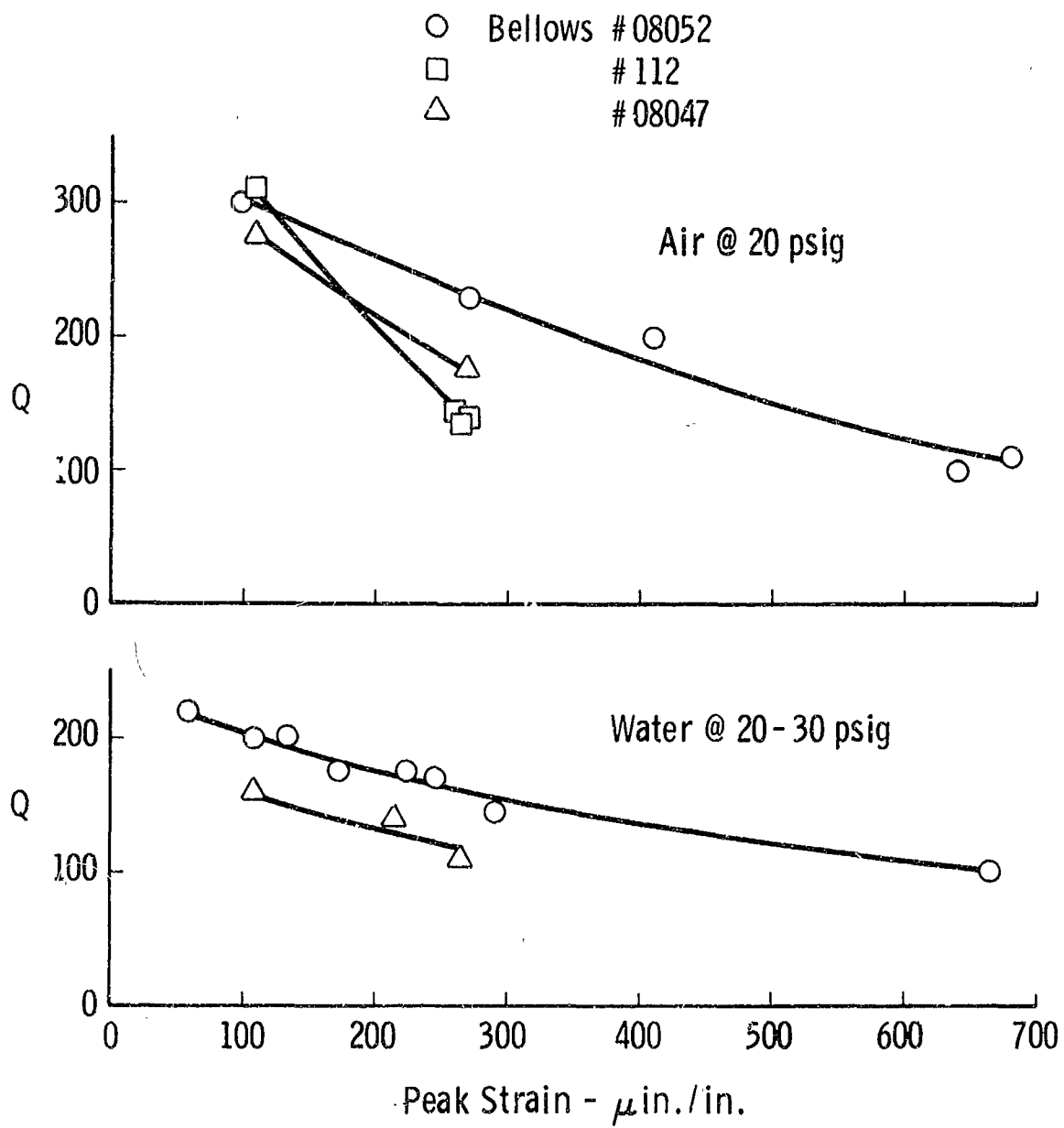Figure 39. Schematic Of Bellows Damping Measurement Test Setup

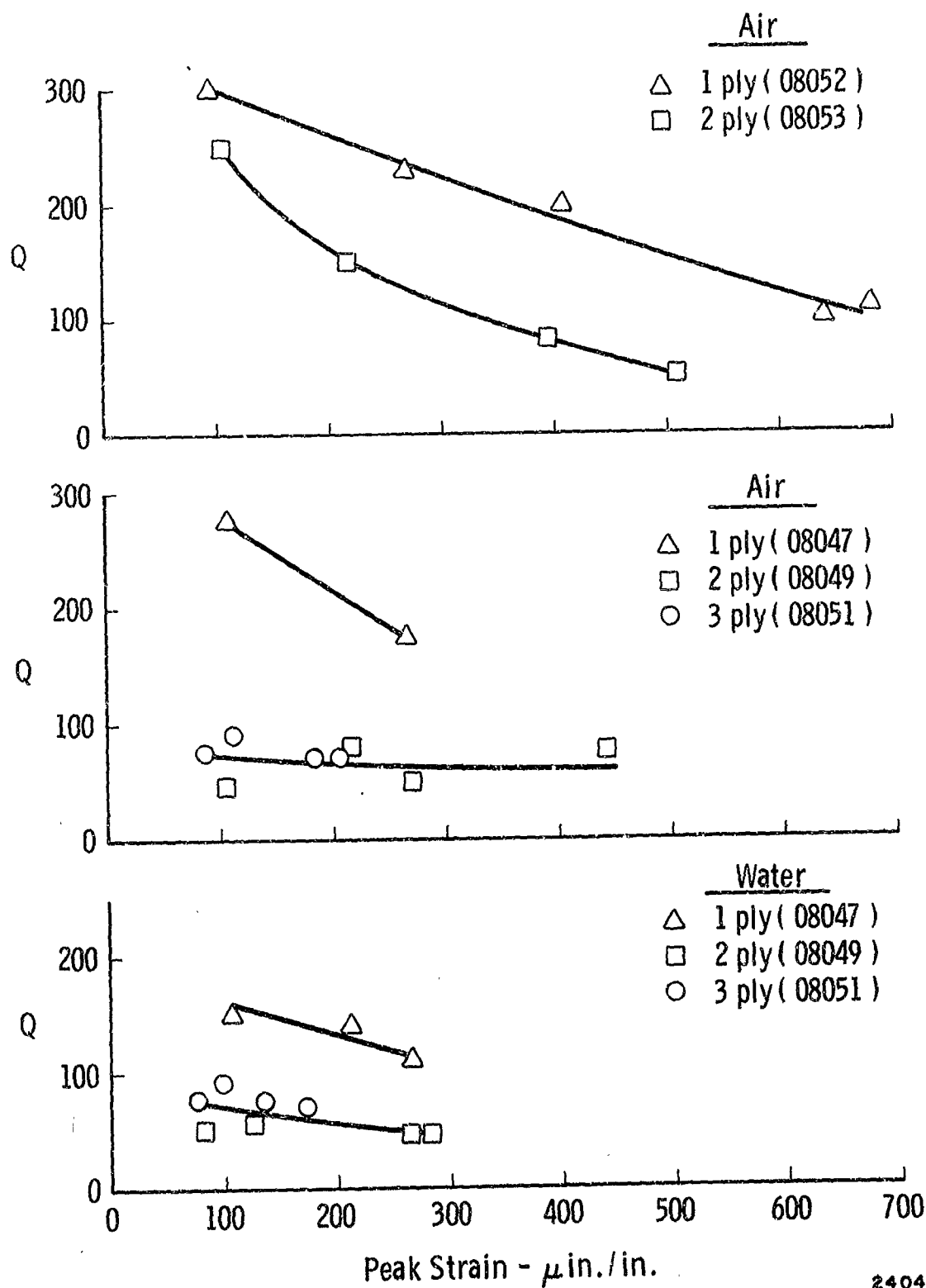Figure 40. Q Values For Single Ply Bellows

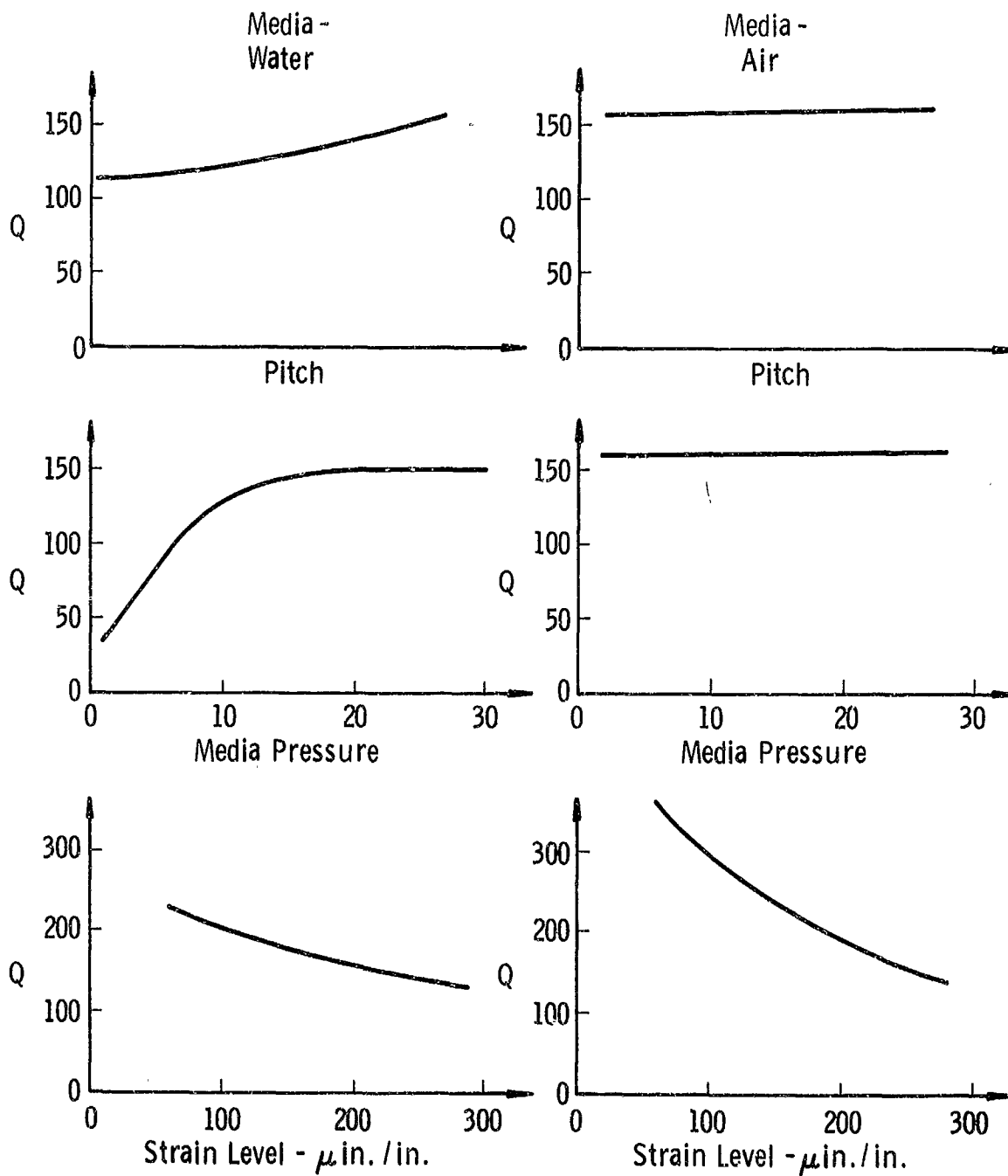Figure 41. Q Values For Multiple-Ply Bellows

Figure 42. Trend Of Q With Various Parameters

2335

74

The fact that damping increases as the strain level increases means that the damping is a nonlinear function of amplitude and, therefore, the linear model in Figure 37 is not necessarily valid. Valid Q values can, however, still be assigned if it is realized that they depend on strain level. The fact that the bellows damping is non-linear is really no surprise, since structural damping is often of this nature (see Lazan's discussion of hysteretic damping in Reference 11).

The second trend noted above is that bellows with different configurations do not necessarily have the same Q values for similar test conditions. This is undoubtedly caused by a lack of a proper correlation model for the bellows damping. In other words, if we could develop an analytical model which allows prediction of damping in terms of convolution configuration, strain level, etc., then the damping data should "correlate". Such a model has not yet been developed, but efforts along these lines will be attempted. For the present, we have no recourse but to use the data in Figures 40 and 41 to define conservative Q values for design and analysis purposes.

Table V and Figure 43 summarize what we consider to be a best estimate of conservative Q values for various situations. The user of this data is advised to always tend toward the higher Q values where a choice must be made.

II.9   Other Influences

In practice, it has been found that several factors, in addition to those already discussed, can have an influence on the magnitude and character of bellows flow-induced vibrations; these factors are, (a) presence of an upstream elbow, (b) angulation of the bellows, (c) non-rigidly attached piping, and (d) acoustic resonances of the duct system. The first three influences are discussed briefly in this section and the subject of "acoustic resonance effect" is treated in the following section.

Upstream Elbow Effect

Because it had been observed that some bellows installed immediately downstream of a duct bend were seemingly more susceptible to flow-induced failure problems than those in straight sections, a small investigation was undertaken to study this. One of the calibrated test bellows was placed in the flow system, as shown in Figure 44, and located immediately downstream of a short-radius 90-degree elbow. Flow-induced strain amplitudes were then monitored as a function of the mean internal fluid velocity. The test was repeated with the same bellows in a straight run with all other conditions kept the same.
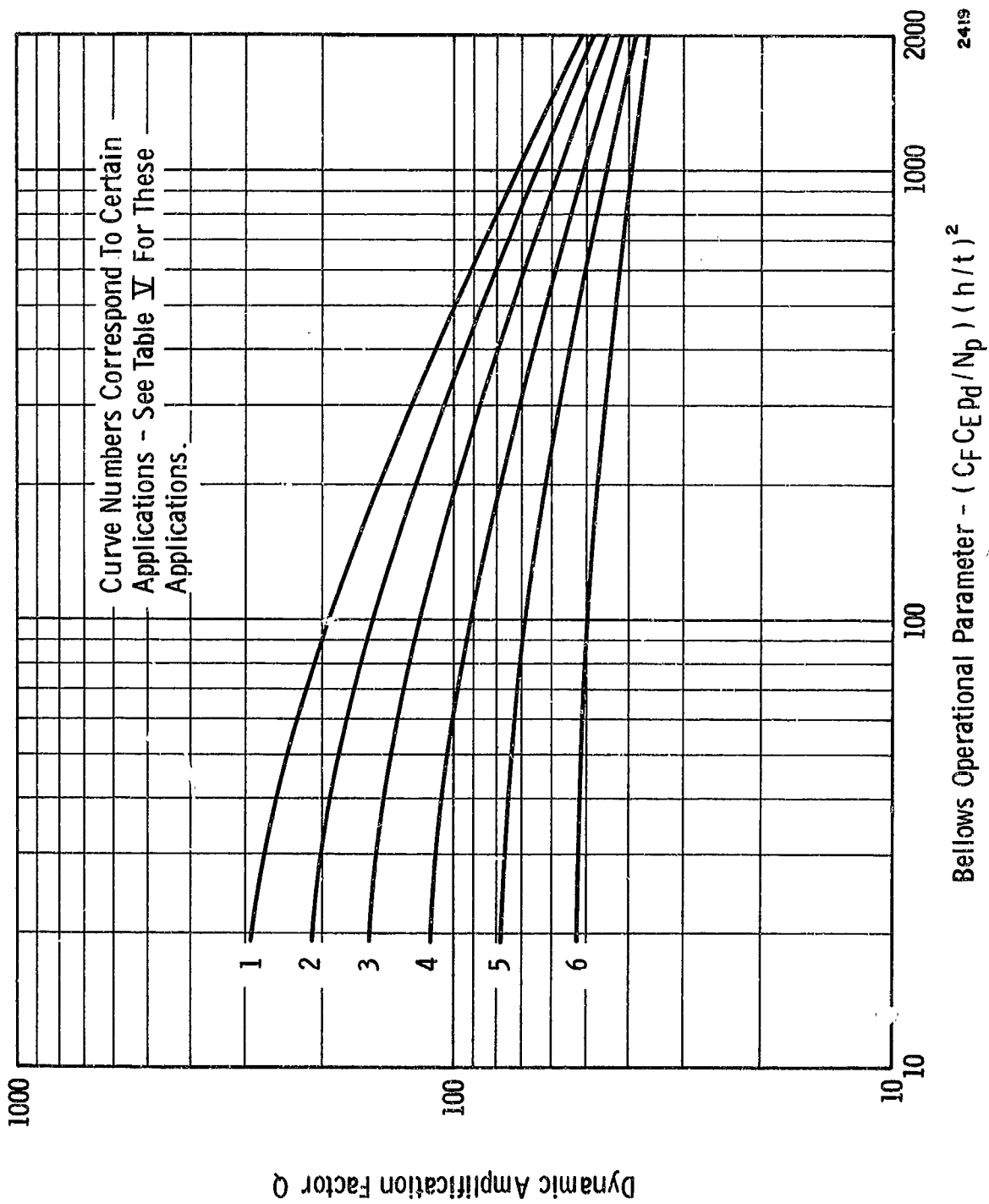
Figure 43. Dynamic Amplification Factors For Various Bellows Applications

2419

Specific Spring Rate (see Note 1)	Number Plies	Internal Media (see Note 2)	Curve No.
all ranges	1	low pressure gases	1
over 2000 lb/in^2	1	high pressure gases, light liquids	1
over 2000	1	water, dense liquids	2
under 2000	1	high pressure gases, light liquids	2
under 2000	1	water, dense liquids	3
over 3000	2	all	3
2000-3000	2	all pressure gases	4
under 2000	2	all pressure gases	5
2000-3000	2	all liquids	5
under 2000	2	all liquids	6
over 3000	3	all	4
2000-3000	3	all	5
under 2000	3	all pressure gases	5
under 2000	3	all liquids	6

Use of Table - To use table, first calculate bellows specific spring rate, then look up application curve number corresponding to this specific spring rate, number of plies, and internal media.

Note 1: The specific spring rate is here defined as

$$S.S.R. = \frac{K_A N_c}{D_m N_p}$$

or is the spring rate per convolute, per ply, per unit of diameter.

Note 2: Low pressure gases will be defined here as being those gases below 150 psia. Light liquids will be defined as having a density, relative to water, of less than 0.2.

TABLE V

Applications Information for Use with Q Values
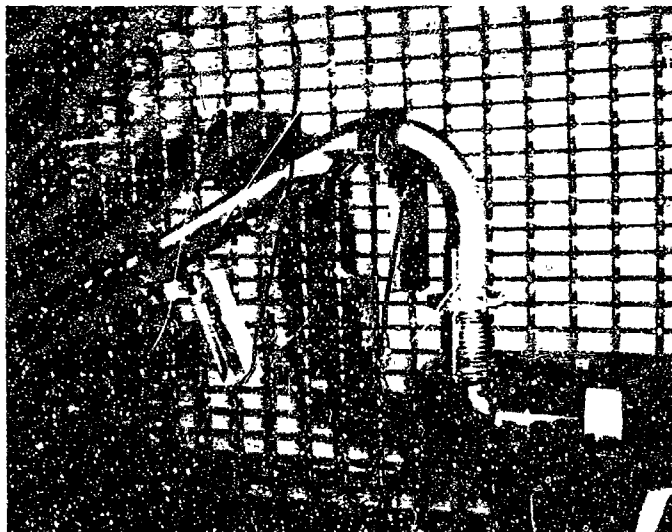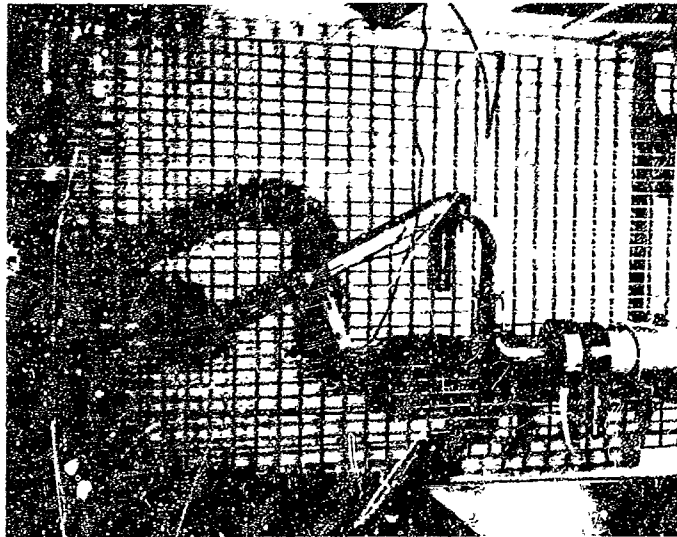Data in Figure 43

Figure 44. Experimental Setup To Determine Effect Of Upstream
Bend On Bellows Vibration

Figure 45 shows the results of these tests. Notice that two things have changed about the response of the bellows with the elbow present, compared with the response with no elbow. First, the <u>mean</u> fluid velocity range over which flow excitation occurs has been shifted down by about 45 percent. Second, note that the strain level for a given mode of vibration has significantly increased, or that the strain amplitude at a given fluid velocity has increased.

The explanation for the difference in bellows vibration with, versus without, an upstream elbow is that the velocity profile is skewed or distorted because of the presence of the elbow (see Figure 45). This causes an excessive dynamic fluid loading on the convolutions downstream of the outer bend region and possibly a reduced loading downstream of the inner region; the net effect is an increased effective value of the fluid velocity along the surface of the bellows, causing the vortex shedding to lock-in on the bellows vibration at a lower-than-normal mean fluid velocity.

While further tests must be performed to better quantify the influence of an upstream elbow on bellows vibration levels, we can say for the present that an increase in stress level by a factor of about 2 is possible for a given mean velocity. Elbows with more generous radii of curvature, or located further upstream, would most likely not cause this great an increase in flow-induced stress levels.

Non-Rigid Ducting

As might be expected, if the ducting attached to the ends of a bellows is not rigid then the character of the flow-induced vibration can be changed compared with the ideal case of perfectly rigid attachments. There are apparently two ways that the bellows vibrations can be affected; first, the modal frequencies can be changed (generally lowered), and second, additional damping can be "added" or energy dissipated through the attachments.

For most cases, the modal frequencies of a bellows will not be significantly changed because of flexible attachments. The reason for this is that the bellows is generally so much more flexible than the attached ducting, particularly in the longitudinal or axial direction. Apparently, however, significant damping can be introduced by allowing duct flexibility as evidenced by some of our experimental observations. While we can't at this time report any quantitative results, the reader should take note of these observations. Whenever a bellows is undergoing a qualification test, our observations indicate that particular care should be

Figure 45. Bellows Flow-Induced Strain With And Without Upstream Elbow
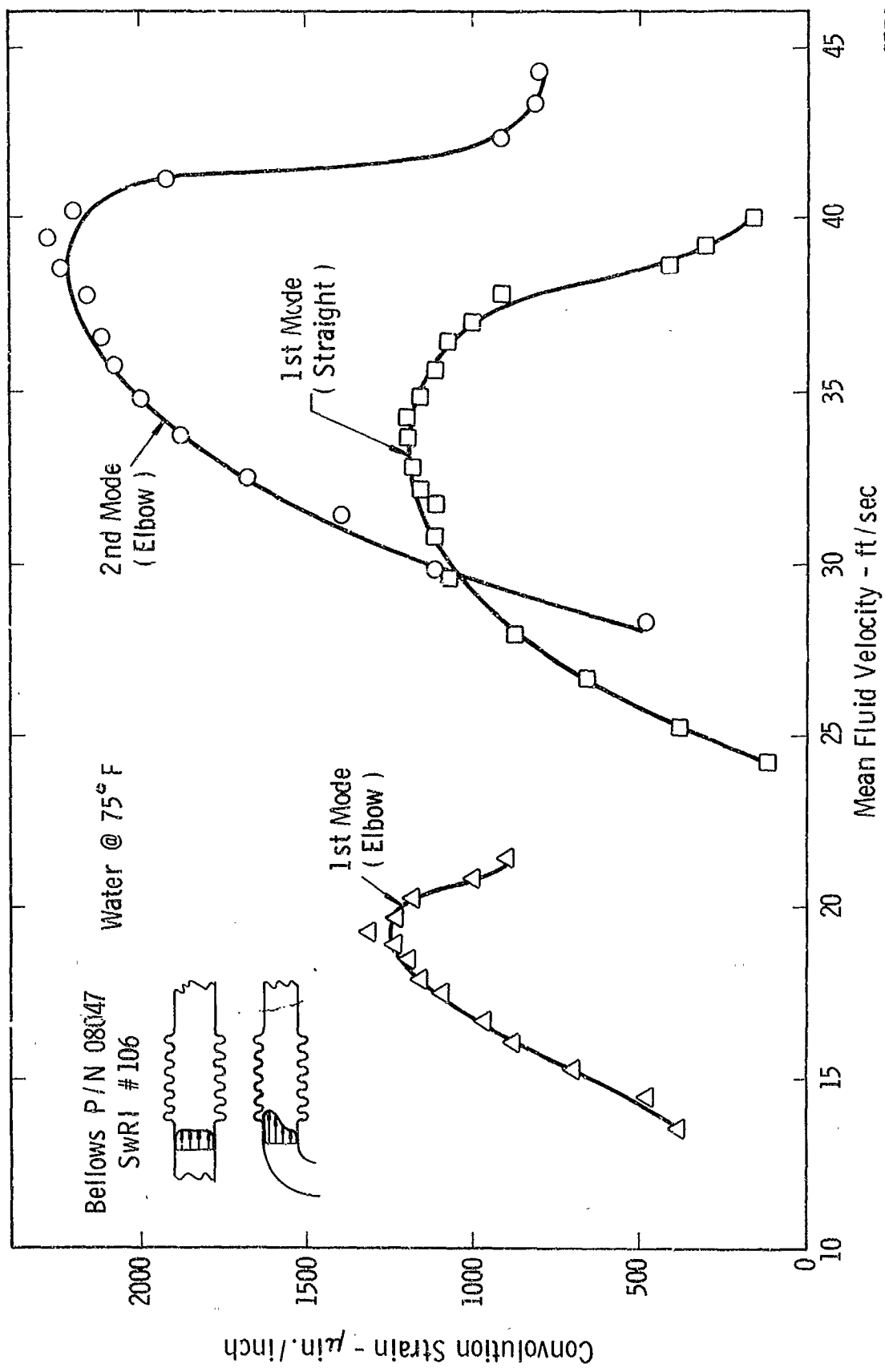
exercised so that the bellows attachments are at least as rigid as in the actual installation. This should help ensure that the flow-induced vibration levels attained in the qualification test are at least as great as the actual installation.

Angulation of Bellows

At the present time, we have no quantitative information to report concerning the effect of angulation on bellows flow-induced vibrations. It would seem, based on the results of the upstream elbow tests discussed above, that angulation might lead to an increase in vibration levels because of the excess fluid loading on the outer bend region. Also, however, angulating a bellows might cause a change in the mode frequencies and damping. At this time, effect of angulation must be considered unknown and we caution the reader to be conservative in dealing with this situation.

II.10   Acoustic Resonance

In a previous section entitled "Fluid Loading Effects," we discussed how acoustic loading can increase the number of degrees of freedom of a bellows system by producing coupled bellows-acoustic modes. When this type of coupling occurs, it has been generally observed that very significant pressure fluctuations can be propagated throughout the fluid system. Appendix D discusses a mechanism of noise production as a result of a vibrating bellows exciting the longitudinal acoustic duct modes. In addition, however, acoustic resonances have been observed to cause a significant increase in the flow-induced stress levels. This second effect is apparently a result of the acoustic resonance flow and/or pressure fluctuations coupling with the vortex shedding process to produce a force amplification, as will now be discussed.

In the preliminary air flow testing of one free bellows, it was noted that the specimen showed virtually no response up to a rather high velocity where, quite suddenly, the response became very significant. This sudden onset of response was accompanied by very significant acoustic radiation from the entire flow loop, indicating that an acoustic resonance existed in the facility. A calculation of the stress indicator (discussed in the next section) value at the air velocity where this phenomena started, gave a value of only a few thousand psi. It was felt that the vibration observed was much more severe than it should have been, and this was attributed to an enhancement of the vortex shedding by the acoustic resonance. At this point it was believed to be a longitudinal resonance which caused this effect.

Following this preliminary air flow test, two different bellows were extensively investigated in order to find out more about the influence of acoustic resonance on the bellows response. One of these bellows was tested using two different gases; air and Freon 12. These two gases were selected because of the great difference in speed of sound. Under ambient conditions, air has an isentropic speed of sound approximately equal to 1100 feet per second, while the isentropic speed of sound for Freon 12 is about 485 feet per second. Also, the Freon has a greater density (by a factor of about 5) under the same conditions. To be able to assess separately the effect of density and speed of sound, flow tests were conducted at different mean pressure levels with each gas. Therefore, by comparing the test results with one gas at different pressures, the effect of density was determined. Figure 46 shows, for example, acceleration level at the predominant response frequency, (measured at the bellows flange) as a function of mean air velocity for two different mean pressure levels. Qualitatively, the response is the same for the two cases, and shows no significant vibration up to a critical flow velocity, where, suddenly the bellows subsequently responds well in various flow-induced modes of vibration as the velocity is further increased. This critical velocity is the same for both mean pressure levels, as may be seen in Figure 46. This onset of bellows vibration is accompanied by a great increase in the acoustic noise level at the same predominant frequencies that exist in the flange acceleration signal.

The results of the tests conducted with the Freon were qualitatively the same as with the air; the critical flow velocity at which the bellows suddenly began to respond was, however, much lower. In fact, the critical flow velocity with the Freon was about half that experienced with the air. This is just what we expected might happen, assuming the responsible mechanism to be an acoustic resonance, since reducing the speed of sound would cause a reduction in the frequency (hence, flow velocity) required to give a resonant condition.

To further verify the acoustic resonance idea, the acoustic pressure field inside the bellows was mapped out, with the aid of a small microphone; the result is illustrated in Figure 47. It was determined that we were getting excitation of coupled radial-axial acoustic modes, with the maximum sound pressure level, in the radial direction, occurring in the vicinity of the bellows internal diameter, while the sound pressure level maximum, in the axial direction, is half way along the convoluted length of the bellows. There is an acoustic pressure minimum all along
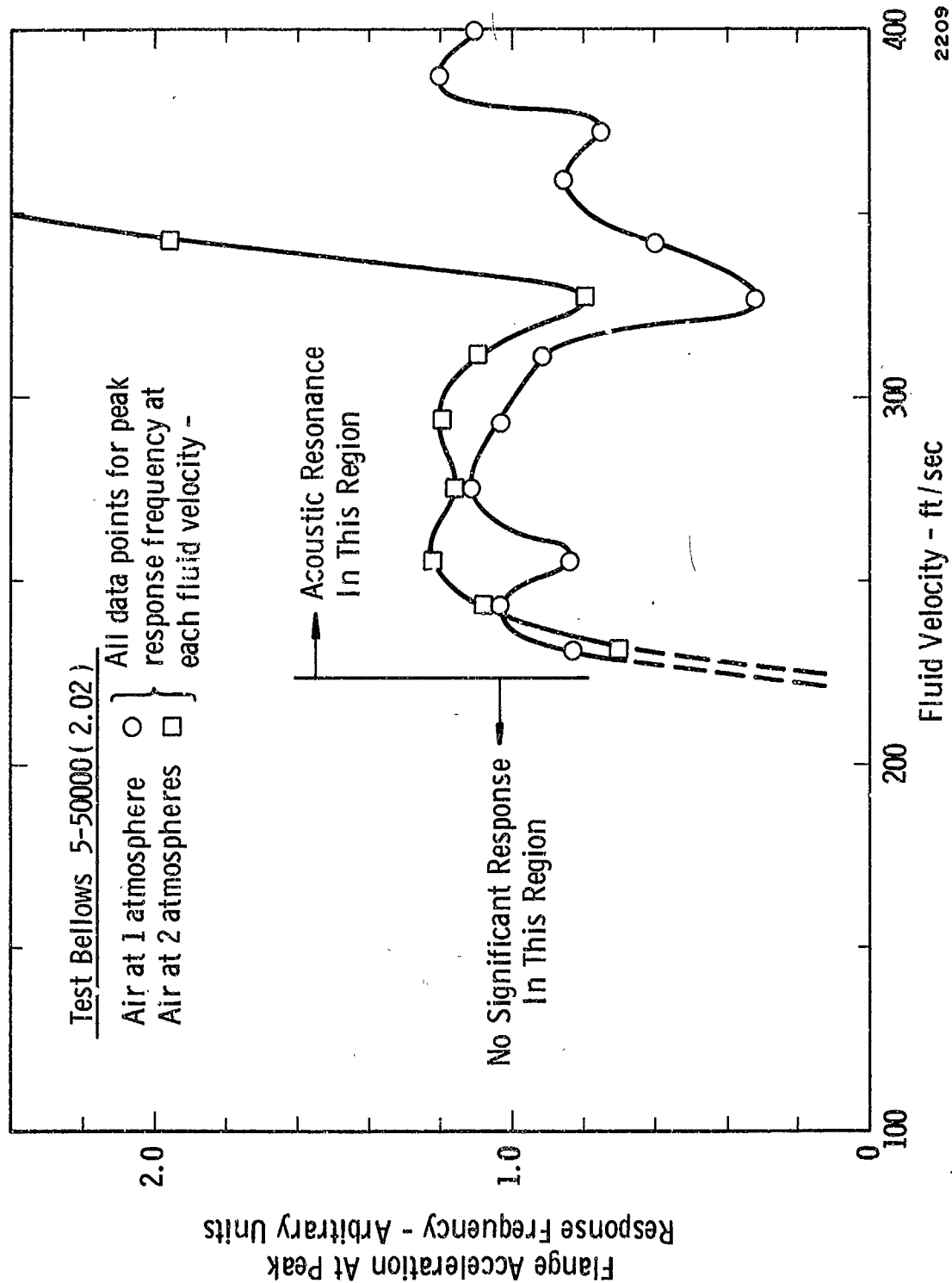
Figure 43. Bellows Acceleration At Peak Response Frequency For Two Different Mean Air Pressures Showing Sudden Response Where Acoustic Resonance Occurs

83

Axis of Bellows

Envelopes of sound
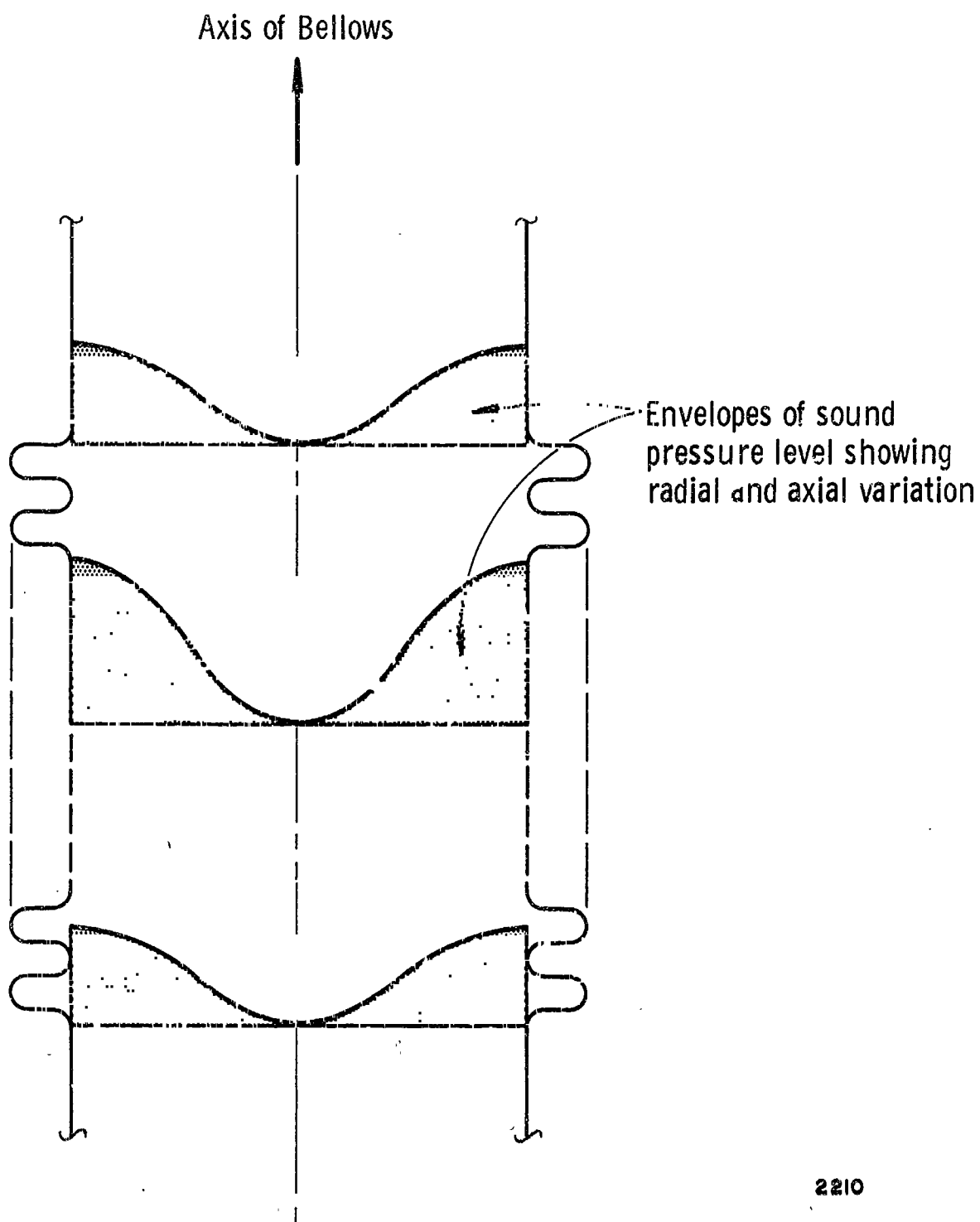pressure level showing
radial and axial variation

2210

Figure 47. Illustration Of Acoustic Pressure Level Variation
With Radial And Axial Position In Bellows

the geometric bellows axis. The acoustic field described above is being excited by the vortex shedding from the bellows convolutions. In turn, the acoustic resonance apparently enhances the vortex shedding, causing "greater-than-expected" response levels.

The reason for the sudden occurrence of this phenomena at some critical flow velocity is as follows: At low fluid velocities, hence low vortex frequencies, the acoustic wavelengths are too long to "fit" in the bellows in a radial direction; therefore, the radial acoustic waves which are generated experience pure attenuation. When a high enough shedding frequency is achieved (hence, a high enough fluid velocity), the wavelengths are short enough to "fit" radially, and, therefore, cause a radial resonance condition and couple with an axial acoustic mode.

It is very important to note that this radial acoustic resonance was observed even when the bellows was completely restrained to prevent any possible convolution vibrations (this was done by covering the bellows on the outside with a thick coat of epoxy). Under these conditions, the acoustic resonance was not as strong as with the bellows free to vibrate. Even so, accelerometer data monitored at the bellows flange showed strong acceleration levels at the acoustic resonant frequency, plus numerous harmonics. This implies that the use of an accelerometer for bellows vibration monitoring where an acoustic resonance occurs can be very misleading. A comparison was made during one test of the spectral content of convolute strain and flange acceleration, and the results were grossly different. The reader should, therefore, be wary of accelerometer data which is taken where an acoustic resonance occurs, and which shows strong response at multiples of the vortex shedding frequency.

In conclusion, the effect of a radial acoustic resonance in bellows leads to greatly increased flow-induced stress levels and sharp increases in the sound level in the duct system at the vortex shedding frequency, and at multiples of this frequency. A rough judgment can be made as to the likelihood of a radial acoustic resonance occurring by comparing the calculated acoustic wavelength with the outside diameter of the bellows. When this calculated wavelength becomes small enough to about equal the bellows outside diameter, then acoustic resonance may occur, and any bellows structural modes corresponding to this frequency may be strongly excited.

85

II.11 Bellows Flow-Induced Stress

Best Model

The present "best model" for predicting bellows flow-induced stress levels involves calculating the maximum relative convolute displacement by the method discussed previously in this chapter, and then calculating a corresponding stress level from an existing stress-deflection theory. The steps in thus calculating flow-induced stress are summarized below:

Step A   -   Calculate the maximum convolute relative displacement of one-half of a convolute from the expression

$$x = \frac{C_m F Q}{K_A} \qquad (31)$$

where

$$C_m = \frac{1}{8N} \left\{ \frac{N}{N_c} + \sin \left(\frac{\pi}{2} \frac{N}{N_c} \right) \right\} \qquad (32)$$

and

$$F = C_F \pi (D_i h + h^2) (1/2 \rho V^2) \qquad (33)$$

The values of C_F and Q may be found from Figures 36 and 43, respectively. The mode number N may be determined as a function of fluid velocity by the method outlined in Section II.4(see Tables III and IV).

Step B   -   Calculate the stress corresponding to the maximum convolute displacement x by an existing method, such as outlined in Appendix B.

Step C   -   If an upstream elbow is present for the subject bellows installation, then some upward adjustment of the calculated stress is necessary. For a severe bend immediately upstream of a bellows, multiply the calculated stress by 2.0 to correct for the elbow. For "less severe" cases, multiply by 1.5 to correct for the upstream elbow.

At this point it is well to point out the currently known limitations and potential limitations of this model, including estimated possible errors. The model, as discussed in this chapter, has evolved from a theory which is supported by some empirically-obtained factors; these are the vortex

force coefficient C_F and the amplification factor Q. Values of C_F and Q were obtained from tests of bell∅ws, and a special single convolute model, having internal diameters of 1.5 inches and 2.0 inches. Bellows with a range of geometries were tested in these two sizes. It is evident, therefore, that the model as it stands has only been verified for bellows of this general size. A potential limitation, then, is in the use of the C_F and Q values reported herein for much larger (or smaller) bellows. Also, C_F data was only obtained with internal water flow. However, we are confident that the C_F values thus obtained can be used for gas flow through this general size bellows <u>if no acoustic resonance occurs</u>.

Probably the greatest potential source of error in calculating flow-induced stress for a given bellows is the value picked for the amplification factor Q from Figure 43. As discussed previously, we have not yet developed what we believed is a satisfactory damping correlation method which includes the effect of all factors illustrated in Figure 42. The data given in Figure 43 is felt to be conservative, or give "high" Q values.

Other sources of error are the occurrence of acoustic resonances in the duct system and non-rigid "end conditions". Acoustical resonances tend to amplify the vortex shedding forces, while non-rigid attached ducts tend to reduce vibration amplitudes because of increased damping.

The sources of error and their potential effect on the calculation procedure are summarized below:

(a) Vortex Force Coefficient C_F - The C_F values given in Figure 36 are conservative in that they represent the upper limit of the experimental data. Our observations show that these C_F values are good for bellows vibrating vigorously so that there is "good coupling" between the vibrating bellows and the vortex shedding. For bellows which do not vibrate vigorously (have low stress values) these C_F values will tend to be high; but this will result in conservative answers.

(b) Dynamic Amplification (Q) Values - The values of Q given in Figure 43 are conservative, or at the upper limit of experimental observations. For a very "stiff" bellows, these values should be quite good, but for a "low spring rate" bellows they will tend to be high but give conservative answers.

(c) Acoustical Resonance (Radial and Helmholtz) - An acoustical resonance of the type discussed in Section II. 10 will tend to make the calculated stress levels <u>very conservative</u>. As a rule of thumb, we suggest that the acoustical resonance may cause a stress amplification of the order of 5.

(d)   Upstream Elbow - The presence of an upstream elbow
        causes excessive flow-induced stresses for a given fluid
        velocity. We don't have much quantitative data on this
        effect but suggest correcting the calculated stresses
        upward by as much as 2.0 to account for the elbow.

(e)   Heat Transfer Effect - A potentially great influence on
        bellows flow-induced stress can be caused by heat transfer
        induced changes of phase or fluid state within the bellows.
        This effect is currently under investigation.

Improved Stress Indicator

In Quarterly Report No. 5 (16) , we developed the preliminary
form of a quick method for estimating the dynamic flow-induced stress
level for a given bellows installation. This method consisted of calculating
a "Stress Indicator" which was a number roughly proportional to stress and
apparently valid for judging the relative severeity of bellows vibrations.
We are still convinced that the "Stress Indicator" approach is useful and
valid. The purpose of this section is to present an "Improved Stress
Indicator" which is based on the "best model" stress calculation procedure
discussed above.

The basic equations which describe flow-induced stress, as given
in Sections II.5 to II.7, are

$$F = C_F \, A_p(1/2 \, \rho V^2) = C_F A_p P_d \tag{34}$$

$$x = \frac{C_m FQ}{KA} \tag{35}$$

and

$$Stress = \frac{C_s Etx}{h^2} \tag{36}$$

The objective of the "Stress Indicator" approach is to combine these
expressions in a simple form so as to give a single expression for stress
which contains only readily-known bellows dimensional data, or parameters,
and flow variables. Therefore, we will assume the following:

(a) A_p can be approximated by

$$A_p \approx \pi D_m h$$

(b) C_F is known from Figure 36

(c) C_m can be approximated by

$$C_m \approx \frac{1}{4N_c}$$

(d) K_A can be approximated by

$$K_A \approx D_m E \, (N_p/N_c) \, (t/h)^3$$

(e)   Q can be found from Figure 43.

(f)   The factor C_s is approximately constant for all bellows.

Based on these assumptions, Equations (34), (35), and (36) may be combined to give

$$\text{Stress} = \pi C_s \left(\frac{C_F Q}{N_p}\right) \left(\frac{h}{t}\right)^2 (1/2 \rho V^2) \tag{37}$$

Since C_s has been assumed constant, we can extract a quantity from Equation (37) which is approximately proportional to flow-induced stress for all bellows; this quantity is

$$\text{Stress Indicator} = \left(\frac{C_F Q}{N_p}\right) \left(\frac{h}{t}\right)^2 (1/2 \rho V^2) = \left(\frac{C_F Q}{N_p}\right) \left(\frac{h}{t}\right)^2 P_d \tag{38}$$

This expression for Stress Indicator is <u>slightly different</u> from that given in Reference (16) and is closer to the real situation. To perform calculations with Equation (38), it is first necessary to find C_F and Q from Figures 36 and 43, respectively.

Bellows Fatigue Life

To supplement the Stress Indicator given in Equation (38), we have prepared a <u>preliminary</u> plot (Figure 48) for predicting bellows fatigue life which gives the number of cycles to failure as a function of Stress Indicator. The actual time to failure can be calculated by dividing the number of cycles by the appropriate modal frequency (see Section II.4, Tables III and IV).
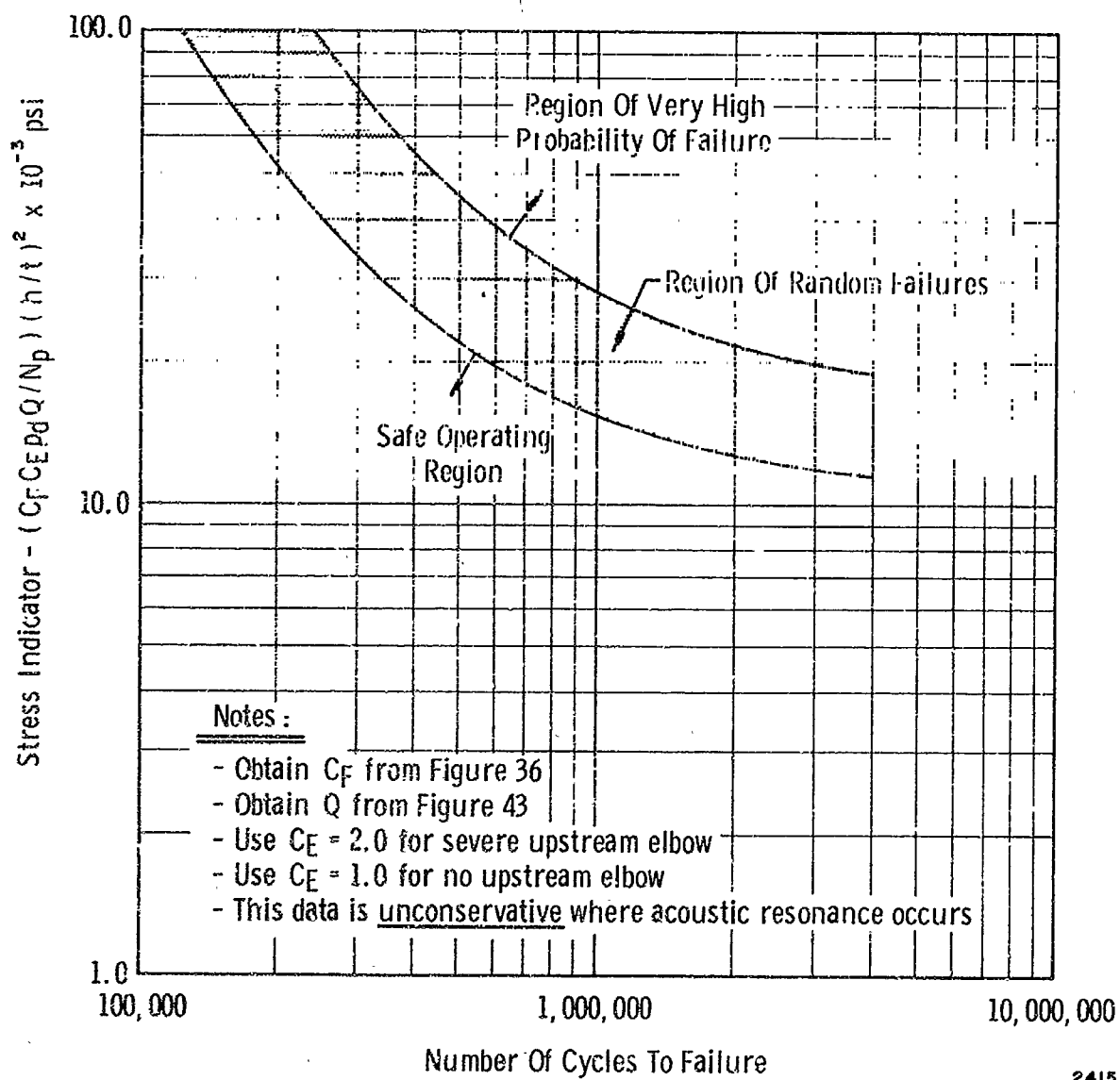
Figure 48. Preliminary Bellows Fatigue Life Data

The data in Figure 48 represents a collection of all failure cases which we have observed in the laboratory, plus some data for the F-1 engine ASI line failures, and for S-IVB J-2 engine LOX feedline bellows (with appropriate accounting of the upstream elbow). This fatigue data must be considered preliminary because of the small number of sample points used in its compilation, but should be good enough, at the very least, to help judge relative severity of various bellows installations.

III. BELLOWS LINER DESIGN AND EXTERNAL DAMPING DEVICES

III.1 Cone Liners for Reduction of Vibrations

A limited study of cone-shaped liners was made with the specific purpose of determining how much of the bellows must be covered by the liner to effectively stop flow-induced vibrations. The liners being considered here are simple, truncated, hollow cones formed from thin sheet metal which are mounted at the entrance of a bellows and extend into the bellows itself. The cone shape allows angular movement of the bellows but also produces a constriction, and a resulting pressure drop, which is discussed in the next section.

An initial aspect of the liner study was to determine the nature of the velocity profiles downstream of the liner; this, it was hoped, would provide some insight into how far the liner should extend into the bellows to prevent vibration. Pitot tube traverses were run downstream of convergent inserts mounted in a 2-inch ID duct to determine the shape of a fluid jet as it emerges from the end of a cone liner. The resultant velocity profiles are shown in Figure 49 where the velocity downstream has been normalized by the velocity at the center of the cone exit.

The influence of the cone angle was not very pronounced, but there was a vena-contracta present with the 30° cone which was not present with the 10° or 20° cones. This was quite noticeable from the Pitot differential pressure which represents the square of velocity. However, the actual center velocity at the vena-contracta was only about 3% greater than at the cone outlet. Comparison of the flow profiles at station #6 with and without the inserts shows that the flow is noticeably affected as far as 5 or 6 outlet diameters away from the insert. This would indicate that a considerable part of a bellows could be left uncovered when a cone-shaped liner is used.

In order to determine the extent to which this information could be applied to an actual situation, two -1/2-inch ID bellows of different convolution geometries (#110 and #112)[*] were flow tested with water using a movable liner that could be positioned at any axial location within the bellows. Since

---

[*] See Appendix A for a list of dimensional data on all test bellows.
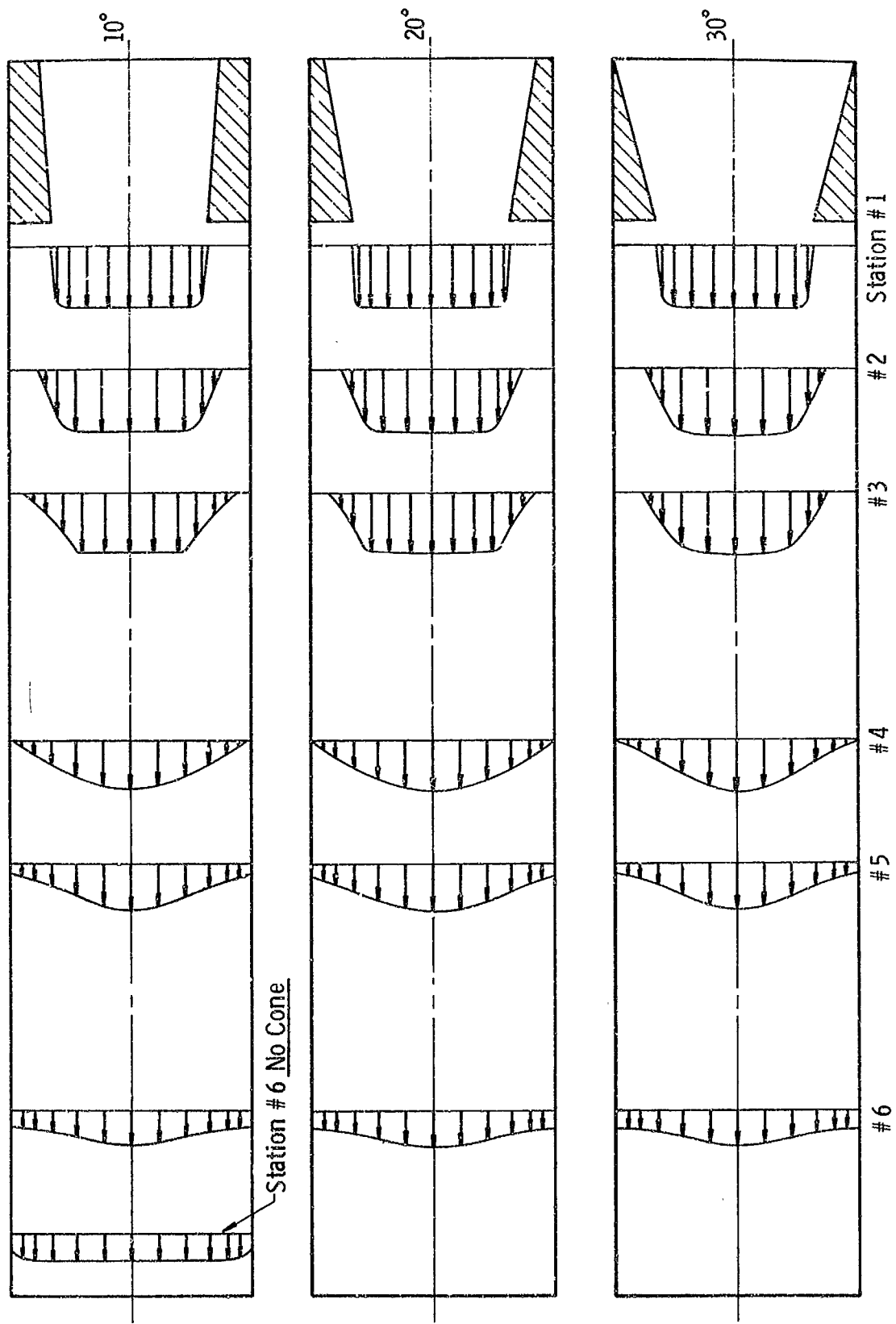
Figure 49. Flow Patterns Downstream Of Cone Shaped Liners

2408

93

the effect of cone angle on the flow pattern was rather small, only one liner configuration was tested. The liner had an outlet diameter of 1-1/4", a length of 11/16", and a 10° included angle. The fluid velocity was varied from 0 to 70 ft/sec based on bellows diameter and maximum dynamic strain was recorded for several liner positions. The results are shown in Figure 50.

Even with the liner completely withdrawn from the bellows, the strain level was reduced from that of an unlined bellows; this result is in agreement with the velocity profile observations. However, all modal vibrations were not stopped until the liner covered all but one or two convolution roots. The modes which were present did not occur in order. In some cases the first mode was present at two different flow rates while the second mode was completely absent over the entire flow range.

Operating the bellows at an angle did not significantly affect the dynamic strain readings for these particular bellows-liner arrangements. There probably are cases where the effects of angulation are significant.

The effectiveness of a cone liner or the effect of angulation would be difficult to predict analytically due to the highly turbulent expansion which takes place at the liner exit. The tests which have been performed can serve as a guide, but more testing of different types of bellows is required before reliable empirical design is possible. At this time, however, we offer the following design guidelines:

(1)   If the bellows failure problem without a liner is severe, then the liner should cover most if not all of the active convolutions. If pressure loss is a problem, the liner might be reduced in length somewhat, possibly allowing some bellows vibration. Testing should be performed to verify the design; preferably, a "before and after" test should be conducted with one or more bellows.

(2)   If the bellows vibrations are not too severe without the liner, then a very short liner extending over, say, about one-fourth of the convoluted length should offer substantial reduction in vibration levels. Again, the design should be verified with testing.

(3)   On any liner design, an important consideration is weight which means the liner thickness, as well as length, should be minimized. Any proposed design should be subjected to a buckling analysis to assure that it will not collapse as a

94
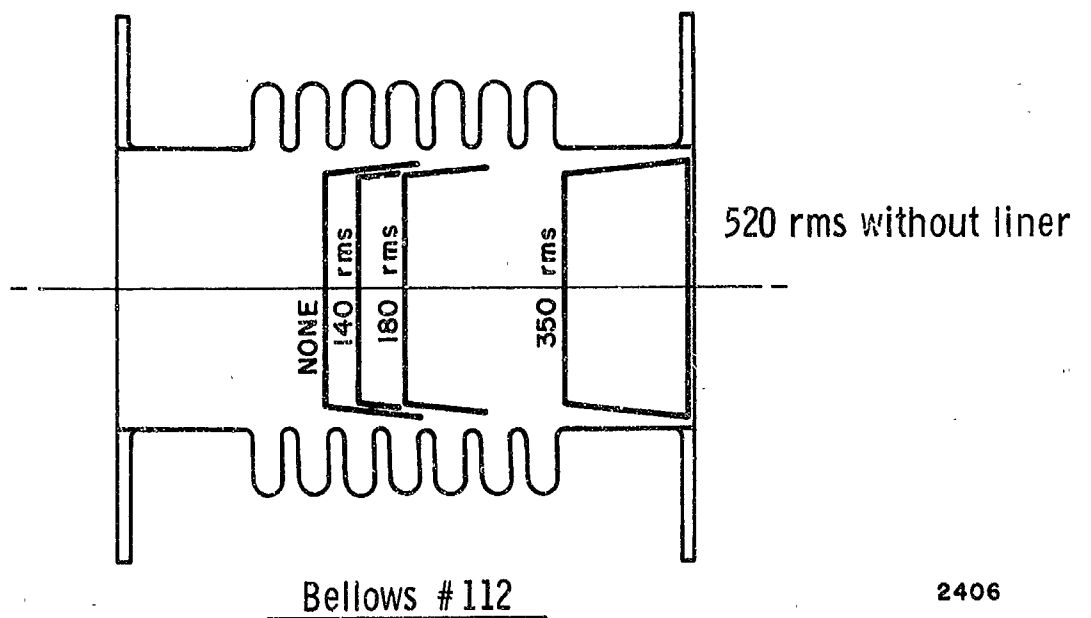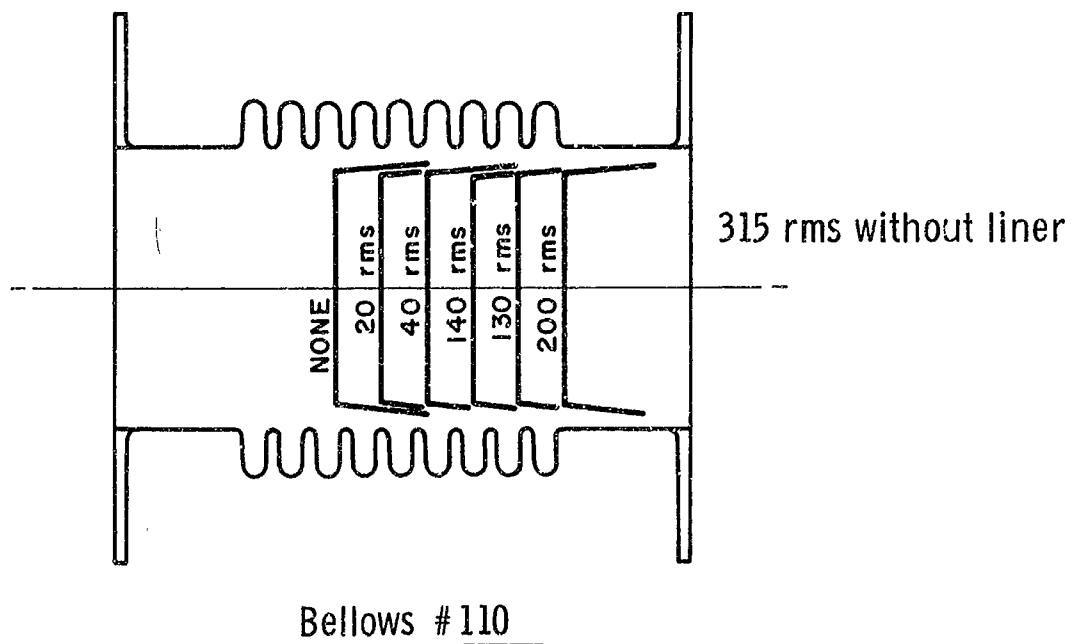
Figure 50. Maximum Dynamic Strain For Fluid Velocities From
0 – 70 ft/sec (Water – 75°F)

95

result of the differential pressure. Also, the designer should be aware of potential "splitting" problems caused by turbulent flow excitation of tne liner. High dynamic pressure situations should be approached with care.

III.2 Pressure Loss of Cone Liners

An important point for consideration in regard to a proposed liner design is that the pressure loss be acceptable. It has been demonstrated that a liner can, in fact, increase the pressure drop compared with the bare bellows. The purpose of the following discussion is to demonstrate a simple procedure for estimating liner pressure drop characteristics.

Usually, a typical liner can be considered, from a fluid mechanics point of view, to consist of a contracting section followed by an expansion or, in some cases, an expansion followed by a contraction or, possibly even a series of expansions and contractions depending on the specific configuration. Assuming this to be true, then using information available in the literature for losses resulting from expansions and contractions, the liner overall pressure loss can be estimated. Figure 51 gives all of the information needed for estimating these losses. Note that for either a contraction or expansion, the pressure drop is characterized by
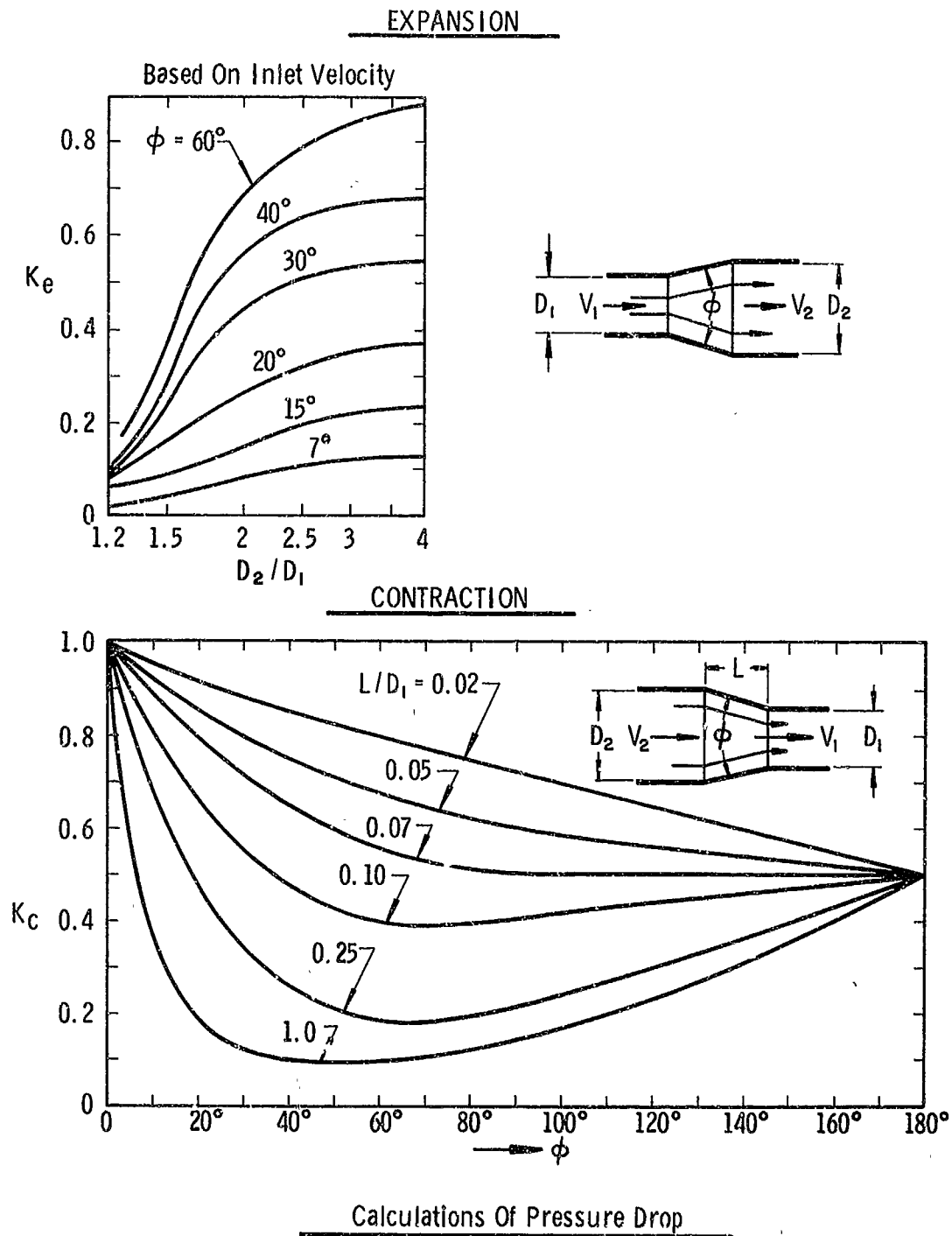
$$\Delta p = \frac{K\rho}{2} \; V_1^2 \left[1 - (D_1/D_2)^2 \right]^2$$

$$= \frac{K\rho}{2} \; V_2^2 \left[(D_2/D_1)^2 - 1 \right]^2$$

where K is a loss factor defined in terms of the geometry of the duct as shown in Figure 51.

This prediction procedure has been checked experimentally for the liner illustrated in Figure 52 which is a conical configuration typical of a currently used design.

For a zero deflection angle, the pressure loss for this case will be the collective result of, first, the contraction in the cone section and, second, the uncontrolled expansion when the fluid exits the cone. The pressure drop will therefore be given by

$$\Delta p = \frac{\rho}{2} \; (K_c + K_E) \left[(D_2/D_1)^2 - 1 \right]^2 \; V_2^2$$

96

Based On Inlet Velocity

CONTRACTION

Calculations Of Pressure Drop

For Either Contractions Or Expansions, The Pressure Drop Is

$$\Delta p = \frac{K\rho}{2}V_1^2 \left[1-(D_1/D_2)^2\right]^2 = \frac{K\rho}{2}V_2^2 \left[(D_2/D_1)^2 -1\right]^2$$

1865
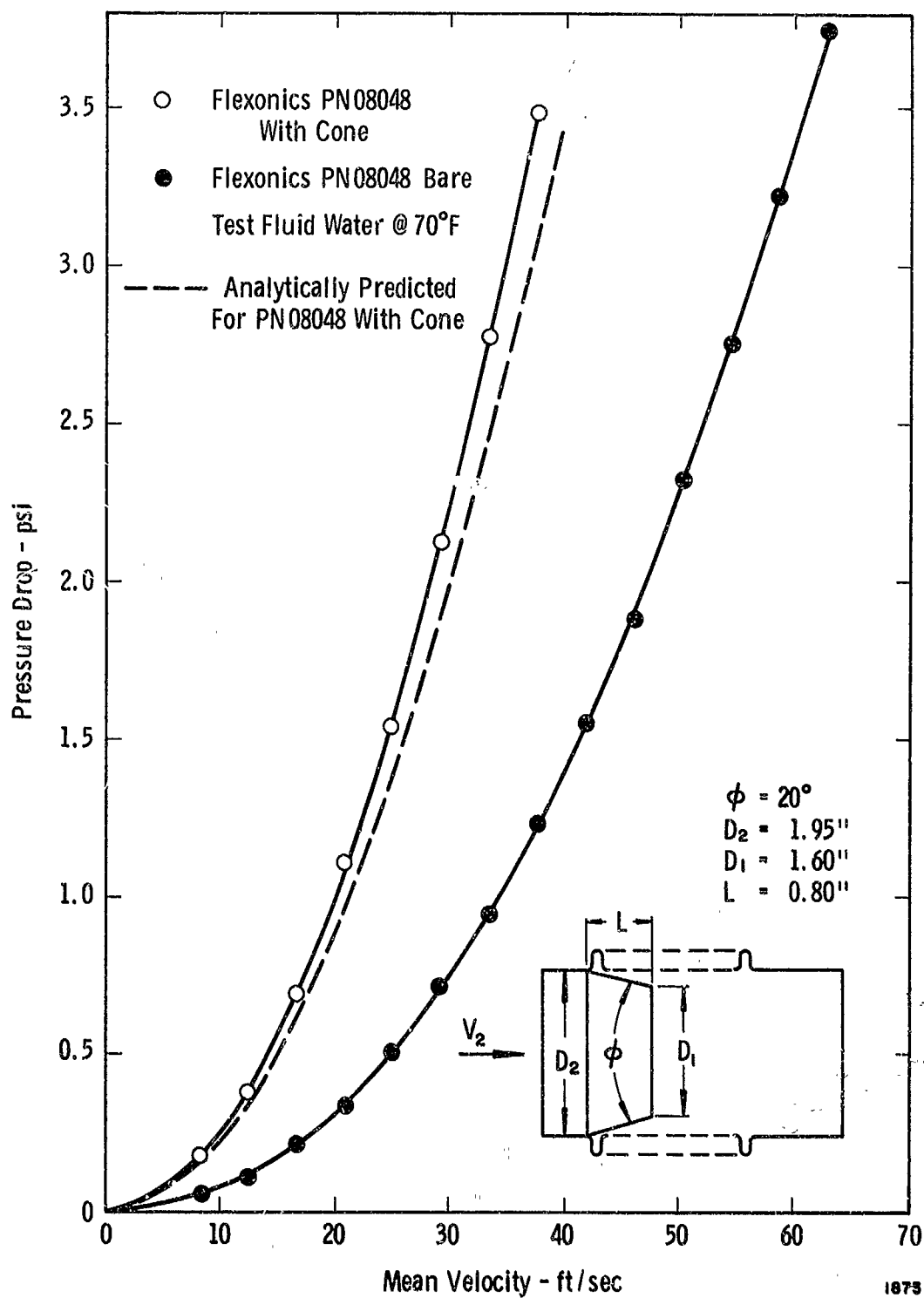
Figure 51. Flow Loss Factors For Contractions And Expansions

Figure 52. Comparison Of Pressure Loss For Bare Bellows And Bellows With Cone Liner

From Figure 51, the value of K_c for this cone geometry is about 0.35. The value of K_E for an uncontrolled expansion is 1.0, thus

$$\Delta p = \frac{\rho}{2} (1.35) [(1.22)^2-1]^2 V_2^2 = (0.324) (1/2 \rho V_2^2)$$

Figure 52 shows pressure drop as a function of mean flow velocity predicted by the above equation, and also the pressure drop obtained experimentally for this same conical liner configuration. Figure 52 also shows the experimentally obtained pressure loss for the bare bellows (no liner) used for the tests. In this case, the liner is responsible for an increase in pressure loss.

III.3   External Damping Devices

One possible means of reducing the stresses in a bellows resulting from internal flow is to add damping to the bellows structure. The attractive feature of this method of reducing stress is that it allows the designer to possibly "fix" a bellows which has demonstrated some fatigue tendencies, but is otherwise satisfactory. Our work to date in this area has been strictly exploratory; several external damping ideas have been tried with two basic objectives, (1) to find out in a quantitative fashion how much the damping can be increased under ideal conditions, and (2) to compare the relative increase in damping for several devices or ideas. Three types of external damping ideas have been tried thus far; these are:

(1)   Filling the convolutions with some damping material, usually a viscoelastic material, such as RTV rubber, 3M strip-caulk (a putty-like material), and a polystyrene foam.

(2)   Placing a metal spring or rubber "O" ring in each convolution.

(3)   Wrapping the exterior of the bellows with screen wire.

Figure 53 shows a photograph of several bellows with various external damping devices added. Flow tests have been run on several of these "damped" bellows to explore very briefly their possibilities. Figures 54 and 55 show some of the test results. In Figure 54, a comparison is shown between an undamped bellows and the same bellows with two types of dampers; the external screen and the neoprene "O" rings. In general,
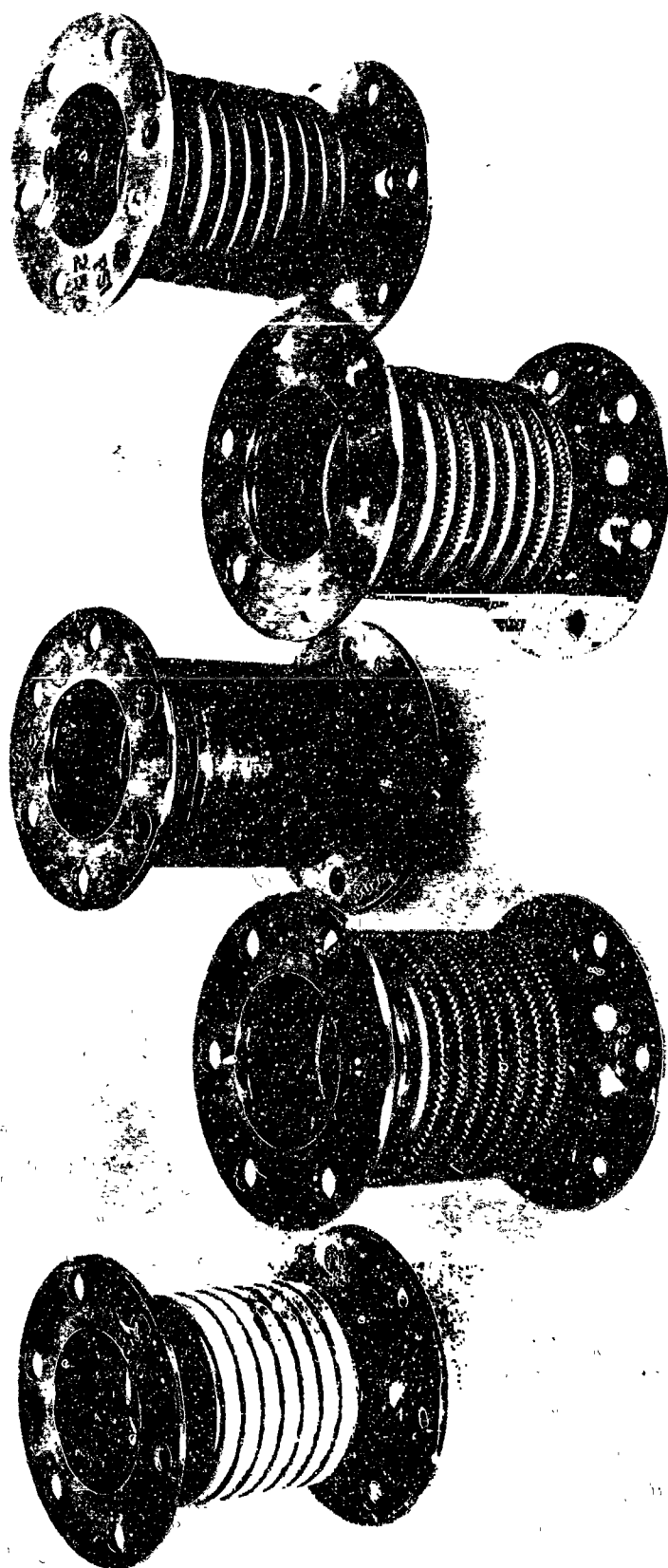
C-31459

Figure 53. Photographs Of Several Bellows With Various External Damping Devices
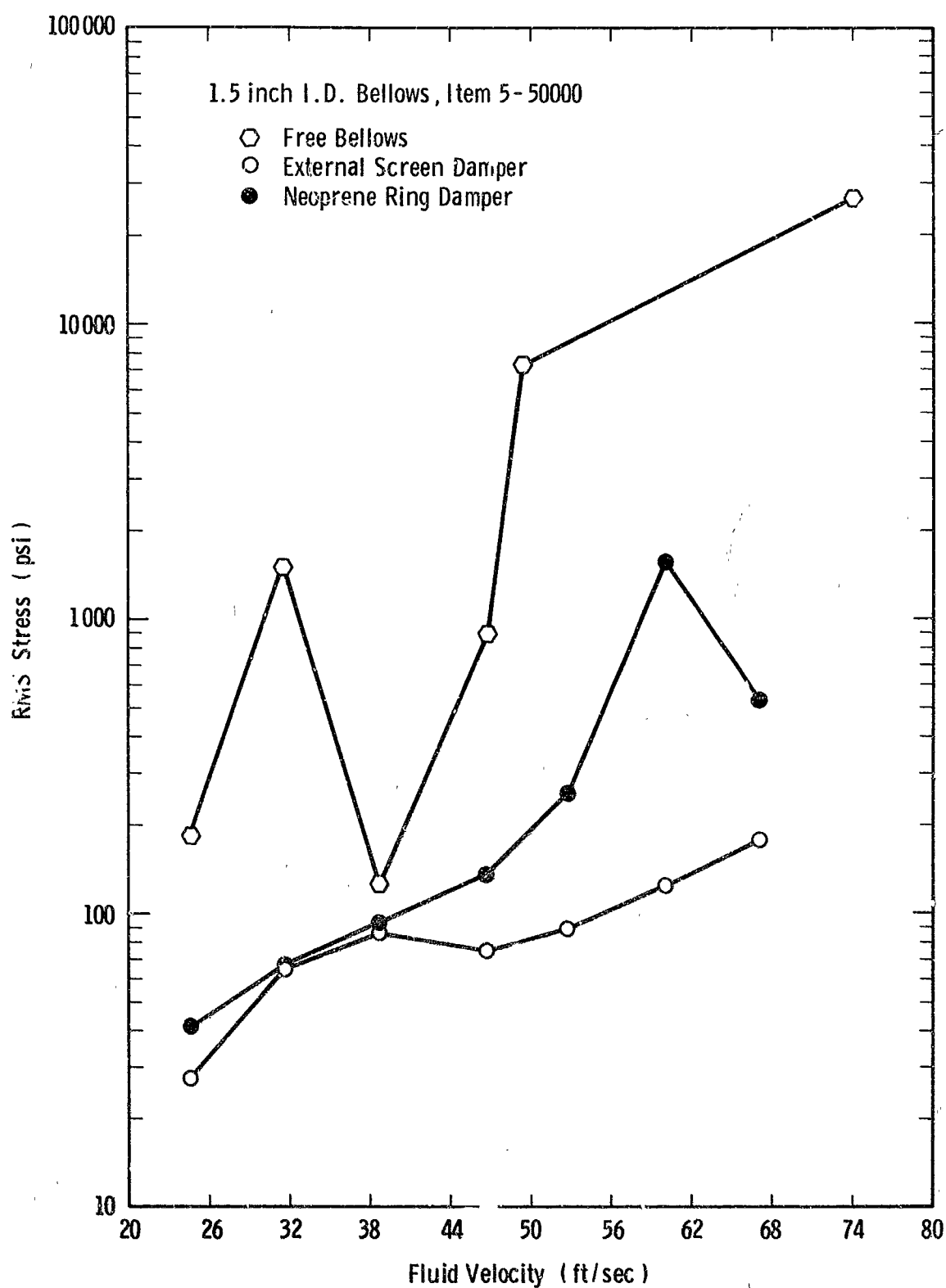
100

Figure 54. Comparison Of External Screen And Neoprene Ring Dampers
With Free Undamped Bellows

both devices provided considerable damping; however, the "O" ring dampers allowed some resonance effect at about 60 ft/sec flow velocity, whereas the external screen did not. Figure 55 shows a comparison of an undamped bellows and two others with damping devices; one of the damped bellows had 3M strip-caulk packed in the convolutions and the other had coil springs wound around the outside of each convolution. The two damped bellows exhibited about the same vibration character- istics, as may be seen from Figure 55, and both reduced the vibration level by a considerable amount (about 2 orders of magnitude near the resonant points).

In general, we believe that these exploratory tests have demon- strated that it is, indeed, possible to add considerable damping to a bellows by use of some external device. A word of caution must be added here, however, because our tests were only conducted on free bellows and for conditions where the first few modes could be excited. For a flexible hose or the higher modes of a free bellows, it is not known what kind of device will be required. Of course, some of the devices which were tried would obviously not work for a flexible hose.

Another point which the reader will undoubtedly note is that some of the damping devices which were tried are absolutely not practical for one reason or another; for example, the external screen, as shown, would not allow a free bellows to flex; a variation of this idea will, how- ever. Also, neoprene, the strip-caulk, and the polystyrene foam will not work at cryogenic temperatures. As mentioned previously, one objective of these tests was to find out how much damping can be intro- duced under ideal conditions, and this is why some impractical devices were tried. The important point of the results is that considerable damping can be added; the problem now is to discover practical devices.

III.4   Summary of Bellows Vibration Suppression

We have demonstrated in this chapter that both cone liners and external damping devices are effective in suppressing bellows flow- induced vibrations. Both types of devices have been used in the past by bellows manufacturers for this very purpose. Some points are important to reemphasize about the use of these devices:

(1)   Cone liners can cause a significant increase in the pressure drop across the bellows.

(2)   Cone liners can experience both buckling failures, because of the large differential pressure, and fatigue failures because of turbulence-induced vibrations.
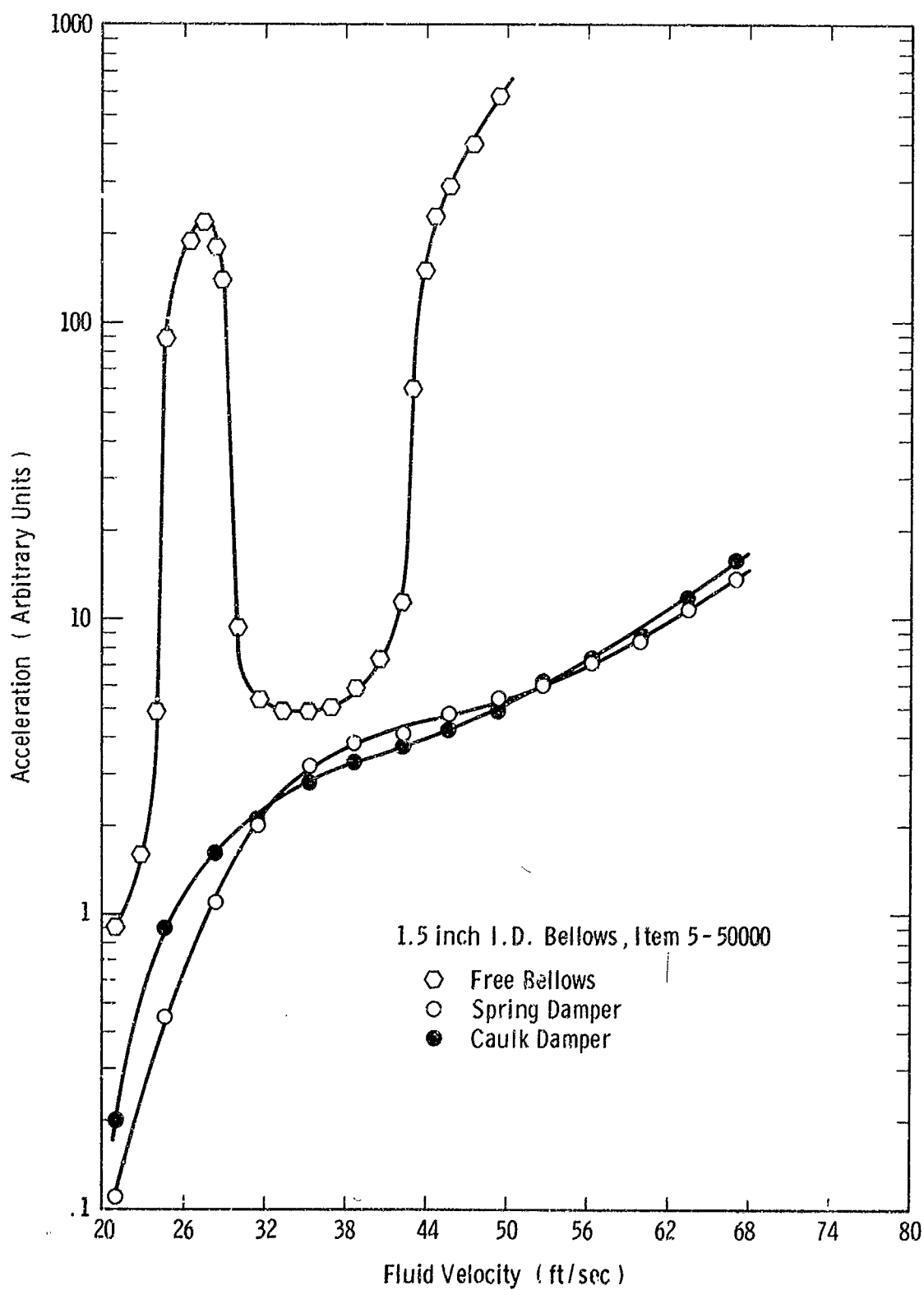
Figure 55. Comparison Of External Spring And Caulk Dampers
With Free Undamped Bellows

(3)   External damping devices can be as effective as a cone liner without causing an increase in pressure loss.

(4)   Care must be exercised in the application of external damping devices to ensure that the damping is actually increased.

IV. BELLOWS AND ELBOW PRESSURE LOSS

IV.1 Description of Pressure Loss Mechanism

As described in Section II.3, the general behavior of the fluid through a bellows involves a generation of vortices in the convolutions. In the absence of vibrations, the vortex motion inside each convolute is steady as was shown in Figure 6. With flow-induced vibrations, toroidal vortices are periodically shed out of the bellows convolutes as shown in Figure 9.

Regardless of whether or not there is flow-induced vibration, the generation of vortices in the convolutes causes an extraordinarily high steady flow pressure loss compared with an equivalent length of smooth tubing. Figure 56 shows a typical plot of the friction factor f as compared with friction factors for flow through tubes. Recall that the friction factor is proportional to the pressure drop in a one-diameter length of tubing (or bellows), and is related to the pressure loss and fluid conditions by the equation

$$\Delta p = (fL/D)(1/2 \; \rho V^2)$$

Note from Figure 56 that the bellows friction factor increases drastically as the Reynolds number is increased over the range from about 10^4 to 10^6. This trend is contradictory to the observed behavior of the friction factor for turbulent flow in a pipe, which shows that f decreases as Reynolds number increases. It is our present belief that the cause for this peculiar behavior can be explained by the presence of the vortices in the convolutes, and the fact that these vortices will transition from a laminar to a turbulent condition at a higher Reynolds number than does the main stream flow. We are planning to explore this idea with a simple analysis in the near future.

IV.2 Compiled Bellows Pressure Loss Data and Some Test Results

All pressure loss data for bellows and flex hose which was available in the open literature, or from unrestricted company reports, has been compiled; this data was presented in Quarterly Report No. 1 (Reference 14). This compiled data included two different correlation methods giving the friction factor f in terms of bellows geometry and Reynolds number; these two correlation methods are illustrated in Figures 57 and 58. Each of these correlations gives f, as a function of Reynolds number, in terms of a one-parameter family of curves. The parameter used in the Daniels
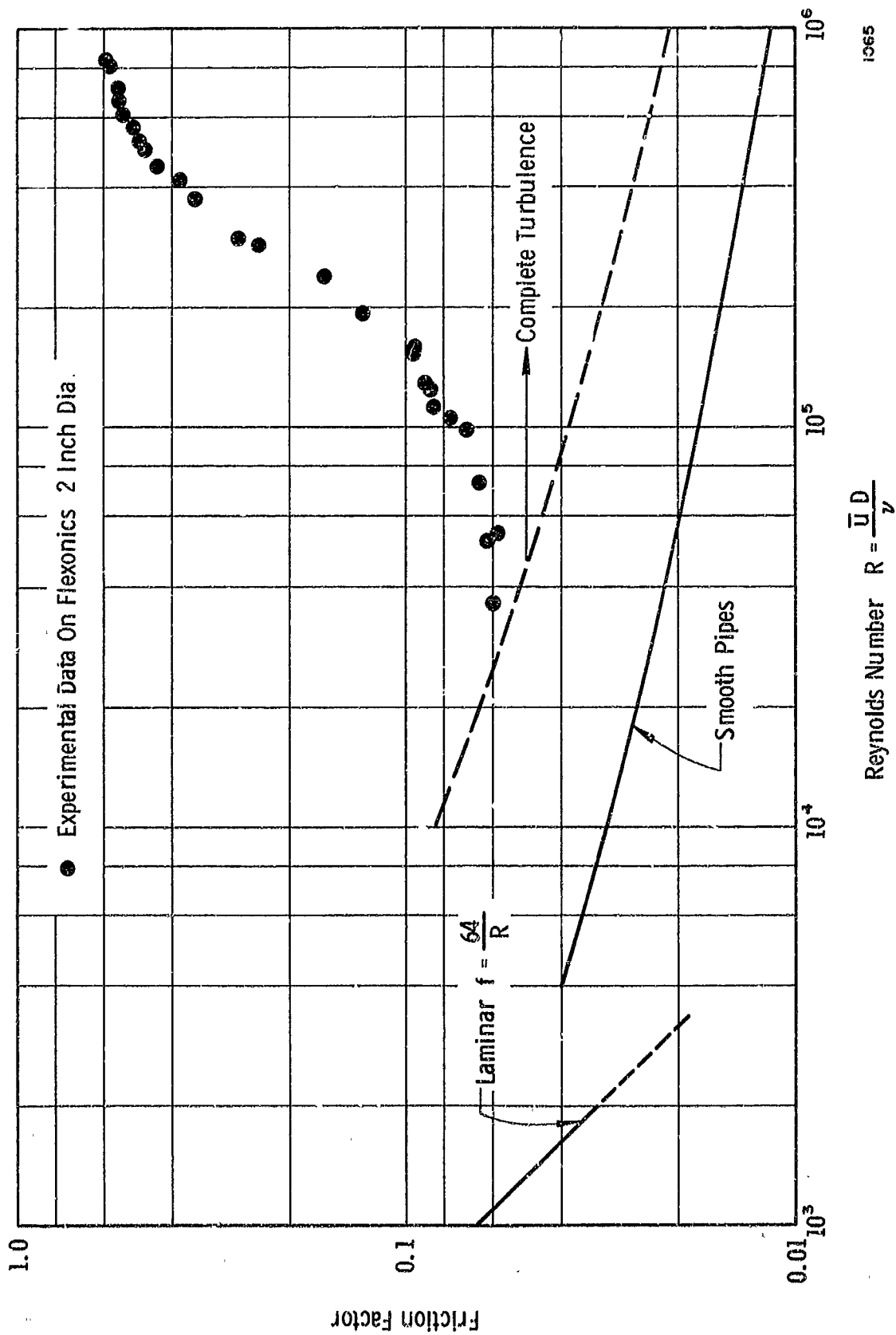
Figure 56. Comparison Of Friction Factors For Smooth Pipes And Flexible Hose

106

Method for Predicting Frictional Loss in Metal Bellows and Flexible Hose

h = Average height of convolution in inches

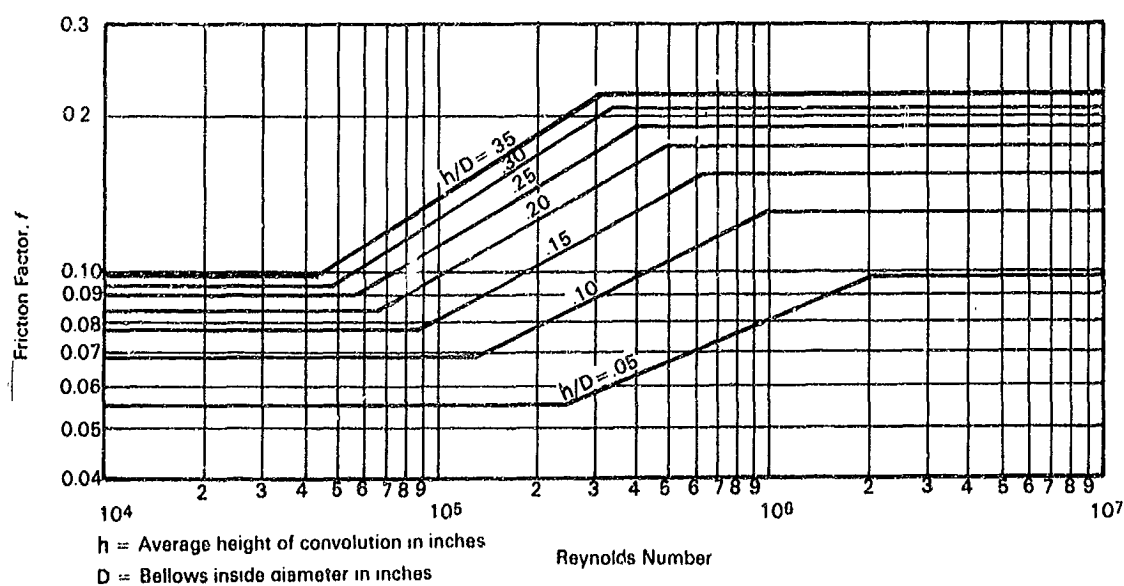D = Bellows inside diameter in inches

Reynolds Number

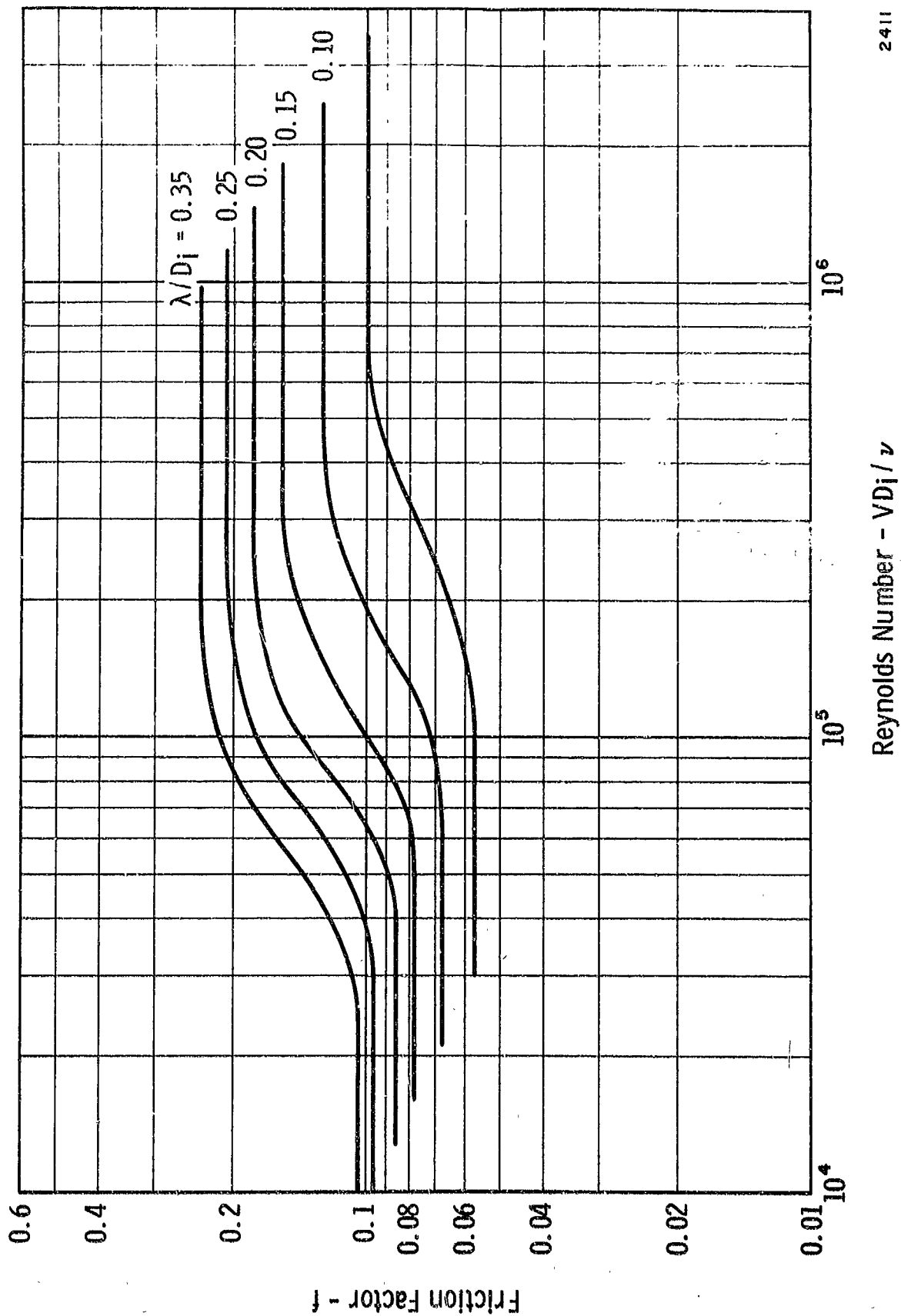Figure 57. Bellows Friction Factor Correlation From Reference [12]

Figure 58. Bellow Friction Factor Correlation From Reference [13]

2411

and Cleveland correlation (Figure 57 and Reference 12) is the ratio of convolute height to bellows internal diameter. The parameter used in the Riley correlation (Figure 58 and Reference 13) is the ratio of convolute pitch to internal diameter. Both correlations can only be valid at the same time for a series of bellows having convolutions with exactly similar geometry; i.e., the ratio of convolute height to pitch, etc., remains constant for all bellows of the series. Therefore, one or both cannot be completely valid for all bellows, in general.

To get a better insight into bellows pressure loss as a function of geometry, and to attempt to clear up the discrepancy of correlation methods noted above, a series of experiments were conducted with some selected bellows, and with a special convoluted test model. The special test model, described in Quarterly Report No. 2 (Reference 15), had provision for changing the convolution geometry so that the effect of geometry on pressure loss could be determined in a controlled manner. Figure 59 shows some pressure drop data obtained with this model. Figure 60 shows friction factor data reduced from the pressure drop data of Figure 59. All of the data in Figures 59 and 60, except one case, were for simulated convolutions with identical depths (or heights). Comparison of the data for this condition (curves 1, 2, 3 and 4) show a distinct variation in the friction factor. This data tends to invalidate the correlation given in Figure 57 since it shows a variation in f for constant values of h/D_i (the ratio of convolute depth to internal diameter). Similarly, a comparison of curves 1 and 2 in Figure 60 shows some variation in f for bellows having the same value of λ/D_i (the ratio of pitch to internal diameter). This tends to invalidate the correlation given in Figure 58. Thus, we can conclude that neither of the correlations given in Figures 57 and 58 is entirely or generally valid. Further detailed evaluation of these two correlation methods has been performed by comparison with more of our experimental data and that of other investigators. We have concluded that:

(1)   The friction factor f is almost entirely independent of h/D_i (the ratio of convolute height to internal diameter); therefore, the correlation given by Daniels and Cleveland (Figure 57 and Reference 12) has no meaning for bellows of general geometry and is invalid.

(2)   The correlation given by Riley (Figure 58 and Reference 13) is roughly valid for all bellows. However, the Riley-type correlation could be improved by making it a three-parameter correlation, with the three parameters being λ/D_i, λ/σ and the fluid density.

109

Dimensional Data

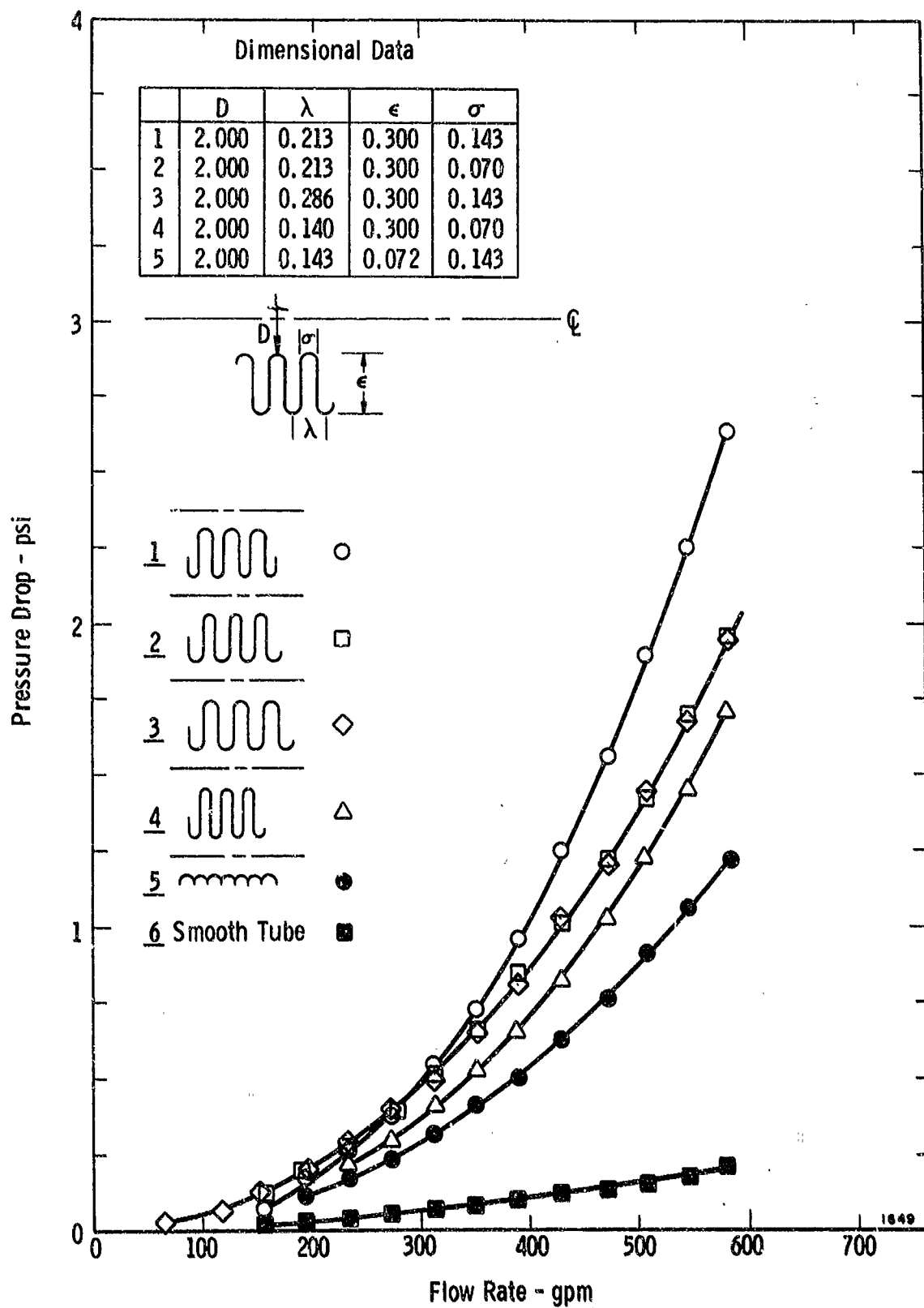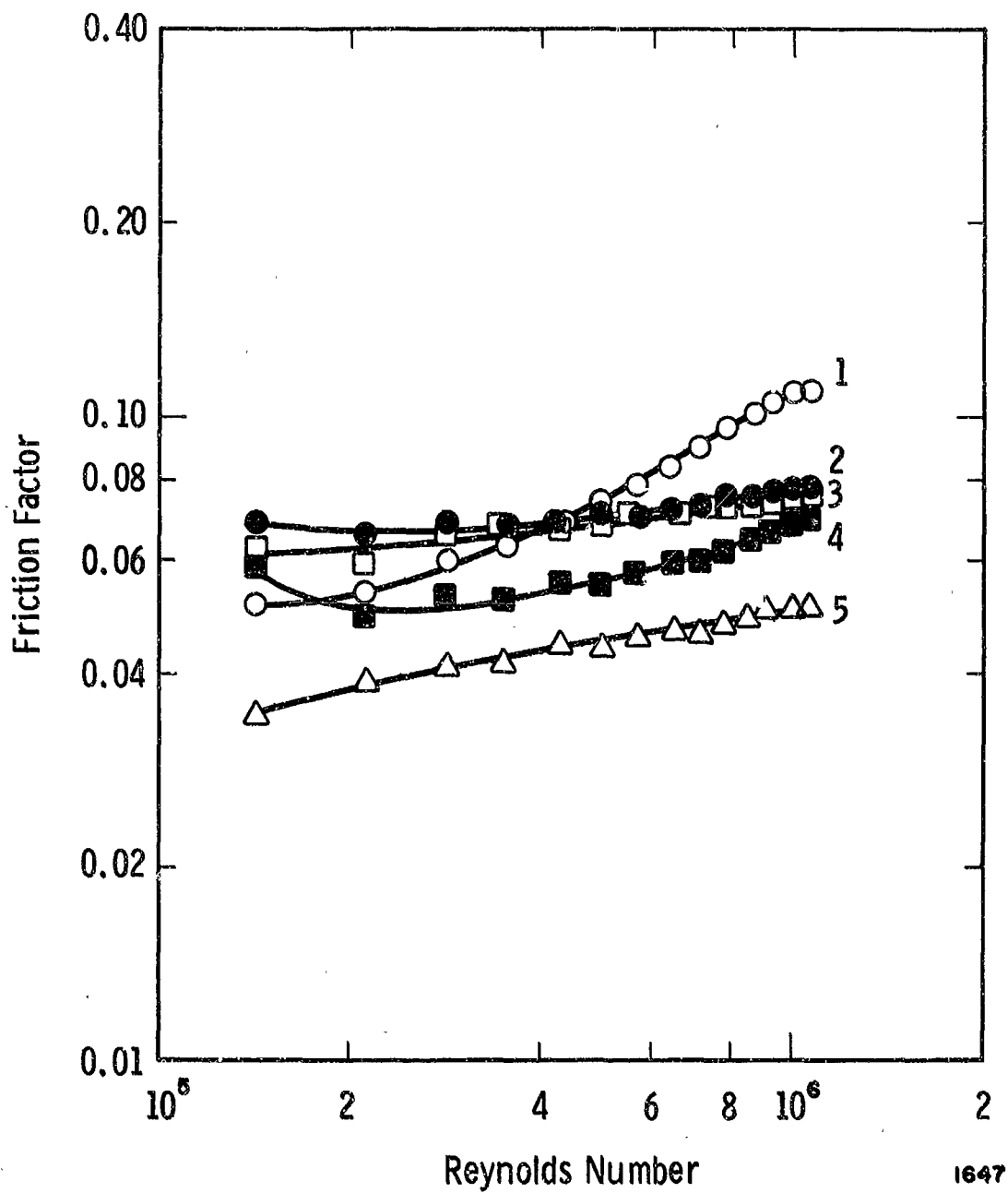|	D	λ	ε	σ
1	2.000	0.213	0.300	0.143
2	2.000	0.213	0.300	0.070
3	2.000	0.286	0.300	0.143
4	2.000	0.140	0.300	0.070
5	2.000	0.143	0.072	0.143

Figure 59. Pressure Drop As A Function Of Flow Rate
For Five Bellows Test Geometries

Figure 60. Friction Factor For Data From Figure 4
For The Five Test Geometries

We recommend that the Riley correlation be used for pressure loss estimate purposes with the user aware of the fact that this method generally overpredicts pressure loss for liquids and underpredicts for gases. Also, the Riley correlation tends to overpredict for bellows with "open" convolution designs ($\lambda/\sigma > 2.0$), and underpredicts for bellows with "closed" convolution designs ($\lambda/\sigma < 2.0$).

In very general and rough terms, the trends of "good" and "bad" convolutions configurations are illustrated in Figure 61. It is interesting to note that the "bad" designs correspond to those geometries which exhibit the more severe flow-induced vibration tendencies.

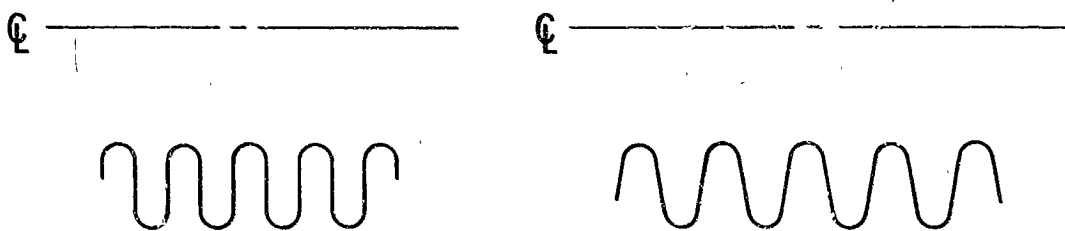## IV.3 Low Pressure Loss Bellows Configurations

As discussed in Chapter III, a conical liner can be effective in suppressing flow-induced vibrations but can lead to a significant increase in the pressure loss if the required contraction is too great. For bellows not required to angulate, a cone liner can reduce the pressure loss if it is properly designed. Therefore, new ways were sought to reduce losses which might be useful for bellows required to angulate.

Several specific configurations have been tested. A sketch of one configuration is shown in Figure 62. This design employs a rigid skirt, but not one of conventional design. Rather than neck down the skirt or liner section, the convoluted section is made slightly larger (on the order of 10%) and the skirt is kept the same diameter as the duct. The ratio of skirt diameter to bellows diameter is, of course, dictated by angulation requirements. Just downstream of the bellows a converging section guides the fluid into the downstream duct. Figure 63 shows pressure loss as a function of flow rate for this new design as well as for a conventional skirt design, and unskirted bellows and a smooth wall section of tubing. Notice that the conventional cone liner model coupling has roughly twice the pressure drop of the unskirted bellows while the new configuration had about one-half the pressure loss of the bare bellows.

Another type of liner which appears to have merit is a screen or wire cloth liner. Because of its flexibility, a cylinder of wire cloth can be fitted directly against the inside of the bellows, allowing some angulation. One test has been performed with this type of liner and the results are shown in Figure 8. Note that a small increase in pressure loss was realized over a bare bellows. It is anticipated that use of a finer mesh wire cloth
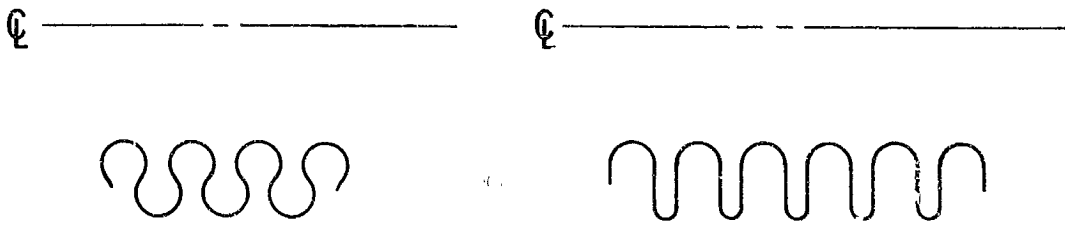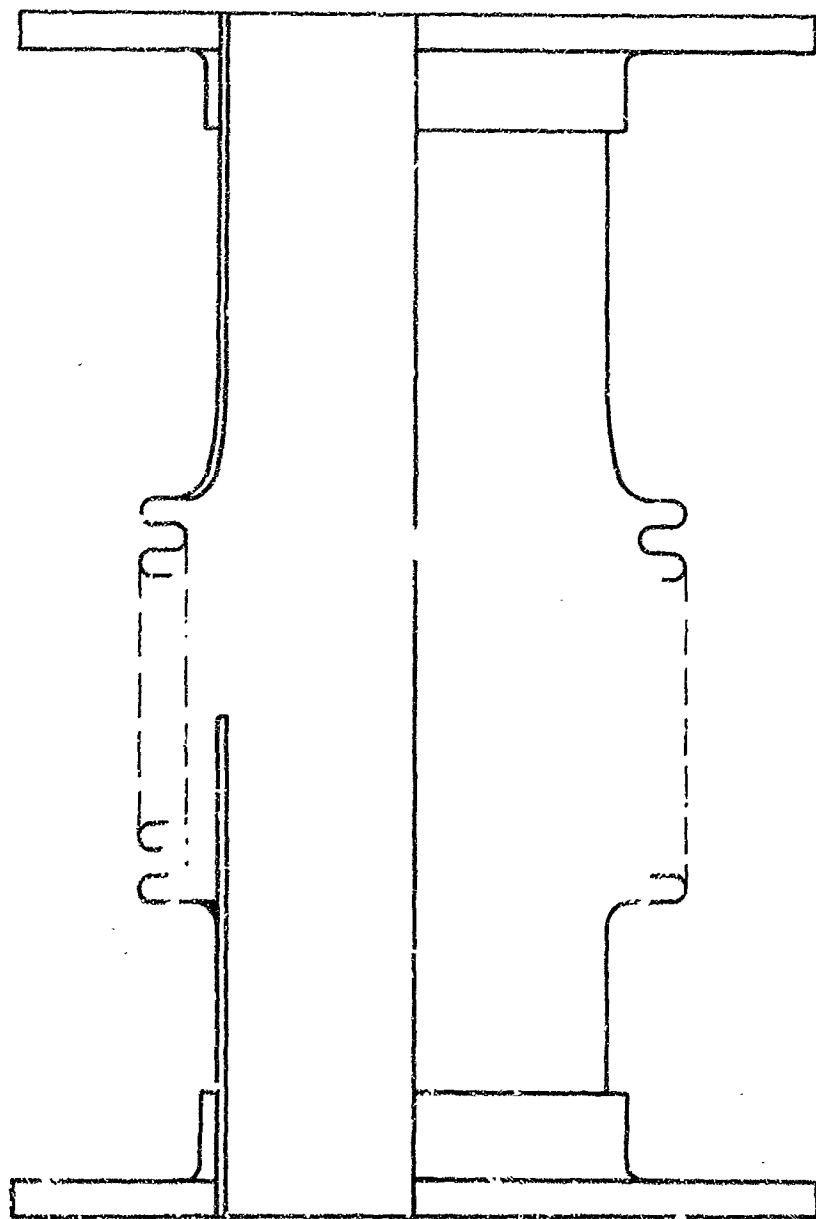
(a) Unfavorable Geometries (Large Losses)

(b) Favorable Geometries (Small Losses)

1654

Figure 51. Sketch Of Bellows Convolutions Giving Unfavorable And
Favorable Pressure Loss Characteristics

113

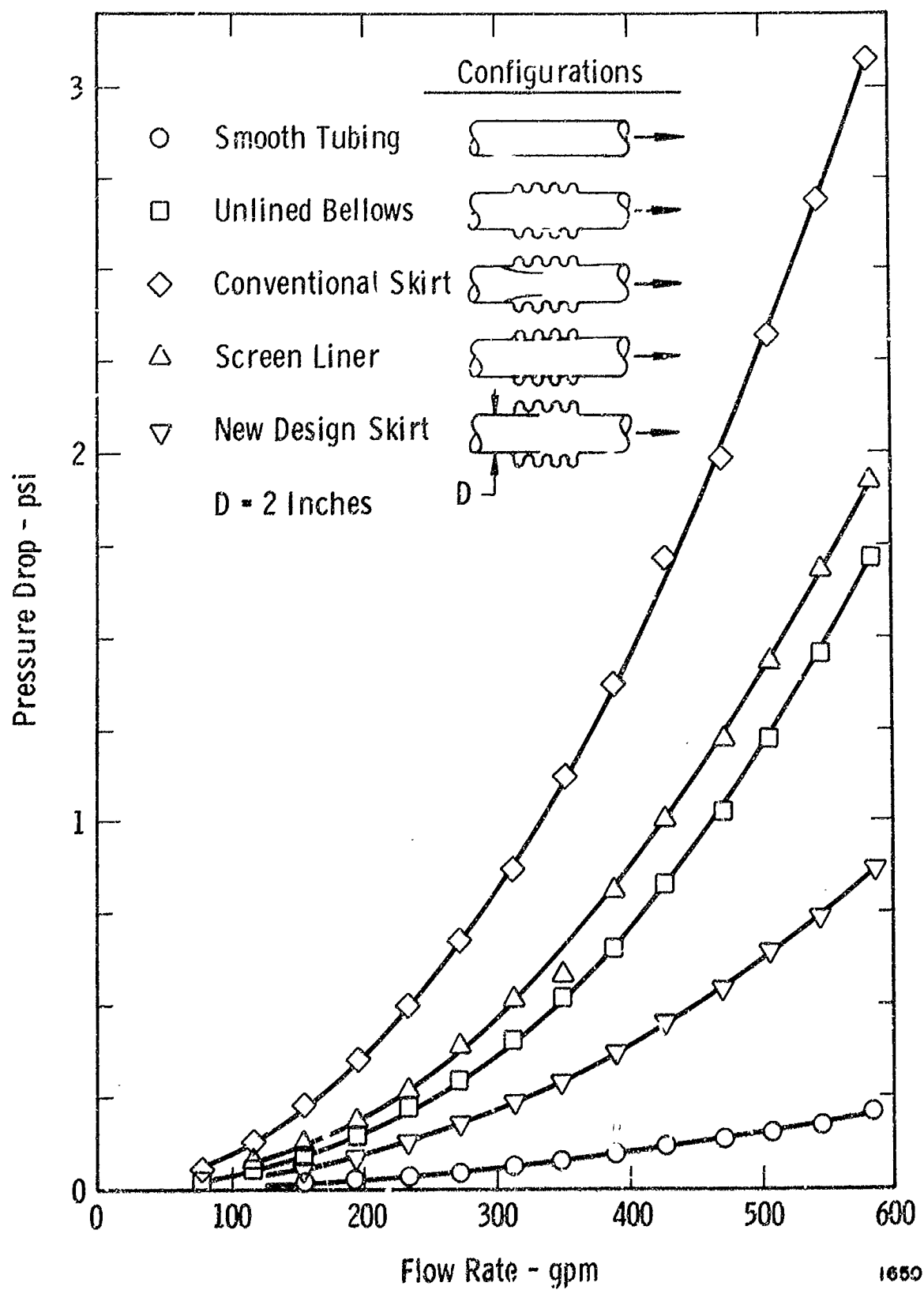Figure 62. Low Pressure Drop Coupling Design #1

1648

114

Figure 63. Pressure Loss Comparison Of Several Skirted
Bellows Configurations

than used in this first test will result in an actual pressure loss reduction. Possibly of most value, however, is the fact that this type of liner suppresses flow-induced vibrations; this fact has been verified by testing. Although we experienced no problems in the laboratory, the reader will likely realize that there are potential problems with a wire cloth liner, should it break loose and be carried downstream in the duct system. Attempts to use this concept should be thoroughly verified with testing.

Two other types of liners were tried, also; a longitudinal wire screen leaf type, and a spiral wound type using either wire screen or metal shim for the liner material. Figures 64 and 65 show examples of the two types. In general, all liners suppressed flow induced bellows vibrations. For example, peak flow induced dynamic stress over the test flow range, in coupling PN 08046 was less than 150 psi with a longitudinal leaf screen liner compared with about 10,000 psi with no liner.

The pressure loss characteristics of the various liner types were quite different. The spiral wound metal shim liner (Figure 66) exhibited the best pressure loss characteristics but still needs some development work. The problem with the spiral wound metal shim liner was that for large bend angles the winding tended to be displaced too far axially, causing separation between adjacent windings. If this problem can be cured, this type of liner has good possibilities. The spiral wound screen liner (test ta not shown) had higher pressure loss than the metal shim liner. Figure 67 shows test results for the longitudinal leaf screen liner. In general, the pressure loss characteristics at high flow rate are better than the unlined bellows for the straight bellows case. For large bend angles, however, the longitudinal leaf screen liner had slightly higher pressure loss than the unlined bellows at the same angle.

IV.4   Low Pressure Loss Duct Bend

Introduction

Duct elbows are known to have a large pressure loss relative to the normal friction loss in straight duct sections. The reason for these large losses can be attributed to secondary flows caused by centrifugal forces and centrifugal force gradients acting on the fluid particles in the bend.

Two experimental elbows have been constructed and tested in order to evaluate a new method of reducing pressure losses and improving velocity profiles in bends. Both elbows were built with square entrance and exit sections to simplify construction, and were identical in every
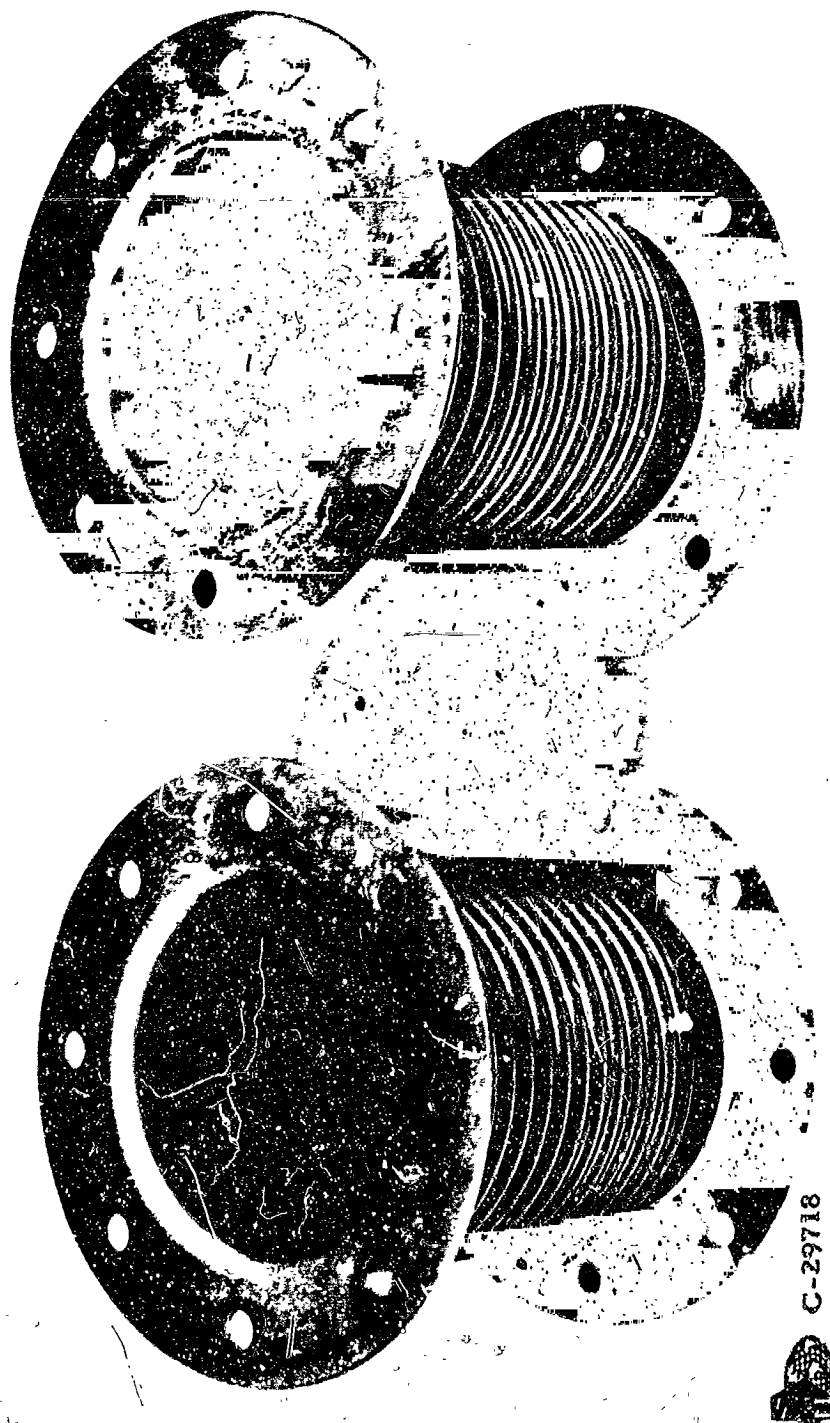
116

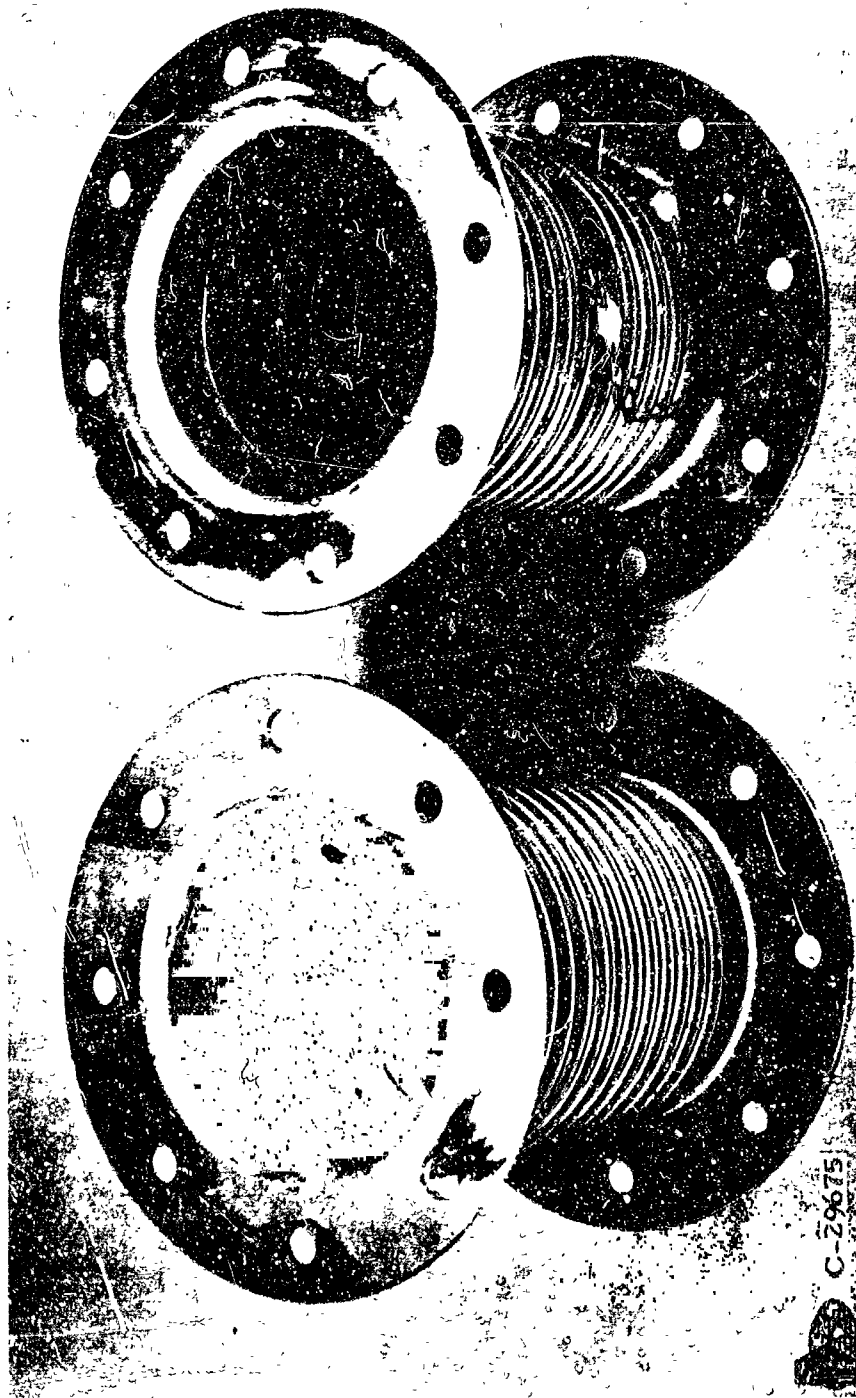FIGURE 64   LONGITUDINAL LEAF SCREEN LINERS

C-29718

Figure 65. Spiral-Wound Liners (Metal Shim On Left - Screen On Right)
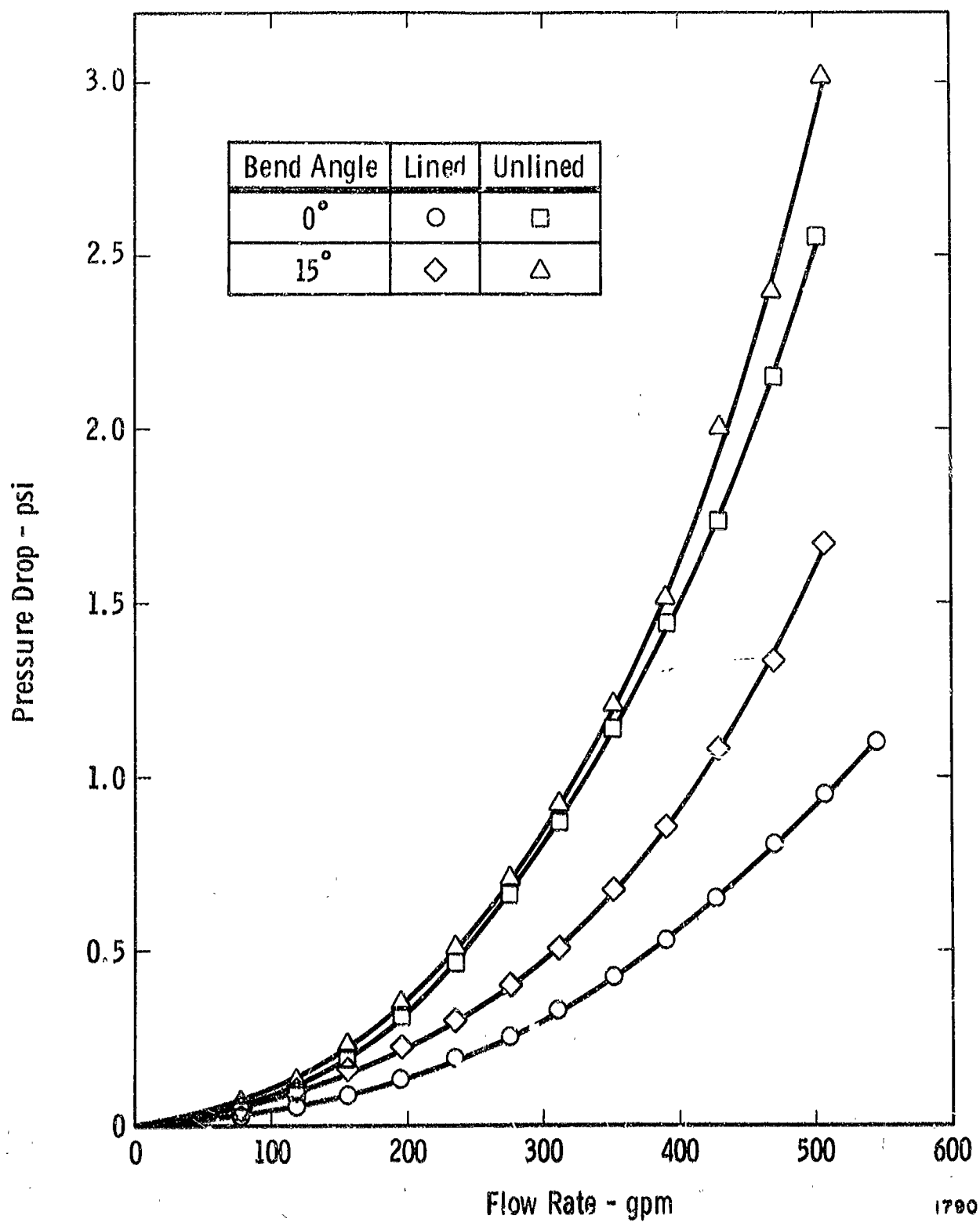
C-29675

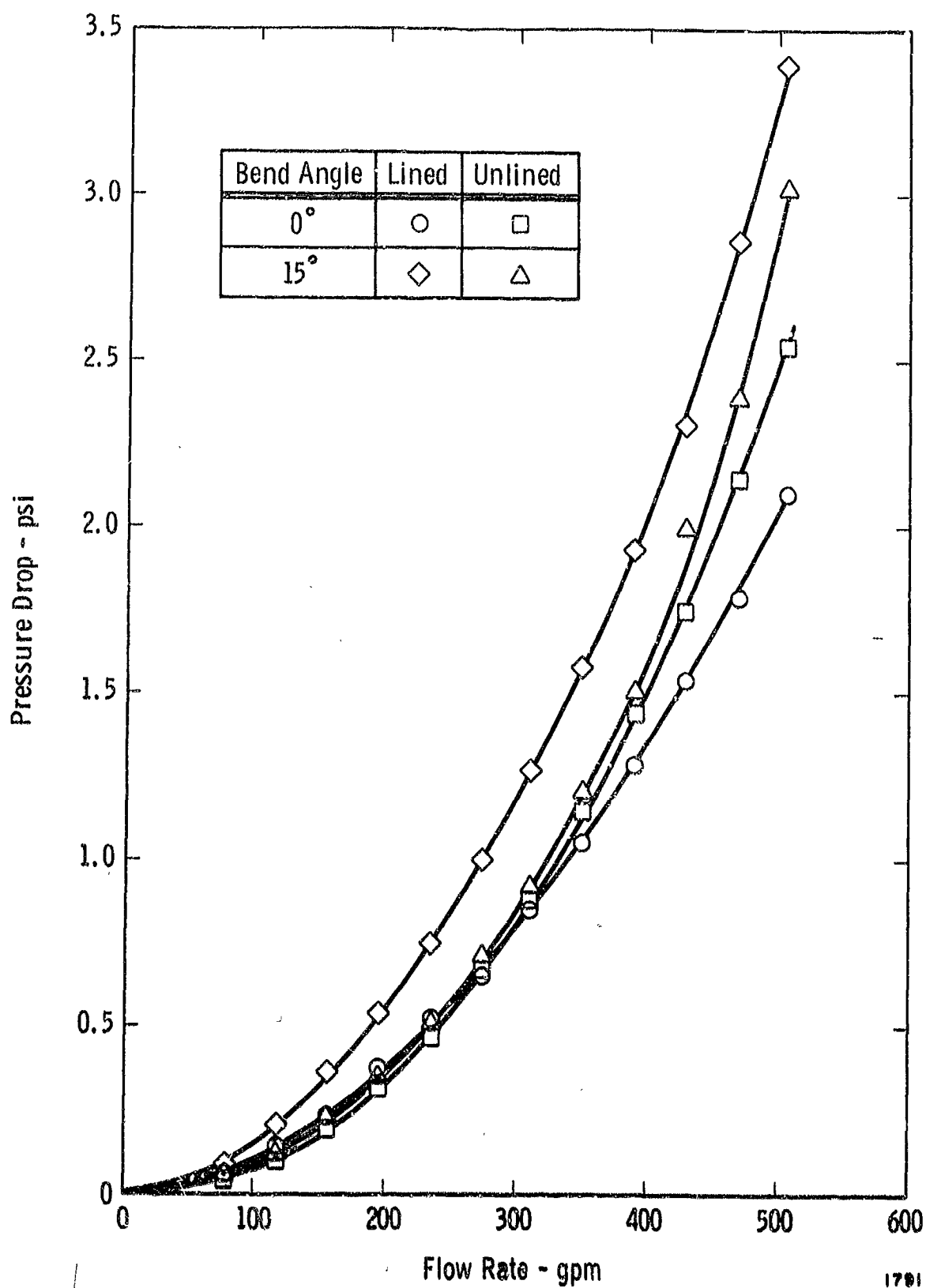Figure 66. Pressure Loss Characteristics Of Spiral Wound Metal Shim Liner

1790

Figure 67. Pressure Loss Characteristics Of Longitudinal Leaf Screen Liner

respect, except that the cross-sectional shapes were different in the bend region. One elbow was conventional in design and had a uniform square cross section. Figure 68 illustrates the new duct design. Note that this new design has an increased area on the inside of the bend but a decreased area on the outside of the bend; the reason for this shape will be discussed below. It was found from testing that the new design had roughly 40 percent less pressure loss than the conventional design. It is anticipated that a greater reduction in loss could be achieved with more detailed changes in the cross sectional shape.

Low Loss Bend Concept

Consider Figure 69, which illustrates the flow of an ideal (no viscosity) fluid through a bend. The predicted velocity profiles immediately upstream and downstream of the bend are uniform. Typical profiles for a real fluid flowing through a bend are shown in Figure 69. Here, because of the centrifugal force gradient which exists at the start of the turn, the high energy fluid tends to migrate to the outside of the elbow while the low energy fluid goes to the inside of the elbow; such a fluid migration constitutes a secondary flow. This mixing plus the mixing which occurs downstream as the fluid develops a normal velocity profile in the downstream duct causes a pressure loss which is nominally about an order of magnitude greater than the normal friction or viscous losses in a straight duct.

If one could, by some means, effectively reduce the driving force for this secondary flow without reducing the mean fluid velocity in the channel, then the overall elbow pressure loss could be reduced. To accomplish this reduction in secondary flow it would be necessary to decelerate the fluid near the suction wall and accelerate the fluid near the pressure, or outer, wall. Once this were accomplished, there should be two results: First, the overall pressure differential across the bend should be decreased and, consequently, low energy fluid migration to the inner wall reduced. Secondly, the centrifugal force gradient should be reduced so that the migration of high energy fluid to the outer wall is suppressed.

The manner in which the duct cross-sectional shape should be changed to bring about these local accelerations and decelerations of the fluid can be estimated analytically.
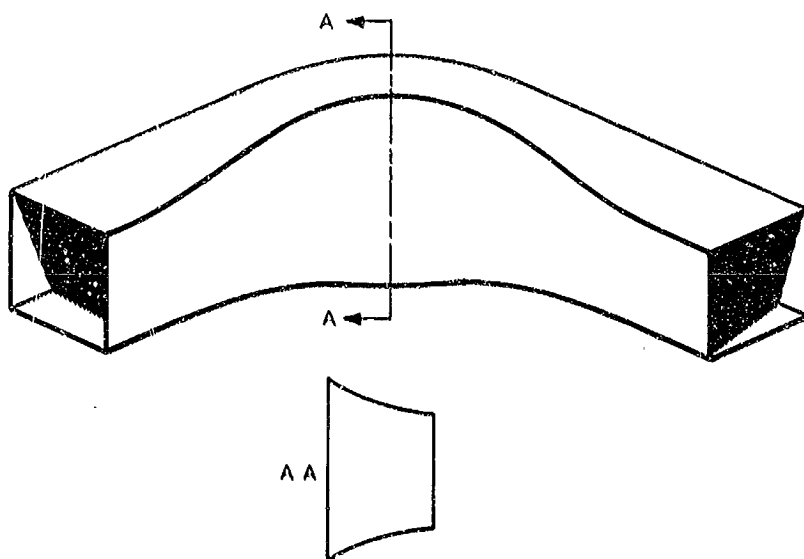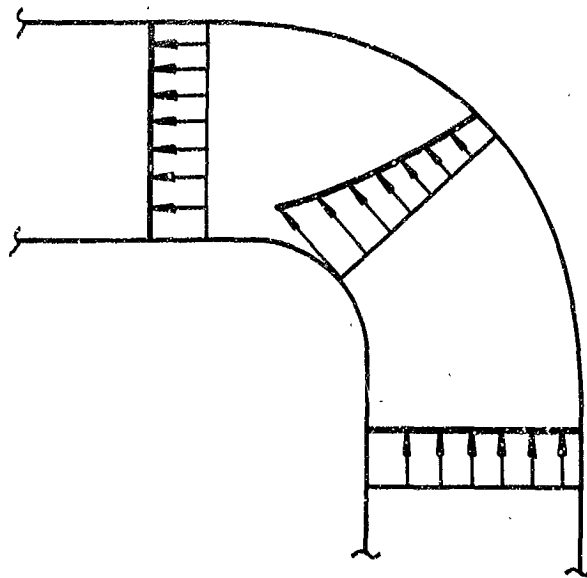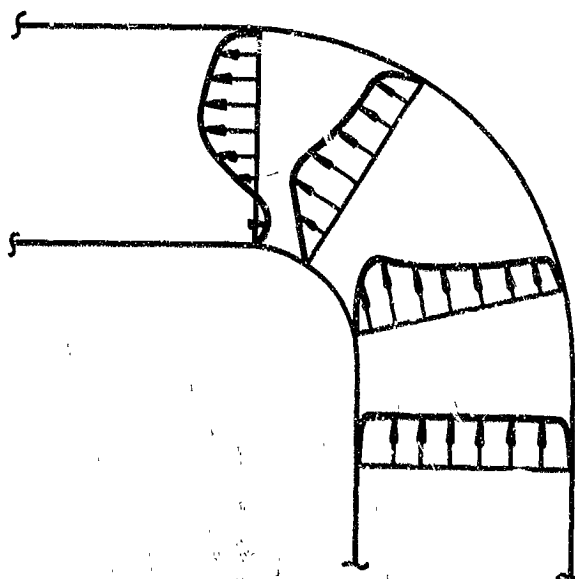
Figure 68. Illustration Of New Elbow Design

(a) Flow Of Ideal Fluid Through Bend

(b) Flow Of Real Fluid Through Bend

1685

Figure 69. Ideal And Real Fluid Flow Through Bend

Neglecting viscous effects, the velocity profile at the start of a bend will tend to be of the form (see Figure 69a)

$$v(r) = \frac{k_1}{r}$$

where

$$k_1 = \frac{(r_2 - r_1)\,\overline{V}}{\ell n\,(r_2/r_1)}$$

Here, $v(r)$ is the local fluid velocity as a function of radius r measured from the center of curvature of the bend, r_2 is the outer wall radius, r_1 the inner wall radius and $\overline{V}$ the mean fluid velocity in the duct.

To suppress the secondary flows it has already been argued that the centrifugal force gradient should be made equal to zero (constant centrifugal force across the bend); this means that the corrected duct local velocity $v'(r)$ should be of the form

$$\frac{v'(r)^2}{r} = k_2$$

where k_2 is a constant. Therefore, the bend duct height must be corrected so that the local velocity in the bend tends to a value

$$v'(r) = (k_2 r)^{0.5}$$

or

$$v'(r) = \frac{v(r)}{C(r)} = \frac{k_1}{r C(r)}$$

The quantity $C(r)$ is a duct correction factor and has a value equal to

$$C(r) = k_1 k_2^{-0.5}\, r^{-1.5}$$

To define k_2, we will arbitrarily spcify that the corrected duct have everywhere a centrifugal force equal to the ideal centerline centrifugal force in the original duct; in other words

$$k_2 = \frac{8 k_1^2}{(r_2 + r_1)^3}$$

and, therefore

$$C(r) = 0.354 \left(\frac{r_2 + r_1}{r}\right)^{1.5}$$

To correct a given duct, the height across the bend must be modified by the quantity $C(r)$. In other words, if $h(r)$ is the uncorrected duct height as a function of radius, then the corrected duct height $h'(r)$ is

$$h'(r) = C(r) h(r)$$

This type of correction can be applied equally well to square, rectangular, circular, etc., ducts.

Experimental Results

Two experimental elbows have been constructed and tested to verify the concept described in the foregoing. Both elbows had identical cross-sectional areas, and inner and outer wall radii; the only difference was that one elbow had a corrected cross-sectional shape in accordance with the above. Figure 68 illustrates the corrected elbow. Both test items were installed in a water flow system and overall pressure loss was monitored. On both elbows, the pressure loss was measured between two points several duct widths upstream and downstream from the bend; Figure 70 shows the resulting overall pressure loss for both test items. It is readily seen that the new design has a lower overall loss, hence, is more efficient.

Figure 71 shows plots of the cross-channel pressure envelopes for the two experimental elbows. Note the reduction in the peak pressure differential for the new design. This reduction in cross-channel pressure differential means that the driving force for the fluid migration, discussed earlier, has been reduced and, therefore, a reduction in overall pressure loss is expected.

Conclusion

The tests performed on the two elbows verified that it is possible to reduce pressure losses in duct elbows by properly designing the duct cross-section in the bend region so as to minimize secondary flows and, hence, flow profile distortion. This concept can be applied to a duct with any basic shape.
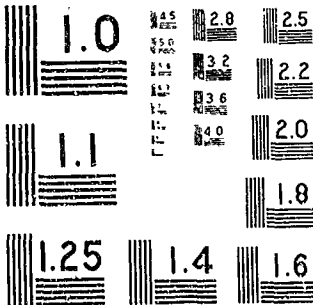
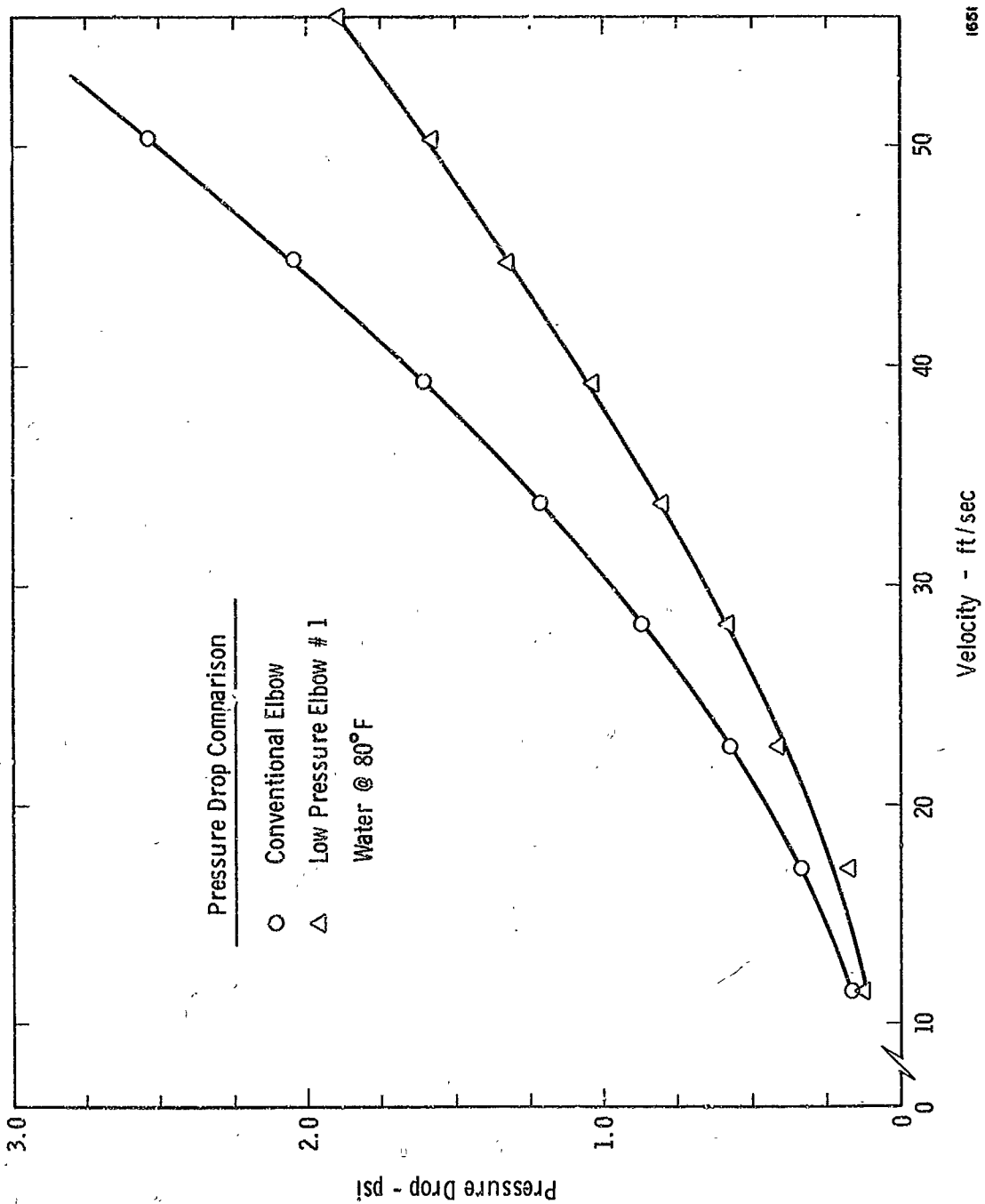MICROCOPY RESOLUTION TEST CHART
NATIONAL BUREAU OF STANDARDS – 1963

Figure 70. Comparison Of Conventional And Low Loss Bend Design # 1
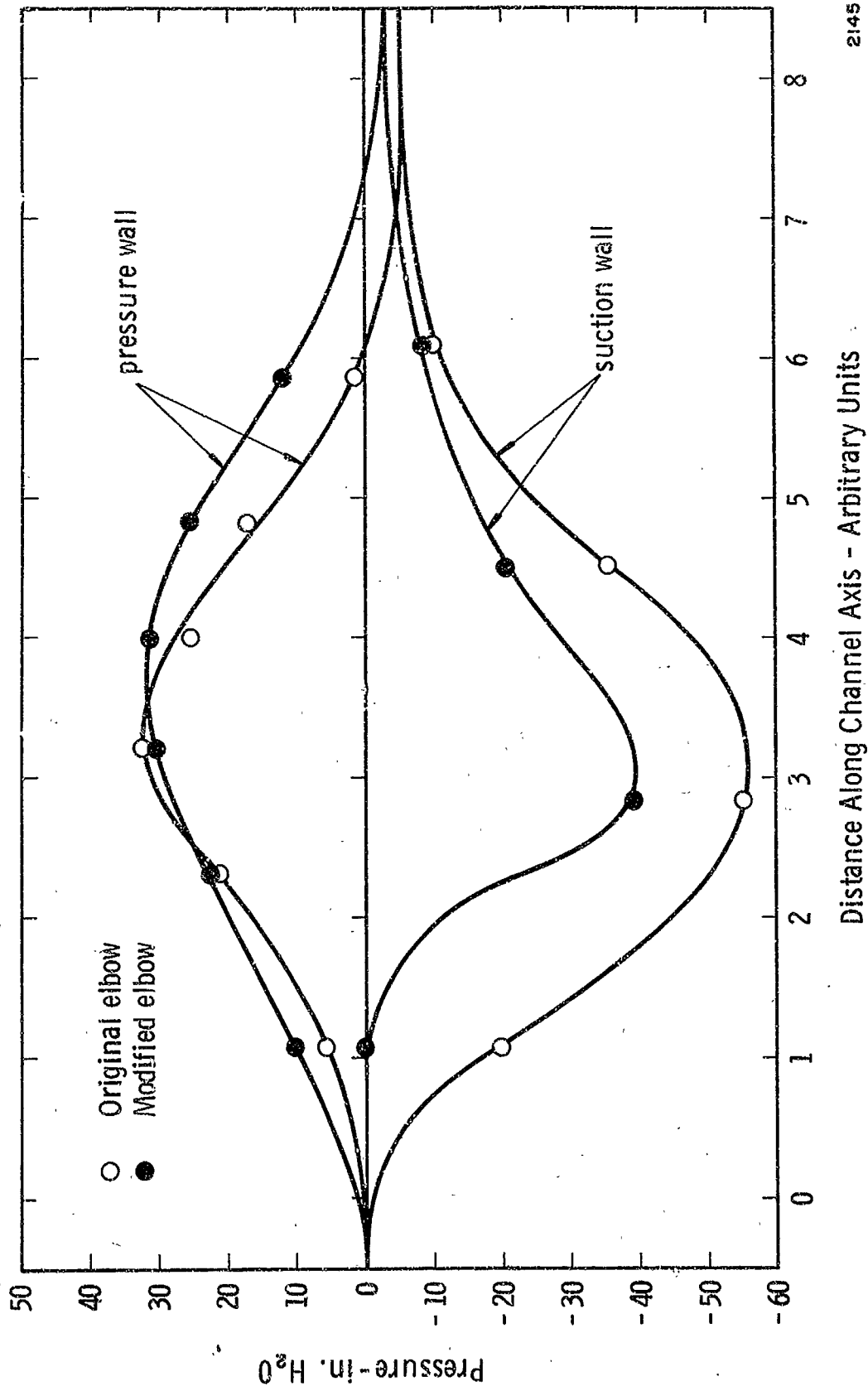
Figure 71. Cross - Channel Pressure Envelopes For Conventional And Modified Elbows

2145

127

V. CONCLUSIONS AND RECOMMENDATIONS

V.1 Conclusions

A number of conclusions have been derived from the study to date; these are listed below:

Bellows Flow-Induced Vibrations

(1) Flow-induced vibration of bellows is caused by a fluid-elastic instability; specifically it is caused by fluid vortex shedding from the bellows convolutions which couples with the convolution vibrations. In the absence of convolute motion there is no well defined large scale vortex shedding.

(2) The frequency of the vortex shedding can be related to the fluid velocity and convolute dimensions through the use of a Strouhal number given by

$$S = f_s \, \sigma/V$$

where f_s is the shedding frequency, V the velocity, and σ the convolute tip width. This Strouhal number appears to be a weak function of only one parameter which is λ/σ, the ratio of pitch to tip width.

(3) The fluid pressure force which is exerted on a single bellows convolute can be expressed in the form

$$F = C_F \, A_p \, (1/2\,\rho V^2)$$

where C_F is a vortex force coefficient, A_p is the height area of the convolute, ρ is fluid density, and V velocity. The data obtained for C_F from a number of bellows tests shows it to be a strong function of the parameter λ/σ.

(4) It appears that, because of a vortex reinforcement phenomena, there are "optimum" values of λ/σ which result in local minimum or maximum values of C_F. Therefore, there might be some advantage in designing the convolute geometry to give a minimum C_F value. In general, "open" convolution designs are better than "closed" designs.

(5) The response of a given bellows to flow excitation can
be predicted with fair accuracy with a method described
in this report. Strictly speaking, and because no support-
ing data is presently available, this method is presently
limited to bellows flowing liquids and having a size of
about 2-inches ID. We believe, however, the method can
safely be extended to include gases and larger bellows. One
important restriction is that no radial acoustic resonance
be present to cause amplification of the forces. Future
work is intended to extend the validity of this bellows flow
excitation method.

(6) A very important factor in bellows vibrations is the value
of the dynamic amplification factor Q. Test results show
that Q is dependent on the bellows specific spring rate
$(K_A N_c / D_m)$, the internal fluid media, and the number of
plies. A preliminary set of universal Q value curves has
been prepared in terms of known bellows and flow parameters,
and can be used for present best-estimate purposes.

(7) A special parameter, called the "Stress Indicator" has been
derived and is felt to be of value in determining the relative
vibration severity of various bellows. All information
required to make "Stress Indicator" calculations is contained
in the report.

(8) A preliminary curve giving fatigue failure information has
been compiled and can be used to estimate the possibility of
failure of a given bellows.

(9) Various kinds of liners can be very effective in suppressing
bellows flow-induced vibrations. Care must be exercised,
however, to keep from causing an increase in pressure loss
because of the liner.

(10) Various kinds of external damping devices can be effected
in reducing bellows vibrations. Care must be taken to ensure
that damping is added to the bellows.

(11) Rather large errors can be expected when using existing
spring rate and stress (in terms of deflection) calculation
methods, largely because of an inaccurate knowledge of true
convolute dimensional data.

(12)   The use of an accelerometer for monitoring bellows
         flow-induced vibrations can give misleading results
         as to the most severe modes of vibration, particularly
         where acoustic resonances occur in the system.

Bellows and Elbow Pressure Loss

(13)   Only one existing bellows pressure loss correlation
         method (see Figure 58) is considered valid for general
         bellows geometry, and this method can lead to rather
         large errors in certain cases.

(14)   Careful attention to convolution geometry design can
         result in a 50 percent or more reduction in pressure
         loss when comparing a good design and a poor design.
         Typical good and bad designs were shown in Figure 61.
         In general, a good design is one with small, open convo-
         lutions. Large, close pitch type convolutions generally
         give large losses.

(15)   A bend with changes in cross section such as described
         in this report can result in a substantial reduction in
         pressure loss compared with a bend of constant geometry
         cross section.

V.2   Recommendations

At this point we have several recommendations:

(1)   It is recommended that the bellows flow-induced vibration
         calculation procedures presented in this report be used
         for predicting the adequacy of bellows designs and appli-
         cations. The reader should be aware, however, of the
         stated limitations of the method. In particular, care
         should be taken in those cases where acoustic resonance
         does, or may, occur.

(2)   It is recommended that the use of external damping devices
         be considered as a practical means of suppressing flow-
         induced vibration levels.

130

(3)   It is recommended that the bellows pressure loss correlation given in Figure 58 be used for prediction purposes.

(4)   It is recommended that more work be done to explore flow-induced vibrations of much larger bellows and thus validate the prediction method for this case. Also, a careful study should be made of the acoustic resonance phenomena.

(5)   Extreme care should be exercised in interpreting accelerometer data which is taken for bellows flow-induced monitoring purposes. Strain gages should be used where feasible.

APPENDIX A

Dimensional Data for Test Bellows Cited
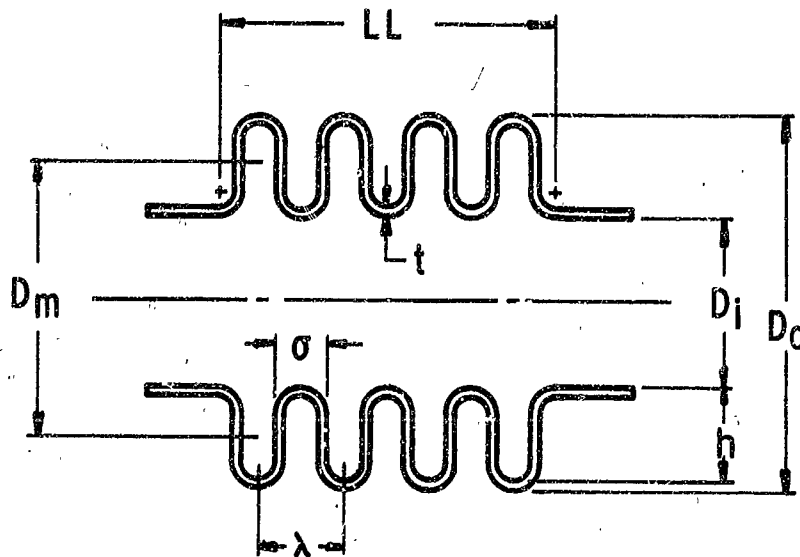
N_C = Number of convolutions counted from the outside.

N_p = Number of plys

Bellows Number	D_i	D_o	D_m	LL	N_c	N_p	h	λ	σ	t
#101, 102, 105, 112	1.49	2.22	1.85	1.80	7	1	.35	.26	.125	.013
#103, 104, 110, 114	1.46	2.03	1.74	1.77	8	1	.27	.22	.144	.013
P/N-08047, #106	1.98	2.32	2.16	2.15	9	1	.16	.24	.095	.006
P/N-08049, #107	1.97	2.33	2.15	2.15	9	2	.17	.24	.140	.006
P/N-08051, #108	2.00	2.34	2.17	2.15	9	3	.15	.24	.140	.006
P/N-08052, #113	1.99	2.45	2.22	2.41	14	1	.22	.17	.090	.013

Note: These dimensions are for geometric description only. Actual dimensions for a particular bellows may vary somewhat from these representative dimensions.

DIMENSIONAL DATA FOR TEST BELLOWS CITED

APPENDIX B

Bellows Spring Rate and Stress-Deflection

BELLOWS SPRING RATE AND STRESS-DEFLECTION

Spring rate and stress-deflection relationships are of interest in bellows vibration studies as well as in quasi-static situations. However, agreement between experimental and analytical methods is quite poor unless a great deal of care is exercised in obtaining the bellows dimensions necessary for calculations. Also, the fact that material thickness is not constant in a formed bellows greatly complicates any analytical method, and necessitates a computer approach or the use of empirical correction factors for accurate results.

Some fairly simple analytical methods are available which can be quite useful if accuracy requirements are not too stringent.

Axial Spring Rate

Probably the most successful analytical method for determining spring rate is the one developed by Battelle Memorial Institute. The computer program NONLIN which was used in this method provides for nonlinear elastic deformations as well as for linear deformation. The program is completely described in Battelle's Technical Report No. AFRPL-TR-68-22.

It was found by Battelle that the dimensional data entered into the program is of critical importance if reasonable accuracy is expected. In fact, the destructive inspection method used in obtaining bellows dimensions is considered absolutely necessary. The bellows were encapsulated in a potting compound, sectioned along the longitudinal axis, polished, and then measured with a machinists microscope. This was done to one sample from each manufacturing lot. The remaining bellows in the lot were then used to obtain the experimental results.

For formed bellows, this technique resulted in calculated values which were consistently within 10% of the experimental values. For welded bellows the results were less accurate but still quite good.

Non-computer techniques are usually similar to or based on equations developed by F. Salzmann (10). The Salzmann method is outlined in Figures B.1 and B.2. These equations were developed for bellows with constant wall thickness and U-shaped convolutions. The results are good when this type of bellows is analyzed. This method should be especially

B1

$$K_A = \frac{\pi}{6} \frac{D_m E N_P}{(1-\nu^2) \zeta_{IV} N_c} \left(\frac{t}{h}\right)^3$$
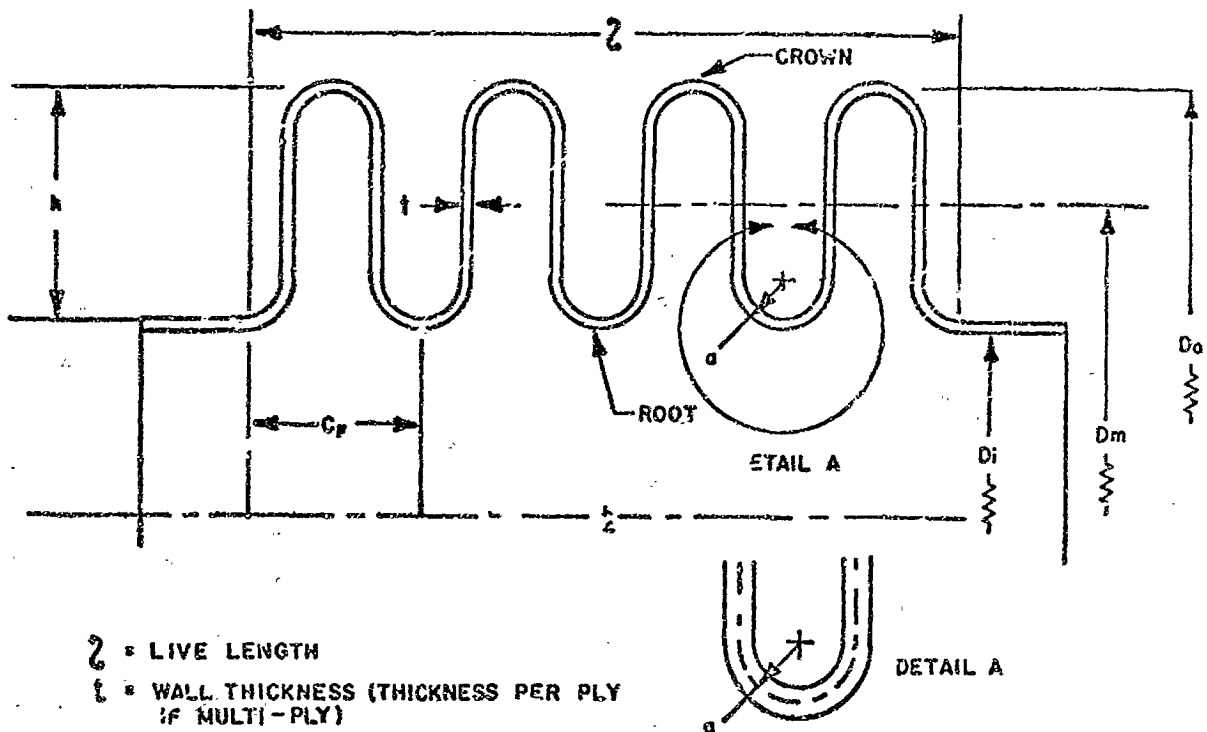
ℓ = LIVE LENGTH

t = WALL THICKNESS (THICKNESS PER PLY IF MULTI-PLY)

C_P = FREE PITCH

h = DISC HEIGHT, MEAN

a = FORMING RADIUS, MEAN

D_m = MEAN BELLOWS DIAMETER = $\frac{Do+Di}{2}$

D_o = OUTSIDE BELLOWS DIAMETER

D_i = INSIDE BELLOWS DIAMETER

N_c = NUMBER OF CONVOLUTIONS

N_p = NUMBER OF PLY

K_A = AXIAL SPRING RATE

P = FORCE TO DEFLECT BELLOWS AN AMOUNT δ

δ = DEFLECTION OF BELLOWS, AXIALLY

E = YOUNG'S MODULUS

ν = POISSON'S RATIO

ζ_{IV} = SALZMANN'S SHAPE FACTOR, See Fig. B.2

Figure B.1.   Bellows Axial Spring Rate

(From Reference 17)

$$X = \frac{\sqrt{RS}}{\sqrt[4]{3(1-\nu^2)}}$$
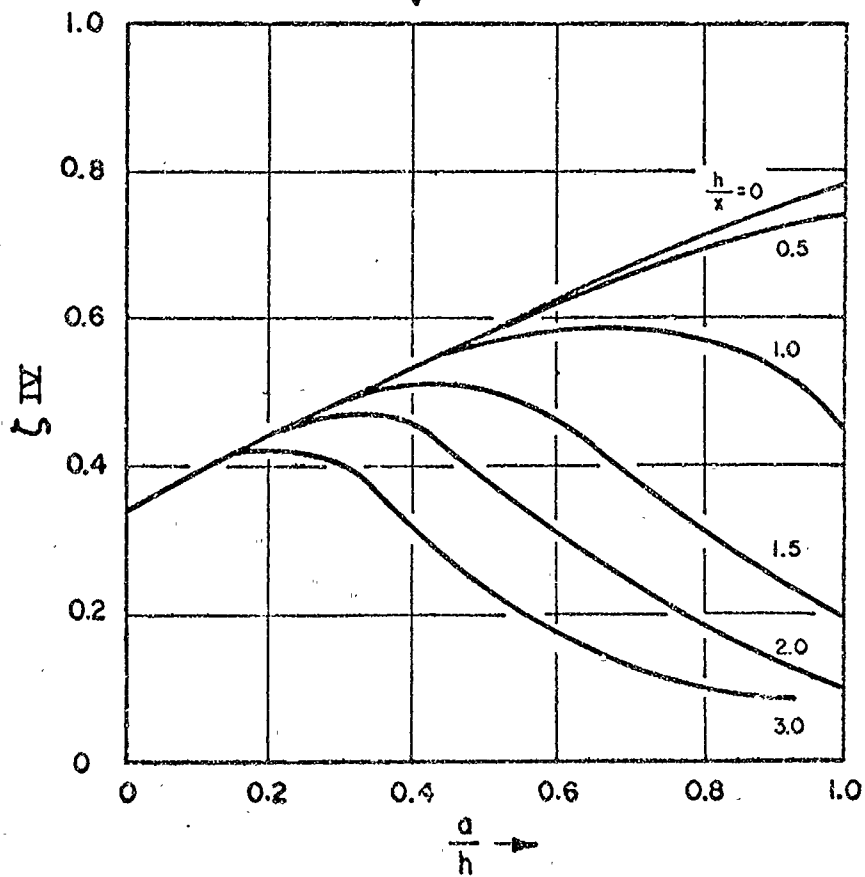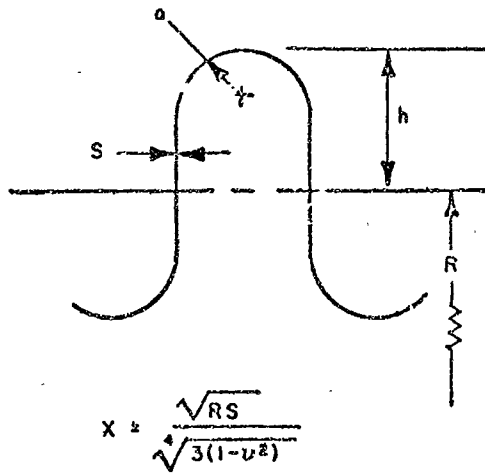
AXIAL EXPANSION OF THE QUARTER CONVOLUTION

$$\delta = \frac{Ph^3}{JE/(1-\nu^2)} \zeta \, \mathrm{IV}$$

Figure B.2. Bellows Axial Spring Rate

(From Reference 17)

useful with deposited bellows or accurately formed bellows where
material thinning is not excessive. The importance of accurate
dimensional data also applies to this method.

Other similar equations for unusual convolution shapes are
given in an article "Bellows Spring Rate," by J. D. Matheny in <u>Machine</u>
<u>Design</u>, January 1962.

The Salzmann method given above is taken from the SAE publi-
cation ARP-735.

When it is impractical to obtain accurate bellows measurements,
and when approximate spring rate is sufficient, the simplified equation
shown below is very convenient:

$$K_A = D_m E \frac{N_p}{N_c} \left(\frac{t}{h}\right)^3$$

The nomenclature here is the same as in Figure B.1.

Table B.1 gives a general idea of what can be expected from the
Salzmann and the simplified methods.

Convolution Shape	S	U	U	U	S
N_c	9	8	7	8	21
N_p	1	1	1	1	1
D_i	2.00	1.5	1.5	1.5	1.5
D_m	2.16	1.74	1.86	1.75	1.71
t	0.006	0.013	0.013	0.013	0.009
h	0.162	0.256	0.345	0.267	0.201
Rate (Test)	282	1000	544	877	251
Rate (Salzmann)	378	980	550	870	300
Rate (Simplified)	364	855	428	755	224

TABLE B.1 Comparison of Calculated and Experimental
Spring Rate

If very accurate results are required, the spring rate should be determined
experimentally for each individual bellows.

Stress-Deflection

In general, the information given in the discussion of spring rate also applies to stress-deflection relationships. Battelle Memorial Institute has obtained very good agreement between theoretical and experimental methods through the use of a computer program. This is reported in the Battelle Technical Report No. AFRPL-TR-6822. The Salzmann method for stress calculation is given in References 10 and 17.

For the bellows vibration studies in this report, strain gages were used mainly as monitors for vibration frequency, displacement, and relative stress level. However, a few tests were performed which compared experimentally determined stress with that given by the Salzmann equation. The experimental values obtained were in variance by from about 10 to 30 percent compared with the calculated values.

In addition to the work of Salzmann and Battelle, other literature of potential value is that of Clark (18), Laupa and Weil (19) and Turner and Ford (20).

APPENDIX C

Prediction of Bellows Added Fluid Mass
for Out-of-Phase Mode

PREDICTION OF BELLOWS ADDED FLUID MASS
FOR OUT-OF-PHASE MODE

Consider the idealized situation shown in Figure C.1; here we have two adjacent convolutions vibrating out of phase. It is assumed that the convolution sides remain straight at all times. This motion of two convolutions toward one another forces some fluid to move in the y direction with a velocity as a function of y given by

$$v(y) = \frac{\dot{x}y^2}{\delta h}$$

(C.1)

From the momentum equation, this fluid motion will cause a pressure gradient along the convolution given by

$$\frac{\partial p}{\partial y} = -\rho_f \frac{\partial v}{\partial t}$$

(C.2)

or

$$\frac{dp}{dy} = -\frac{\rho_f y^2}{\delta h} \ddot{x}$$

(C.3)

Integration gives (see Figure C.1)

$$p(y) = \frac{\rho_f \ddot{x}}{3\delta} \left[h^2 - \frac{y^3}{h} \right]$$

(C.4)

This is, then, the pressure acting along one side of the convolution because of out-of-phase acceleration of two adjacent convolutions. The problem now is to compute an effective force which acts on the convolution as it vibrates. If we knew precisely the mode shape of vibration of the convolution (it has been assumed linear) then this effective force could be calculated exactly (as could the fluid velocity distribution); we don't know the mode shape, however, so that the effective force must be estimated. It is reasonable to assume that it falls somewhere between two limiting values. The first is computed by calculating the total force acting over the convolution (both sides) which gives

$$F = \frac{\pi D_m \rho_f h^3}{2\delta} \ddot{x}$$

(C.5)
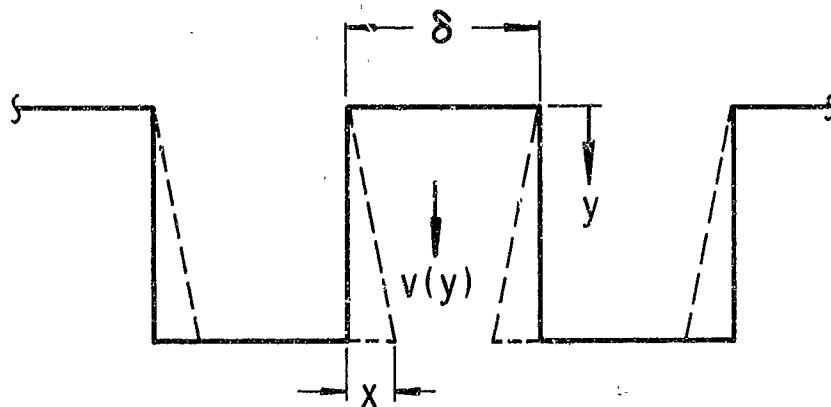
(a) Idealization Of Fluid Motion For Out-of-Phase Mode
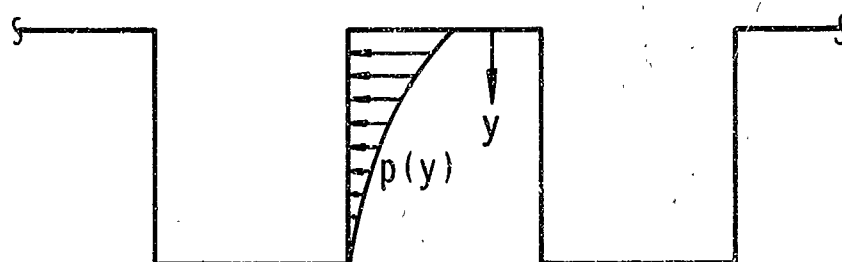
(b) Pressure Distribution Along Convolutions

2004

Figure C.1 Idealization Of Fluid Added Mass Effect
For Out-of-Phase Mode

This value of force is believed to be too high. A lower limiting value is felt to be obtained by weighing $p(y)$ with y and integrating over the convolution, hence

$$F = \int_0^h \left(\frac{\pi D_m}{h} \right) p(y) \, y \, dy$$

$$= \frac{\pi D_m \rho_f h^3}{5 \delta} \, \ddot{x} \tag{C.6}$$

A more reasonable value is believed to be

$$F = \frac{\pi D_m \rho_f h^3}{3 \delta} \, \ddot{x} \tag{C.7}$$

which gives an effective added mass for the out-of-phase mode of

$$m = \frac{\pi D_m \rho_f h^3}{3 \delta} \tag{C.8}$$

For two different cases, use of this value of added mass has given good results when experimental resonant frequency data was compared with calculated data; one was the ring convolution test model discussed previously, the other was a flexible hose for which the in-phase and out-of-phase modes were both calculated and observed.

APPENDIX D

Excitation of Longitudinal Acoustic Resonance
in Flow System

EXCITATION OF LONGITUDINAL ACOUSTIC RESONANCE
IN FLOW SYSTEM

When a bellows in a fluid line is experiencing vibrations induced by the fluid flow, it is generally noted that strong acoustic longitudinal standing waves are excited in the flow system piping. This phenomenon is caused by the bellows vibration exciting some fluid system acoustic mode(s), or more generally stated, resulting in a coupled bellows-liquid mode of the type discussed in the previous section. This coupling effect may be important for two reasons; first, it is feasible that the acoustic properties of the entire flow system may have a significant effect on the bellows flow-induced vibration characteristics and, second, strong acoustic resonance in the flow, with the bellows as a source, may adversely affect the performance of other components in the system, for example, the turbopump.

For the present discussion, the problem will be simplified by considering the bellows vibration as uncoupled from the flow system acoustics and simply representing a sound source in the system.

Consider Figure D.1 which shows an idealized case in which we have a ring vibrating in a pipe; this simulates the vibration of a single-bellows convolution. From an acoustic standpoint, this vibrating ring is a dipole sound source. Without going into the mathematical details of the near field sound characteristics of this source, we will assume that, for all practical purposes, this vibrating ring produces a fluctuating difference in pressure between a point immediately upstream and another point immediately downstream of the ring.

Now, consider Figure D.2, which shows a simplified schematic of our flow system with this idealized dipole source located as shown. Acoustically, we are assuming the system to consist of a line or duct with a dipole source at some intermediate point and with a constant pressure reservoir at each end. It is important to note that the pressures p and velocities v shown in Figure D.2 denote acoustic or nonsteady disturbance quantities, not total quantities. This explains why the acoustic pressure is zero in each reservoir, even though the steady-state pressure is not zero. The problem now is to calculate the response of the fluid system to this dipole source.

With little loss of accuracy, the fluid lines on either side of the source (L_1 and L_2) will be assumed frictionless and one-dimensional from an acoustic point of view. The acoustic impedance of each line (L_1 and L_2)
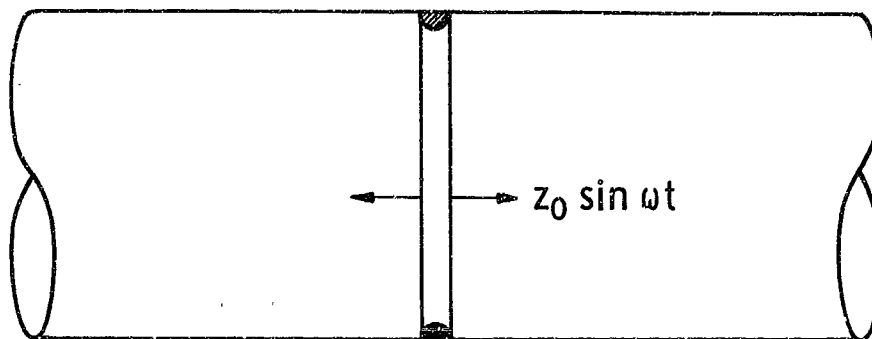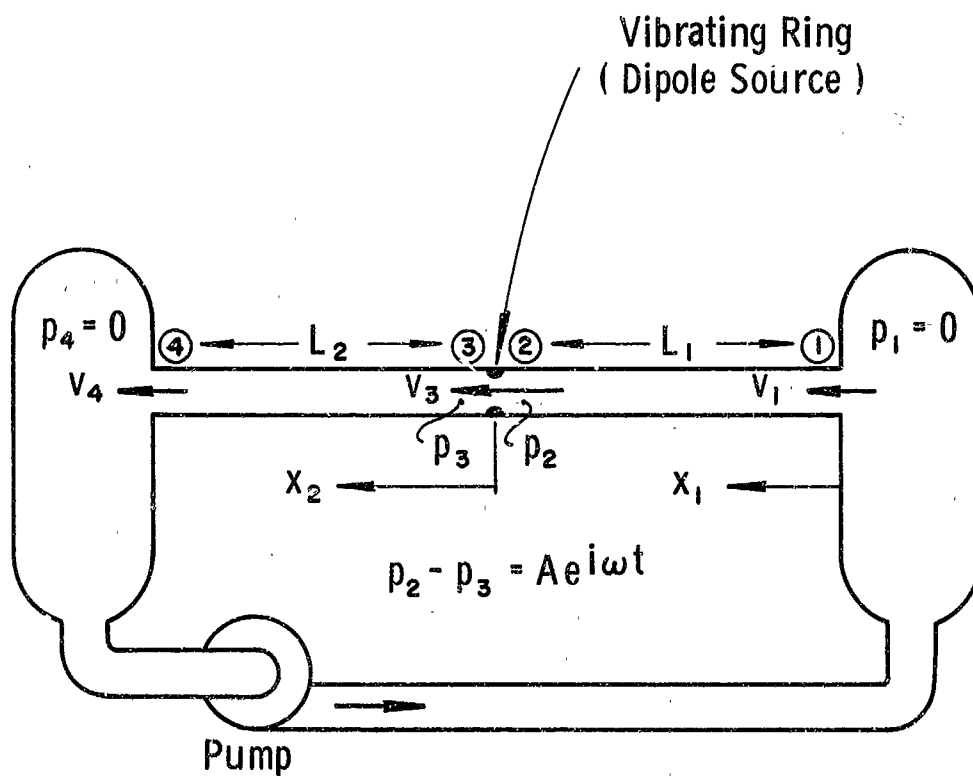
Figure D.1 Idealized Sound Source For A Single Convolution

Figure D.2 Simplified Acoustic Representation Of Flow
System And Dipole Source

looking away from the vibrating ring sound source is

$$\frac{p_2(i\omega)}{V_3(i\omega)} = -i\rho c \, \tan(\omega L_1/c) \qquad (D.1)$$

and

$$\frac{p_3(i\omega)}{V_3(i\omega)} = i\rho c \, \tan(\omega L_2/c) \qquad (D.2)$$

where ρ is fluid density and c speed of sound. These two relations can be combined to give

$$p_2(i\omega) - p_3(i\omega) = -i\rho c \, v_3(i\omega) \left\{ \tan(\omega L_1/c) + \tan(\omega L_2/c) \right\} \qquad (D.3)$$

From Equation (D.3) the magnitude and phase of v_3 can be determined for a given $p_2 - p_3 = A \, e^{i\omega t}$ (value of sound source). Knowing $p_2(i\omega)$, $p_3(i\omega)$ and $v_3(i\omega)$, then the acoustic pressure and velocity at any position x_1 or x_2 along the ducts can be determined from the equations

$$p(x_1, i\omega) = p_2(i\omega) \cos[\omega(L_1 - x_1)/c] + i\rho c \, v_3(i\omega) \sin[\omega(L_1 - x_1)/c] \qquad (D.4)$$
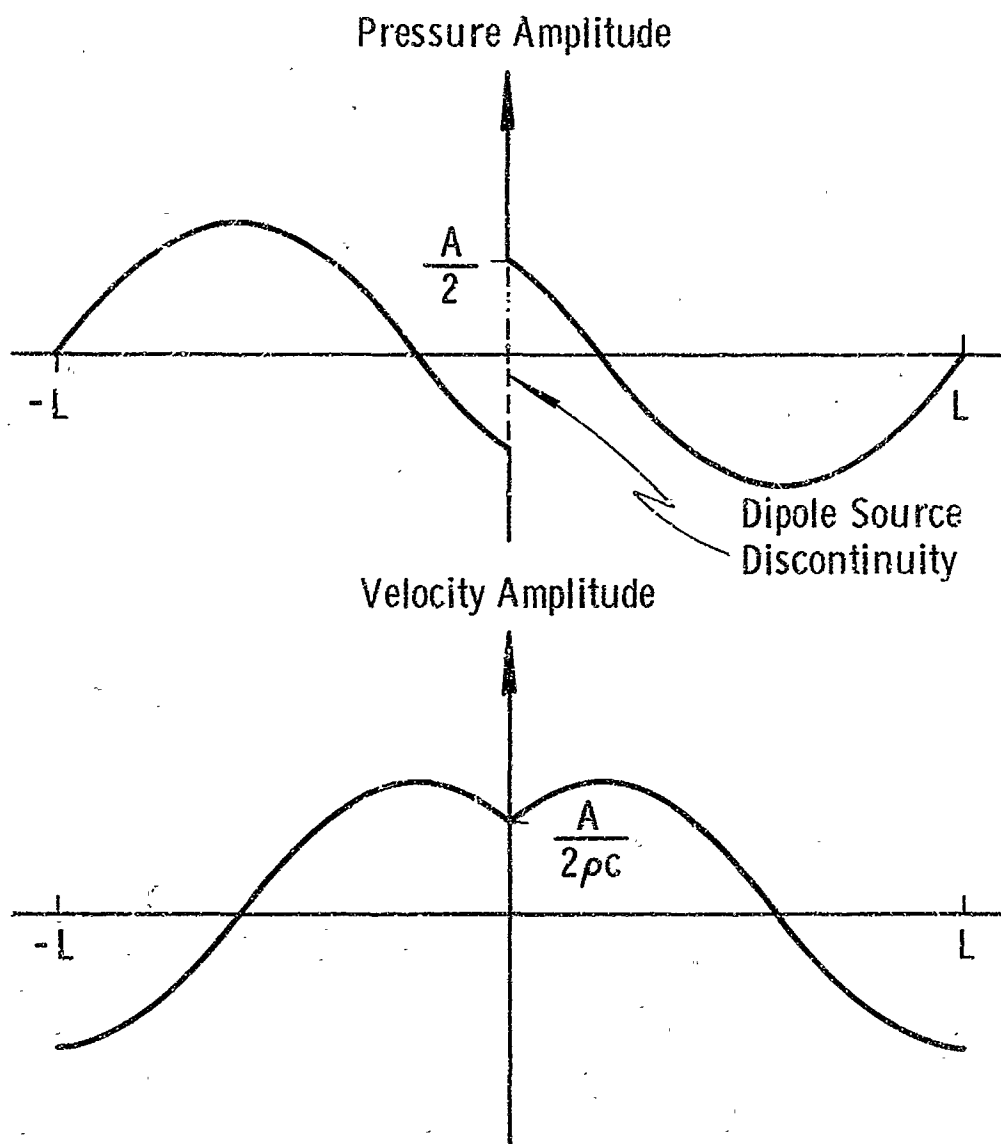
$$v(x_1, i\omega) = v_3(i\omega) \cos[\omega(L_1 - x_1)/c] + \frac{i}{\rho c} p_2(i\omega) \sin[\omega(L_1 - x_1)/c] \qquad (D.5)$$

and

$$p(x_2, i\omega) = p_3(i\omega) \cos(\omega x_2/c) - i\rho c \, v_3(i\omega) \sin(\omega x_2/c) \qquad (D.6)$$

$$v(x_2, i\omega) = v_3(i\omega) \cos(\omega x_2/c) - \frac{i}{\rho c} p_3(i\omega) \sin(\omega x_2/c) \qquad (D.7)$$

The above relations describe standing waves in the flow system ducts. The properties of these standing waves, that is the location of pressure nodes, antinodes and possible resonances, depend essentially upon the values of L_1 and L_2.

Figure D.3 System Acoustic Standing Wave Mode Shape
For $L_1 = L_2 = L$, $\omega L / c = 5\pi/4$

For example, assume $L_1 = L_2 = L$, and also put $x_3 = L_1 - X_1$; eliminating P_2, P_3 and V_3 from Equations (D.4) through (D.7) gives

$$p(x_1, i\omega) = \frac{A\, e^{i\omega t}}{2} \left\{ \cos(\omega x_3/c) - \sin(\omega x_3/c) \cdot \cot(\omega L/c) \right\} \qquad (D.8)$$

$$v(x_1, i\omega) = \frac{iA\, e^{i\omega t}}{2\rho c} \left\{ \cos(\omega x_3/c) \cot(\omega L/c) + \sin(\omega x_3/c) \right\} \qquad (D.9)$$

$$p(x_2, i\omega) = -p(x_1, i\omega) \qquad (D.10)$$

and

$$v(x_2, i\omega) = v(x_1, i\omega). \qquad (D.11)$$

Notice that the system will exhibit a resonance condition when $\omega L/c = n\pi$, (n is any integer); antiresonance occurs when $\omega L/c = \frac{\pi}{2} = n\pi$. Figure D.3 shows the system standing wave patterns predicted by Equations (D.8) through (D.11) with $\omega L/c = 5\pi/4$ as an illustration of a typical situation. Note the jump discontinuity in pressure at $x = 0$ with the value of the jump being equal to the strength of the dipole source. Further, note that the peak system acoustic pressure does <u>not</u> occur at the source, but rather occurs at some point along the line(s); this fact is generally true whenever $\omega L/c > \pi/2$.

As mentioned previously, the above formulation considered the vibrating ring (bellows idealization) to be simply a sound source for the flow system, hence, uncoupled from the system acoustic properties. In the more general case, the influence of the system upon the bellows vibration should be considered.

REFERENCES

1.   Daniels, V. R., "Dynamic Aspects of Metal Bellows," The Shock and Vibration Bulletin, No. 35, Part 3, Jan. 1966. pp. 107-124.

2.   Lytle, A. D., "Dynamics of Bellows Filled with an Incompressible Liquid," Journal of Spacecraft and Rockets, Vol. 5, No. 1, 1968, pp. 9-13.

3.   Toebes, G. H. and Eagleson, P. S., "Hydroelastic Vibrations of Flat Plates Related to Trailing Edge Geometry," Journal of Basic Engineering, Trans. ASME, Vol. 83, Dec. 1961, pp. 671-678.

4.   Marris, A. W., "A Review of Vortex Streets, Periodic Wakes, and Induced Vibration Phenomena," Journal of Basic Engineering, Trans. ASME, Vol. 86, Sept. 1964, pp. 165-196.

5.   Toebes, G. H., "Flow Induced Structural Vibrations," Journal of Engineering Mechanics, Proceedings, ASCE, Vol. 91-EM6, 1965.

6.   Toebes, G. H. and Ramamurthy, A. S., "Fluidelastic Forces on Circular Cylinders," Journal of Engineering Mechanics, Proceedings, ASCE, Vol. 92-EM, 1967.

7.   Protos, A., Goldschmidt, V. W. and Toebes, G. H., "Hydroelastic Forces on Bluff Cylinders," Journal of Basic Engineering, Trans. ASME, Vol. 90, Series D, No. 3, September 1968, pp. 378-386.

8.   Haugen, R. L. and Dhanak, A. M.,"Momentum Transfer in Turbulent Separated Flow Past a Rectangular Cavity," Journal of Applied Mechanics, Trans. ASME, Vol. 33, Sept. 1966, pp. 641-646.

9.   Townes, H. W. and Sabersky, R. H., "Experiments on the Flow Over a Rough Surface," International Journal Heat Mass Transfer, Vol. 9, 1966, pp. 729-738.

10. Salzmann, F., "Ueber die Nachgiebigkeit von Wellrohrexpansionen," Schweiz. Bauztg., Band 127, Nr. 11, March 1946, pp. 127-130.

11. Lazan, B. J., Damping of Materials and Members in Structural Mechanics, Pergamon Press, Oxford, England, 1968.

12. Daniels, C. M. and Cleveland, J. R., "Method of Predicting Frictional Loss in Metal Bellows and Flexible Hose," NASA Tech. Brief No. 66-10662, December 1966.

13. Riley, K. L., "Flow Losses in Flexible Hose," Ph.D. Dissertation, Louisiana State University, May 1967.

14. Gerlach, C. R., "Study of Minimum Pressure Loss in High Velocity Duct Systems," Quarterly Report No. 1, Contract No. NAS8-21133, Southwest Research Institute, August 1967.

15. Gerlach, C. R., "Study of Minimum Pressure Loss in High Velocity Duct Systems," Quarterly Report No. 2, Contract No. NAS8-21133, Southwest Research Institute, November 1967.

16. Gerlach, C. R. and Schroeder, E. C., "Study of Minimum Pressure Loss in High Velocity Duct Systems," Quarterly Report No. 5, Contract No. NAS8-21133, Southwest Research Institute, August 1968.

17. Aerospace Recommended Practice (ARP) No. 735, Society of Automotive Engineers Publication, 1966.

18. Clark, R. A., "On the Theory of Thin Elastic Toroidal Shells," Journal of Mathematics and Physics, Vol. 29, 1950, pp. 146-178.

19. Laupa, A. and Weil, N. A., "Analysis of U-Shaped Expansion Joints," Journal of Applied Mechanics, Vol. 29, 1962, pp. 115-123.

20. Turner, C. E. and Ford, H., "Stress and Deflexion Studies of Pipeline Expansion Bellows," Inst. of Mechanical Engineers, Vol. 171, November 1957, pp. 526-552.